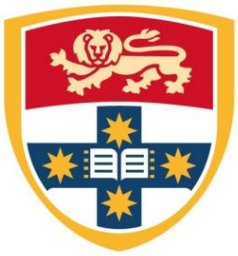

THE UNIVERSITY OF SYDNEY

Influence of the MuSK-system on muscle pathology in the *mdx* mouse model of Duchenne Muscular Dystrophy

A thesis submitted in fulfilment of the requirements for the degree of

Master of Philosophy

Besa Beqaj

Faculty of Medicine & Health

Discipline of Physiology

University of Sydney

2020

Declaration

The work in this thesis was carried out during the period of October 2017 to December 2019 in the Discipline of Physiology at the University of Sydney. The content of this thesis is my own work and all assistance received in preparing the thesis and sources have been acknowledged. All experiments were performed by myself, except where explicit reference to the work of others is mentioned in the text of the acknowledgments. All work in this thesis was carried out with approval from the University of Sydney Animal Ethics Committee and the University of Sydney. This thesis has not been presented for any degree or diploma at this university or elsewhere.

Besa Beqaj

December 2019

Acknowledgements

I would like to thank everyone who helped me throughout the course of my masters, whether it be technical or emotional support. I am grateful for the patience, support and guidance from my supervisor A/Prof Bill Phillips throughout my masters. I would also like to thank everyone in Chris Murphy's lab for adopting me into their lab family and making me feel like one of their own. I would like to thank all my family and friends for their love and support, without you all I wouldn't be where I am today.

The editorial feedback on this thesis was received from my supervisor A/Prof Bill Phillips. Some figures in this thesis arise from the work of others: Joanne Ban performed the experiments that produced Figure 1.12, 1.13 and 3.36. Additionally, the muscles used in chapter 3 were injected and dissected by Joanne Ban during her PhD, while the muscles used in chapter 4 were injected by our post-doc Dengyun Ge and dissected by me. I would also like to thank Prof Frank Lovicu for supplying me with the neonatal mice used in chapter 4. Besides that, I'd like to thank Tim De Solom for plotting the force-frequency curves based on Joanne's contraction data and Joanna Huang for helping me with TA and soleus muscle dissection/freezing and the blinding of my immunofluorescence slides. I would like to thank my supervisor A/Prof Bill Phillips and our post-doc Lorenzo Odierna for helping me with culling the animals used in chapter 4.

I would also like to thank Donna Lai and Sheng Hua from the Molecular Biology Facility for their technical support with cryosectioning; Sadaf Kalam, Chad Moore and Nasir Uddin from the Advanced Microscopy Facility for their training and technical advice on microscopy. Finally, I would like to thank all past and present members of the Phillips lab for providing an enjoyable and supportive environment.

Table of Contents

Chapter 5: Conclusions

List of Figures

Chapter 1: Introduction

Chapter 2: Materials and methods

Chapter 3: MuSK-GFP supplementation does not alter the composition of *mdx* muscle

Chapter 4: Effect of MuSK-system on muscle fibre regeneration

List of Tables

Chapter 2: Materials and methods

Chapter 4: Effect of MuSK-system on muscle fibre regeneration

List of Abbreviations

AAV	Adeno-associated viral vector
AChR	Acetylcholine receptors
ALS	Amyotrophic Lateral Sclerosis
BMP	Bone Morphogenetic Protein
CMV	Cytomegalovirus
DAPC	Dystrophin associated protein complex
DMD	Duchenne muscular dystrophy
Dok7	Downstream-of-tyrosine-kinase 7
DSHB	Developmental Studies Hybridoma Bank
ECM	Extracellular matrix
EDL	Extensor digitorum longus
FAPs	Fibro-adipogenic progenitors
GFP	Green fluorescent protein
LRP4	Low density lipoprotein receptor related protein 4
MCK	Muscle-specific creatine kinase
MHC	Myosin heavy chain
mRNA	Messenger ribonucleic acid
MMPs	Matrix metalloproteases
MuSK	Muscle specific kinase
NMJ	Neuromuscular junction
P1	Postnatal day 1

List of Abbreviations

PBS	Phosphate buffered saline
PGC- 1α	Proliferator activated receptor gamma coactivator - 1 alpha
RDS	Research data store
SOPs	Standard operating procedures
TA	Tibialis anterior
TGF-β1	Transforming growth factor- beta 1
TIMPs	Tissue inhibitors of metalloproteases

Abstract

Duchenne Muscular Dystrophy (DMD) is a severe muscle wasting disorder caused by a mutation in the dystrophin gene. The dystrophin-deficient *mdx* mouse is the most common animal model of DMD. Muscle fibres lacking dystrophin go through cycles of degeneration followed by progressively impaired regeneration. Eventually, degeneration dominates and fibres are replaced with extracellular matrix (fibrosis). The receptor tyrosine kinase muscle specific kinase (MuSK) has a well-established role in the maintenance of the neuromuscular junction. However, recent work in the lab suggests that it can also reduce the fragility of muscle fibres in the *mdx* mouse. In this thesis, the tibialis anterior (TA) muscles of 3-4 week old *mdx* mice were injected with AAV-MuSK and culled at 12 weeks of age for histological analysis (chapter 3). Supplementation with MuSK-GFP did not alter the composition of the muscle, with no differences in fibre type populations or in the proportion of the muscle occupied by extracellular matrix (collagen I) vs muscle fibre area (pan-myosin). Additionally, in chapter 4 *mdx* TA muscles were supplemented with other members of the MuSK-system (Dok7 and Rapsyn). This batch of *mdx* mice were injected at 4 weeks of age with one of the following AAVs encoding: MuSK, mutant MuSK lacking the Ig3 domain (MuSK-ΔIg3), Dok7 or Rapsyn before being culled at 9 weeks of age for histological analysis. Supplementation with AAV-Dok7 was found to improve muscle pathology by reducing the number of recently degenerated/regenerated muscle fibres. Moreover, AAV-MuSK and AAV-Rapsyn were found to reduce muscle fibre girth. Together, these findings suggest a novel role for MuSK-system in protecting dystrophic muscles from damage. Thus, supplementation of MuSK-system components (MuSK, Dok7 and Rapsyn) may present a therapy for DMD and other neuromuscular disorders.

CHAPTER ONE:
Introduction

1.1 Duchenne Muscular Dystrophy

1.1.1 Clinical symptoms & progression

Duchenne Muscular Dystrophy (DMD) is an x-linked muscle wasting disorder caused by a loss of function mutation in the dystrophin gene (Guiraud & Davies, 2017). DMD is the most common and the most severe of all muscular dystrophies (Chang, Chevalier & Rudnicki, 2016), with an incidence of 1 in 5000 live male births (Guiraud & Davies, 2017). Boys with DMD are typically diagnosed at about 2-5 years of age as they experience proximal muscle weakness, delayed walking and hypertrophy of the calf muscle (Cros, Harnden, Pellissier & Serratrice, 1989; Guiraud & Davies, 2017). After the age of 7, muscle wastage begins to supersede muscle growth and by the age of 12 most boys with DMD are wheelchair bound (Guiraud & Davies, 2017; Kole & Kreig, 2015; Figure 1.1). Typically, assisted ventilation and intensive care are required for boys with DMD to survive into their mid-twenties. While assisted ventilation and corticosteroids have been used to prolong the life of DMD patients, there remains no effective treatment or cure for DMD (Kole & Kreig, 2015).

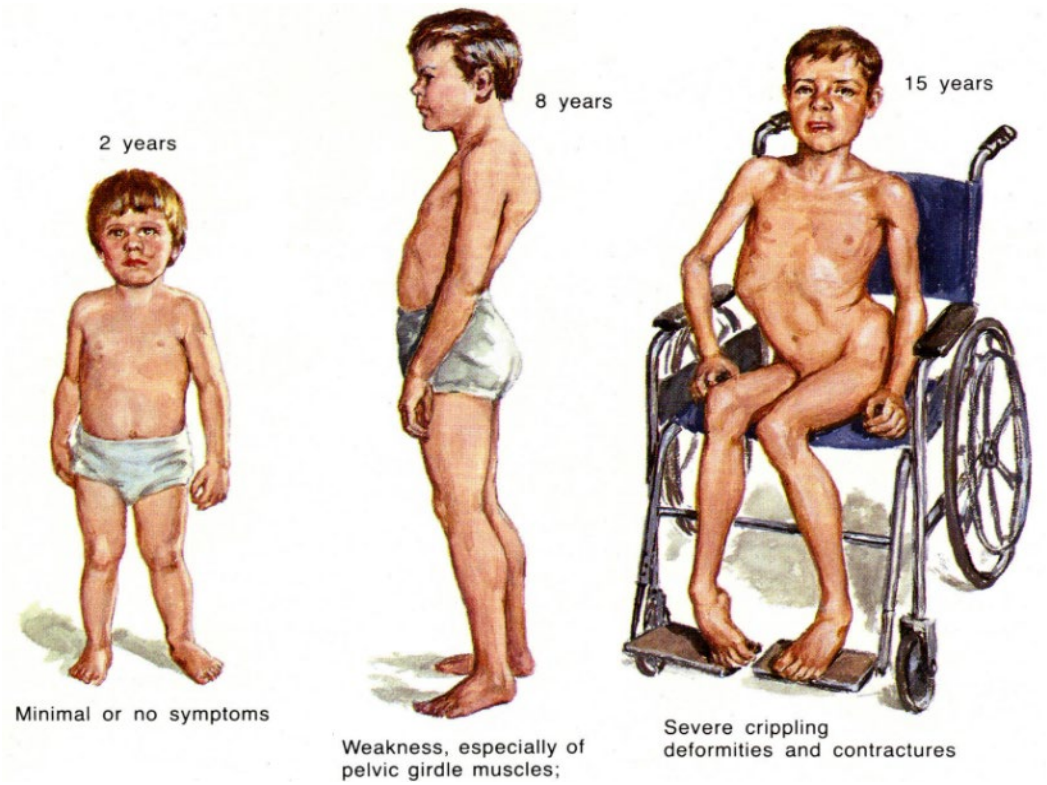

Figure 1.1: Typical presentation/progression of Duchenne Muscular Dystrophy from 2 years through to 15 years. Modified from Jones *et al.* (2011).

1.1.2 The DMD gene

The DMD gene, which encodes for a cytoskeletal protein called dystrophin, is one of the largest known genes in humans (Guiraud & Davies, 2017). The DMD gene is 2.4Mb long with 79 exons and 78 introns. Due to its large size, the DMD gene is susceptible to spontaneous mutations (Kole & Krieg, 2015). In fact, the DMD gene has one of the highest rates of spontaneous mutation (Guiraud & Davies, 2017). Most mutations causing DMD are deletions in one or more exon, resulting in either the partial or complete absence of dystrophin (Fairclough *et al.,* 2013). These deletions result in a frameshift, where the mRNA no longer encodes for a functional protein. Any non-functional proteins produced are believed to be degraded by the proteasome (Kole & Krieg, 2015). The remainder of DMD cases are caused by duplications and insertions/deletions of a single base pair (Guiraud & Davies, 2017).

1.1.3 Dystrophin

Dystrophin, the product of the DMD gene, is a cytoplasmic protein and a key component of the dystrophin-associated protein complex (DAPC). Other members of the DAPC include the: dystrobrevins, dystroglycans, sarcoglycans, sarcospans and syntrophins (Wallace & McNally, 2009; Figure 1.2). Together, these proteins anchor the actin-cytoskeleton of muscle fibres to the surrounding extracellular matrix (ECM), providing muscle fibres with the strength and flexibility needed to protect against contraction-induced injury (Manning & O'Malley, 2015). Dystrophin binds directly to the actin cytoskeleton of muscle fibres via its amino-terminal and spectrin-repeat domains (Manning & O'Malley, 2015). To complete the ECM-cytoskeletal link, dystrophin binds with β-dystroglycan via its cysteine-rich domain. This

dystrophin-β-dystroglycan binding indirectly links dystrophin to laminin within the ECM, via β- and α-dystroglycan (Figure 1.2). The remaining members of the DAPC have signalling roles, with sarcospan and the sarcoglycans playing both a signalling and structural role (Wallace & McNally, 2009).

In the absence of dystrophin, the DAPC becomes destabilised and is partially or completely lost from the sarcolemma (Chang, Chevalier & Rudnicki, 2016). This causes muscle fibres to become fragile and susceptible to contraction-induced injuries such as membrane tears. In turn, this leads to the premature death of muscle fibres, resulting in cycles of fibre degeneration and regeneration that ultimately lead to muscle wastage and weakness (Manning & O'Malley, 2015).

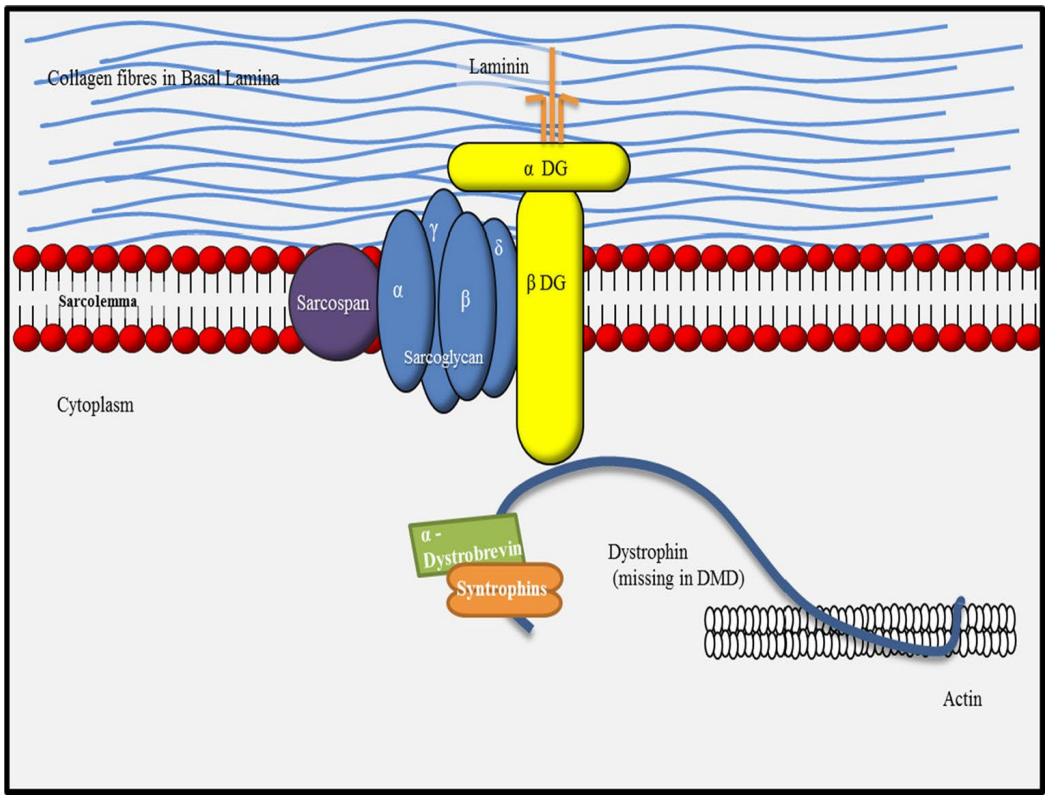

Figure 1.2: Schematic of the Dystrophin Associated Protein Complex, showing the anchoring of muscle fibres to the surrounding extracellular matrix. Reproduced from Manning & O'Malley (2015).

1.2 Skeletal muscle fibre organisation

1.2.1 Skeletal muscle is made up of several different fibre types

Adult skeletal muscle is a heterogeneous tissue composed of muscle fibres that vary in their speed of contraction, metabolic activity and myosin heavy chain (MHC) composition (Bloemberg & Quadrilatero, 2012). Muscle fibres were first categorised as either a type I or type II fibre. Type I (slow) fibres, named for their expression of the MHC-I isoform, are considered to have a slow contraction speed and are involved in tonic muscle contraction. Type I (slow) fibres are often referred to as red, oxidative fibres due to their high levels of myoglobin and mitochondria. Type II (fast) fibres express various isoforms of MHC-II resulting in a fast contraction speed suitable for phasic contraction. These fibres are referred to as white, glycolytic fibres due to the low density of mitochondria and myoglobin (Schiaffino, 2010). The use of histochemical techniques led to the discovery of three different type II (fast) muscle fibres: type IIa, type IIb and type IIx named after their MHC composition (Schiaffino *et al*., 2015). Even within the larger type II (fast) group, each fibre type has varying contraction speed (IIB > IIX > IIA) and glycolytic capacity (IIA> IIX > IIB) (Schiaffino, 2010).

Generally, adult mammalian muscle is thought to be composed of four fibre types: type I, type IIa, type IIb and type IIx. However, the proportions of these various types differ between species and anatomical location (Schiaffino and Reggiani, 2011; Bloemberg & Quadrilatero, 2012). For example, the human diaphragm consists of equal proportions of type I and type II fibres, whereas the rodent diaphragm consists of mostly type II fibres (Polla *et al*., 2004; Schiaffino & Reggiani, 2011). The proportion of fibre types also seems to vary between different muscle groups. For example, type I fibres are more

common in the posterior compartment, where the soleus is found. While hind limb muscles such as the tibialis anterior (TA) and Extensor digitorum longus (EDL) consist of entirely fast fibres (Schiaffino & Reggiani, 2011).

During development, two specific isoforms of MHC are expressed in skeletal muscle. These developmental isoforms are known as embryonic myosin and neonatal myosin (Schiaffino & Reggiani, 2011). During the first weeks of postnatal development, embryonic and neonatal myosin expression is down-regulated as the fast and slow-type adult MHC begins to be expressed (Schiaffino *et al*., 1988). Moreover, slow-type fibres are thought to disappear from fast muscles in this early stage of postnatal development. This suggests that this slow-to-fast switch that occurs in fast-type muscles is inhibited in slow-type muscles such as the soleus (Schiaffino *et al*, 2010). Although embryonic and neonatal myosin are expressed only transiently during development, these developmental isoforms are re-expressed in adult muscles that have undergone injury and subsequent regeneration. Both embryonic and neonatal myosin are expressed 2-3 days after injury and are thought to persist for another 2-3 weeks (Guiraud *et al*., 2018). Antibodies specific for embryonic myosin can be used as a marker for recently regenerated muscle fibres in muscular dystrophy research (Guiraud *et al*., 2018).

1.2.2 Skeletal muscle extracellular matrix

The ECM is a three-dimensional network composed of many proteins including collagens, proteoglycans, elastin, fibronectin, laminins and many more (Theocharis *et* al., 2016). While the ECM is only a small component of skeletal muscle, it is known to greatly impact muscle function. Specifically, the ECM plays a key role in force transmission as well as

in the maintenance and repair of skeletal muscle (Gillies & Lieber., 2011). The skeletal muscle ECM consists of the inner basement membrane and three outer components: the endomysium, epimysium and perimysium (Figure 1.3a-c). The basement membrane is the innermost layer that makes direct contact with the sarcolemma (Figure 1.3d). The basement membrane itself is thought to make a great contribution to the overall strength and elasticity of muscle (Grounds 2008, p.271; Sanes, 2003). Although considered to be distinct from each other, the endomysium is closely associated with the basement membrane (Figure 1.3d) and surrounds individual muscle fibres (Chaturvedi *et* al, 2015; Gillies & Lieber. 2011). The perimysium then surrounds bundles of muscle fibres, termed fascicles. The final component is the epimysium, the connective tissue sheath that encapsulates the entire muscle (Chaturvedi *et* al, 2015).

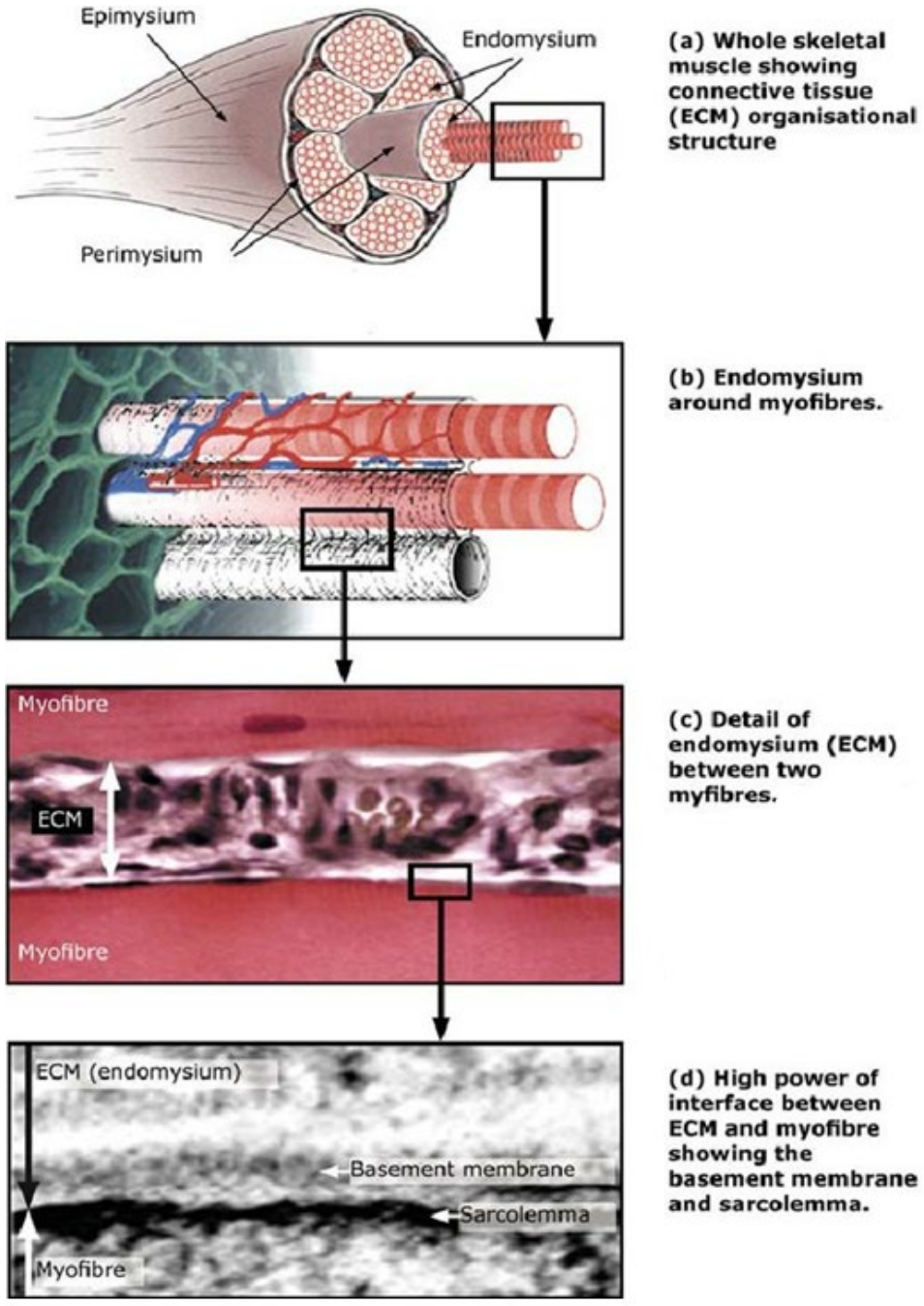

Figure 1.3: Structure of skeletal muscle extracellular matrix. (a) Shows the epimysium surrounding the entire muscle, the perimysium surrounding bundles of muscle fibres (fascicles) and (b, c) the endomysium which surrounds individual muscle fibres. (d) Shows the interface between the endomysium and the muscle fibre, showing the basement membrane and sarcolemma. Modified from Grounds (2008, p.271).

While the ECM is composed of many constituents, the collagens are said to be the major component of the skeletal muscle ECM, accounting for 1-10% of muscle dry mass (Gillies & Lieber, 2011). There has been a total of 26 different types of collagen reported (Gelse, Pöschl & Aigner, 2003) and 10 of these are found in the skeletal muscle ECM (Gillies & Lieber. 2011). Collagen I and collagen III are fibrillar in structure and are thought to be the most abundant collagen types in the skeletal muscle ECM. Interestingly, collagen I alone is said to make up anywhere between 30% and 97% of the total collagen in the skeletal muscle ECM (Gelse *et al.,* 2003; Gillies & Lieber, 2011). Interestingly, the different components of the ECM seem to consist of different types and amounts of the collagens. For example, the perimysium consists of mostly collagen I and a small amount of collagen III. Whereas the endomysium and epimysium consist of equal amounts of collagen I and III. Even the closely associated basement membrane and endomysium differ in their collagen composition, with the basement membrane consisting of mostly type IV collagen (Gillies & Lieber, 2011).

1.3 Skeletal muscle repair in healthy and dystrophic muscles

Healthy skeletal muscle can be damaged by exercise, eccentric (lengthening) contractions or trauma and this leads to a process of regeneration. The mechanism of skeletal muscle repair includes a cycle of: degeneration, inflammatory cell invasion, regeneration and ECM deposition (Urso, 1985). When a muscle is physically injured, vascular damage occurs and the muscle fibres burst and necrotise. In response to the vascular damage, monocytes leave the blood stream and enter the muscle, where they become macrophages and clear necrotic fibres (Kharraz *et al,* 2013). At the same time, there is ECM deposition. Together, the macrophages and ECM release growth factors that activate muscle fibre satellite cells. These

are the stem cells of skeletal muscle, resident in the endomysium (Urso, 1985). The activated satellite cells begin to proliferate and form myoblasts (muscle pre-cursor cells) which subsequently differentiate and fuse to form multi-nucleated muscle fibres. This satellite cell system can activate and fully regenerate muscle fibres just days after the injury (Vidal et al, 2012; Wallace & McNally, 2009).

Dystrophic muscles are more susceptible to contraction-induced injury than healthy (non-dystrophic) muscles and consequently they go through multiple cycles of degeneration (Guiraud & Davies, 2017). These repeated cycles of degeneration eventually exhaust the regenerative capacity of the satellite cell system, resulting in limited fibre regeneration (Wallace & McNally, 2009). Fatty and fibrous tissues eventually replace the necrotised fibres and the muscle becomes weak (Manning & O'Malley, 2015). While the exact mechanism for the exhaustion of the satellite cell system in DMD is unknown, it has been hypothesised that persistent inflammation and/or the untimely deposition of ECM may play a role (Kharraz *et al.,* 2013).

1.3.1 Inflammation in skeletal muscle repair

A transient inflammatory response is required for skeletal muscle repair and it begins when macrophages enter the injured muscle (Figure 1.4), as mentioned above (Kharraz *et al*., 2013). At this early stage of muscle repair, macrophages are active in their M1 (pro-inflammatory) phenotype, where their main role is to clear necrotic fibres (Villalta *et al*, 2008). These M1 macrophages also release signalling molecules that stimulate cell proliferation in the myoblasts (Kharraz *et al.,* 2013). As muscle regeneration advances, the macrophages switch to their M2 (anti-inflammatory) phenotype. It is these M2 macrophages that are

thought to stimulate myoblast differentiation, fusion (Kharraz *et al.,* 2013) and the transient ECM deposition needed for skeletal muscle repair (Villalta *et al*.,2008).

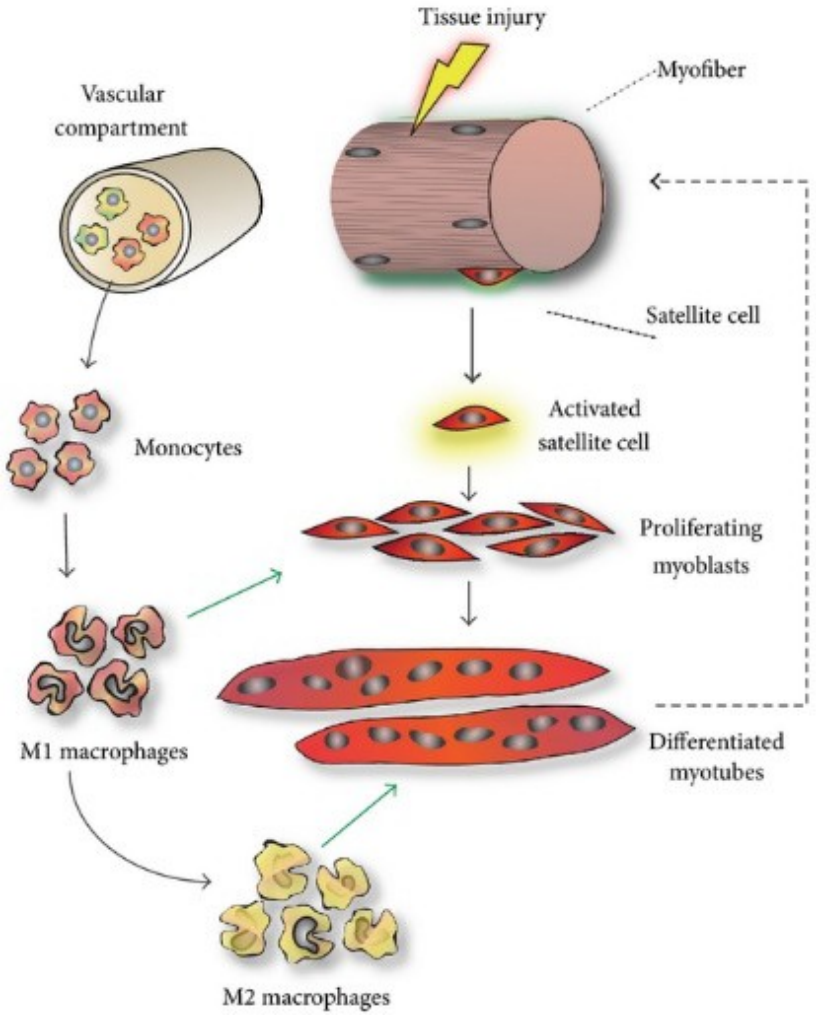

Figure 1.4: Schematic of skeletal muscle regeneration in response to muscle damage, showing the activation of satellite cells (muscle stem cells) within the muscle and the extravasation of monocytes from blood vessels. In the early stages of muscle regeneration, the monocytes differentiate into M1 (pro-inflammatory) macrophages which clear any necrotising fibres and stimulate myoblast proliferation. M2 (anti-inflammatory) macrophages are active in the later stages of repair and stimulate myoblast differentiation and fusion. Reproduced from Kharraz *et al*. (2013).

In DMD, this inflammatory response is chronic. This is due to the persistent activation of macrophages, as the muscle fibres undergo repeated cycles of degeneration (Kharraz *et al*, 2014). While the precise mechanism behind this persistent inflammation is unclear, it has been suggested that an imbalance between the M1 and M2 macrophage phenotypes could play a role (Nitahara-Kasahara *et al.,* 2014). Furthermore, it has been suggested that deposits of fibrin and fibrinogen, found only in dystrophic muscles, may activate M1 macrophages and thus, contribute to the persistent inflammation (Vidal *et al*., 2012). This model proposes that muscle injury causes the extravasation of fibrin and fibrinogen from the damaged blood vessels. Together, fibrin and fibrinogen form a temporary matrix between the muscle fibres that is never seen in healthy muscle (Figure 1.5). This matrix is then thought to interact with macrophages (via $\alpha_M \beta_2$ integrin), causing them to switch to the M1 phenotype. It is the additional activation of these M1 macrophages, by fibrin and fibrinogen that is thought to further promote muscle degeneration and possibly negatively regulate satellite cell function by preventing the differentiation of myotubes (Vidal *et al*., 2012).

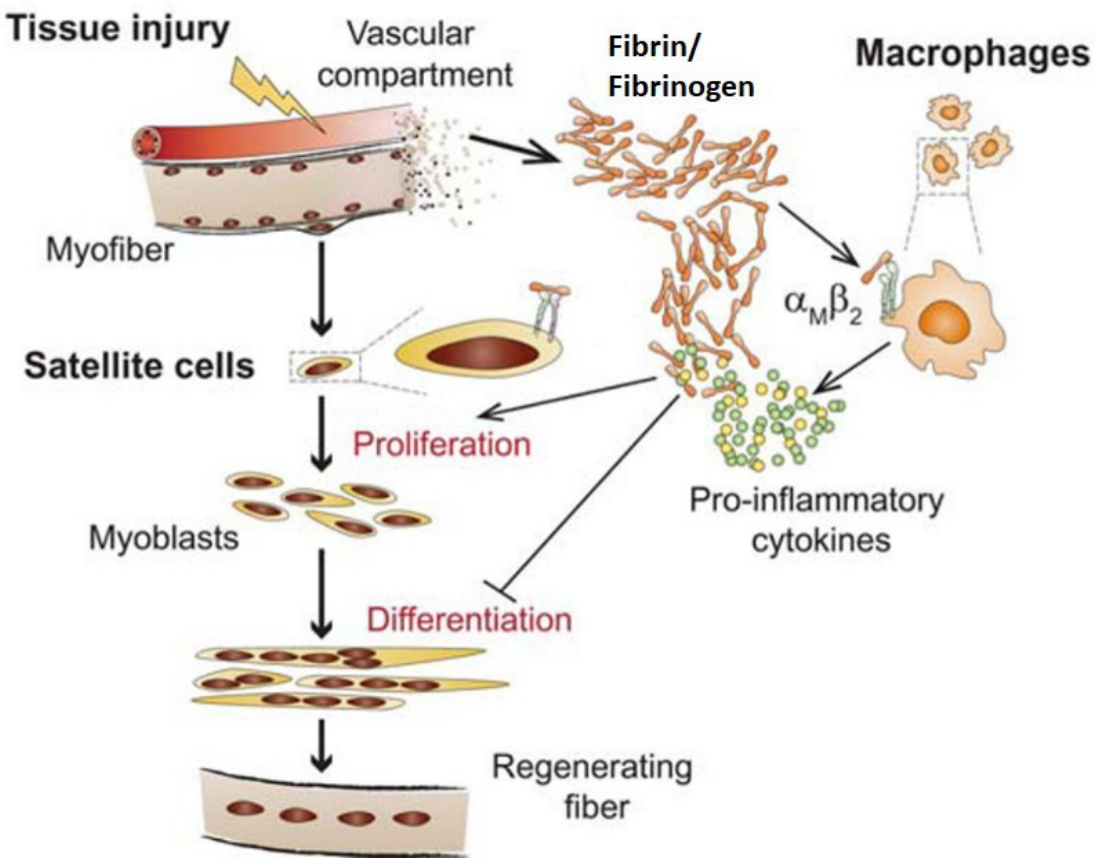

Figure 1.5: **Schematic of inflammatory response to tissue injury in dystrophic muscles**. Fibrin and fibrinogen are released from blood vessels and interact with macrophages, causing them to release pro-inflammatory cytokines which promotes myoblast proliferation and possibly negatively regulates satellite cell function by preventing differentiation. Modified from Vidal *et al*. (2012).

1.3.2 Extracellular matrix deposition in skeletal muscle repair

Upon muscle injury, the controlled deposition of ECM around individual muscle fibres helps provide the muscle with strength and support for contraction (Kharraz *et al.,* 2013; Kharraz *et al.,* 2014). It also provides a scaffold for regenerating fibres, ensuring that all new fibres adopt the correct spatial architecture (Kharraz *et al.,* 2013). This process of ECM deposition is tightly regulated by various signalling molecules, such as growth factors, extracellular proteases and their inhibitors (Kharraz *et al.,* 2013; Kharraz *et al.,* 2014). One growth factor, Transforming Growth Factor-β1 (TGF-β1) is released from the ECM and/or macrophages upon tissue damage and stimulates transient deposition of ECM by fibroblasts (Kemaladewi *et al.,* 2012; Kharraz *et al.,* 2014). Additionally, macrophages are known to release matrix metalloproteases (MMPs; which break down the ECM) and tissue inhibitors of metalloproteases (TIMPs) (Kemaladewi *et al.,* 2012). When TGF-β1 is released by macrophages (upon muscle damage), TIMPs are also active, allowing for transient ECM deposition required for muscle repair. This ECM scaffold is no longer required once new fibres are formed and thus the ECM is degraded by MMPs (Kharraz *et al.,* 2013; Kharraz *et al.,* 2014). This ECM degradation also leads to the production of protein fragments that aid tissue repair (Mann *etal.,* 2011).

In DMD, this ECM deposition becomes excessive or uncontrolled and is thus defined as fibrosis (Kharraz *et al*., 2014). Interestingly, the persistent activation of macrophages seen in DMD (due to the continuous cycles of degeneration/regeneration) seems to contribute to this fibrosis (Nigro & Piluso*,* 2015). As mentioned above, macrophages can release TGF-β1 and thus stimulate ECM deposition. The constant activation of macrophages in DMD is thought to up-regulate TGF-β1 signalling which in turn promotes ECM deposition. This

continuous up-regulation of TGF-β1 signalling could lead to the excessive ECM deposition that ultimately leads to fibrosis in DMD (Figure 1.6; Kemaladewi *et al.,* 2012).

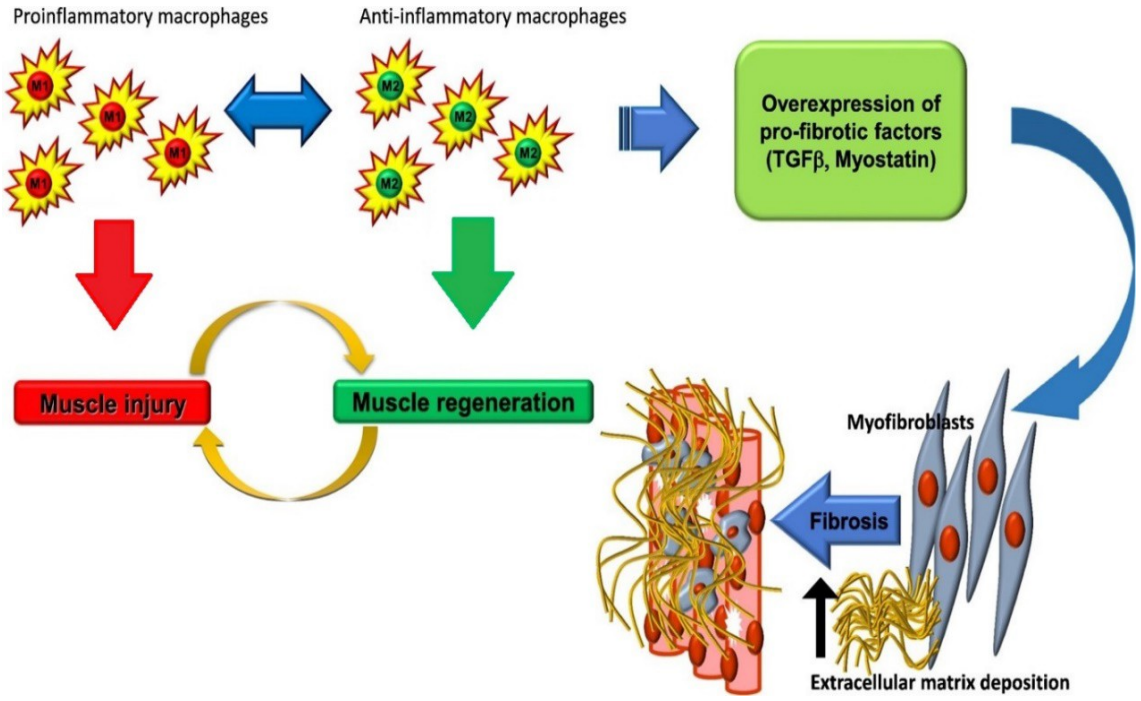

Figure 1.6: Schematic of excess extracellular matrix deposition (fibrosis) in DMD. Persistent macrophage activation leads to an up-regulation in pro-fibrotic factors such as transforming growth factor β (TGFβ), causing excess extracellular matrix deposition and ultimately fibrosis. Modified from Nigro & Piluso (2015).

Moreover, TGF-β1 is also known to stimulate a cell population known as Fibro/adipogenic progenitors (FAPs). FAPs are mesenchymal progenitors that contribute to fibrosis by differentiating into adipocytes or collagen-producing cells, when stimulated by TGF-β1 (Farup *et al.,* 2015; Uezumi *et al*., 2011). It is the up-regulation of TGF-β1 signalling in DMD which stimulates FAPs to differentiate into adipocytes and collagen-producing cells (Lemos *et al*, 2015). This then results in excessive deposition of collagens, a major component of the fibrotic ECM (Uezumi *et al*., 2011).

1.3.3 Hypertrophy and pseudohypertrophy

Hypertrophy or enlargement of the calf (Figure 1.7) is a characteristic feature of DMD. Hypertrophy is described as an increase in the number or size of muscle fibres without an increase in non-contractile material. This hypertrophy is commonly seen in the gastrocnemius and soleus muscles of DMD patients but has also been identified in other muscles such as the TA (Kornegay *et al.,* 2012). Early clinical data has suggested that this hypertrophy occurs early in the disease course of DMD, while the patients are still ambulatory (Cros *et* al., 1989). It has been suggested that the hypertrophy observed later in the disease course is pseudohypertrophy, which refers to an increase in non-contractile materials such as fat and connective tissue in the muscle (Kornegay *et al.,* 2012). Pseudohypertrophy is thought to occur as a result of myofibre necrosis, with fat and ECM replacing the necrotic fibres. Ultimately, this results in a muscle that is enlarged but weak (Manning & O'Malley,2015).

Figure 1.7: Photograph of a 9-year-old boy with DMD showing the characteristic hypertrophy (enlargement) of the calf muscles. Reproduced from Kornegay *et al.* (2012).

While this early study seemed to indicate a 2-stage process of true hypertrophy followed by pseudohypertrophy, it was only semi-quantitative, and it seemed that this 2-stage process could not be applied to all muscle groups. For example, Cros *et al.* (1989) found that boys with DMD had an increased mean fibre diameter in their gastrocnemius muscle, indicating hypertrophy. However, there was also an increase in non-contractile elements, so true hypertrophy was ruled out. In the quadriceps muscle, true hypertrophy was reported early in the disease course of DMD and was followed by muscle atrophy. For these reasons, it remains uncertain whether the enlargement of muscles seen in boys with DMD is due to hypertrophy, pseudohypertrophy or both.

1.4 *Mdx* mouse model of DMD

1.4.1 The *mdx* mutation

For the last 30 years, the dystrophin-deficient, *mdx* mouse has been used as a model to study the pathophysiology of DMD (McGreevy *et al.*, 2015). The *mdx* mouse model of DMD was discovered in the 1980s when a colony of C57BL/10ScSn mice exhibited evidence of myopathy. A point mutation that prevented the translation of full-length dystrophin was identified as the cause (Bulfield *et* al., 1984; McGreevy *et al.*, 2015). Much like in human DMD, the lack of dystrophin causes muscle weakness, pseudohypertrophy and respiratory insufficiency in the *mdx* mouse. Due to these similarities in the pathogenesis of DMD and its genetic similarity to human DMD, the *mdx* mouse has been extensively used in DMD research, leading to much of what is currently known about the pathogenesis arising from dystrophin deficiency (Manning & O'Malley, 2015).

1.4.2 Pathogenesis of DMD in *mdx* mice

Histological analysis of *mdx* mouse muscle reveals muscle fibre necrosis and subsequent replacement with fatty and fibrous tissues, as is seen in DMD patients (Manning & O'Malley, 2015). In the hind limb muscles of *mdx* mice, necrosis begins at about 21 days of age and is thought to progress until it reaches its peak at 25-26 days of age. There is then a reduction in necrosis until it stabilises at 8 weeks of age. From this point onwards, only about 5% of fibres undergo necrosis at any given time point. As the mice move into adulthood, necrosis becomes almost undetectable (Grounds *et al*., 2008). The deposition of fatty and fibrous tissues (fibrosis) is reported after this peak in necrosis, at about 10-12 weeks of age. However, the fibrosis reported at this age is considered to be quite mild and a severe fibrosis is only reported at 16-20 months of age (Grounds *et al*., 2008; Manning & O'Malley, 2015).

While *mdx* muscles do undergo bouts of necrosis and subsequent fibrosis, the pathology of *mdx* mice is much less severe than the human form of DMD. Interestingly, *mdx* mice also show a shortened lifespan when compared to controls but there is only a 25% reduction. This is much less severe than the 75% lifespan reduction reported in humans with DMD (McGreevy *et al*., 2015). The less severe phenotype of *mdx* mice is thought to be due to the up-regulation of utrophin, a homologue of dystrophin. Utrophin shares an 80% homology with dystrophin and is thought to interact with the same proteins as dystrophin (Manning & O'Malley, 2015). In humans, utrophin is expressed at the sarcolemma during development and is then progressively replaced by dystrophin. In the absence of dystrophin, utrophin can mimic the stabilising function of dystrophin. In this way, utrophin is up-regulated at the sarcolemma in *mdx* mice and compensates for the lack of dystrophin (Guiraud & Davies,

2017). It is this up-regulation of utrophin in *mdx* mice that seems to dampen muscle degeneration, leading to a less severe phenotype. While up-regulation of utrophin has been reported in human DMD, it seems that the levels of utrophin are not high enough to impact disease progression (Manning & O'Malley, 2015).

1.4.3 Parameters to measure pathology in *mdx* mice

Various parameters have been used to assess muscle pathology in *mdx* mice. In fact, standard operating procedures (SOPs) for the pre-clinical assessment of DMD pathology in *mdx* mice have been established and made available globally by the Treat-NMD network (https://treat-nmd.org/). Some of these SOPs by Treat-NMD assess pathology using histological stains, collection of blood samples and functional tests such as contraction recordings. The histological assessments make use of transverse sections of *mdx* muscles to visualise the overall muscle pathology. Haematoxylin & Eosin (H&E) staining is commonly used to assess the extent of damage in *mdx* muscles as it can identify damaged fibres, regenerated fibres and any areas of inflammation. Typically, a damaged fibre will have a fragmented sarcoplasm and a disrupted sarcolemma. These areas of damaged fibres may also show some inflammatory cell invasion, characterised by areas of basophilic staining (Figure 1.8). H&E staining can also be used to identify fibres with centralised nuclei, a marker of regeneration (Grounds *et al*., 2008). For these histological assessments, it is particularly important to consider the age of the mouse as histological features are age-dependant and can greatly differ between the earlier and later stages of disease (Grounds *et al*., 2008; Grounds, 2014; Manning & O'Malley 2015). For example, it is more useful to measure muscle fibre necrosis in young *mdx* mice, before and after florid the degeneration reported at 3

weeks of age, compare to older (1-year-old) *mdx* mice, which show necrotic fibres in less than 5% of the TA muscle. Since the values for older mice are so low, it becomes difficult to detect a relative change in necrosis. Whereas, the higher ~30% necrosis reported in 3-week-old *mdx* mice allows for a highly sensitive assay (Grounds, 2014).

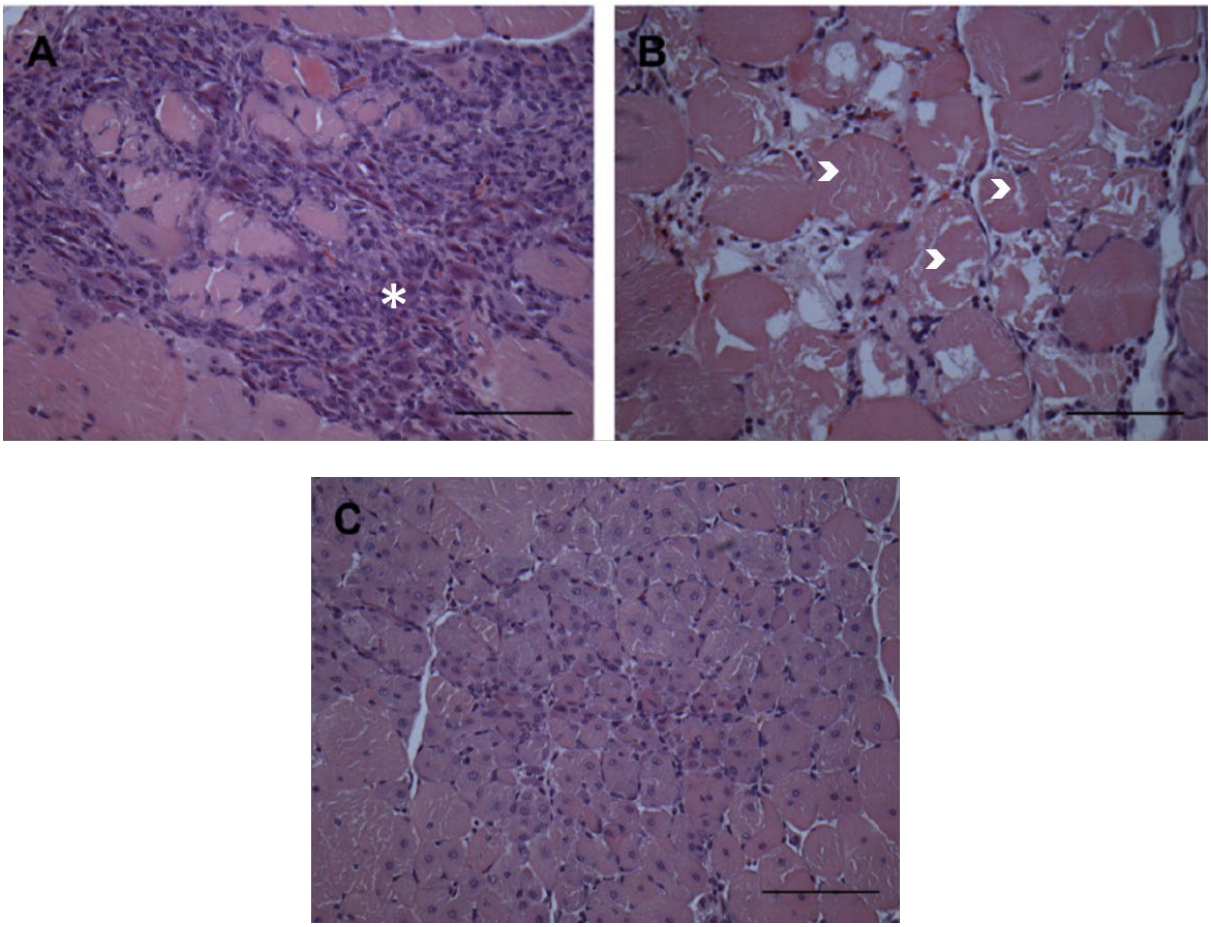

Figure 1.8: Haematoxylin & Eosin staining of adult *mdx* quadriceps muscle. (A) Few damaged fibres surrounded by a large area of inflammation (asterisk). (B) Damaged myofibres with fragmented sarcoplasm (arrowheads). (C) Fibres that have regenerated with centralised nuclei. Modified from Grounds *et al.* (2008).

Moreover, other histological stains such as Sirius red are used to visualise and quantify fibrosis by staining all collagens red (Figure 1.9). Typically, this stain is used to quantify fibrosis in the diaphragm muscle, where the fibrosis can be quite severe. However, it is important to note that the fibrosis in the limb muscles is quite mild, with severe fibrosis only being reported in *mdx* mice that are 16 months old or older (Grounds *et al*., 2008; Pessina *et al*., 2014).

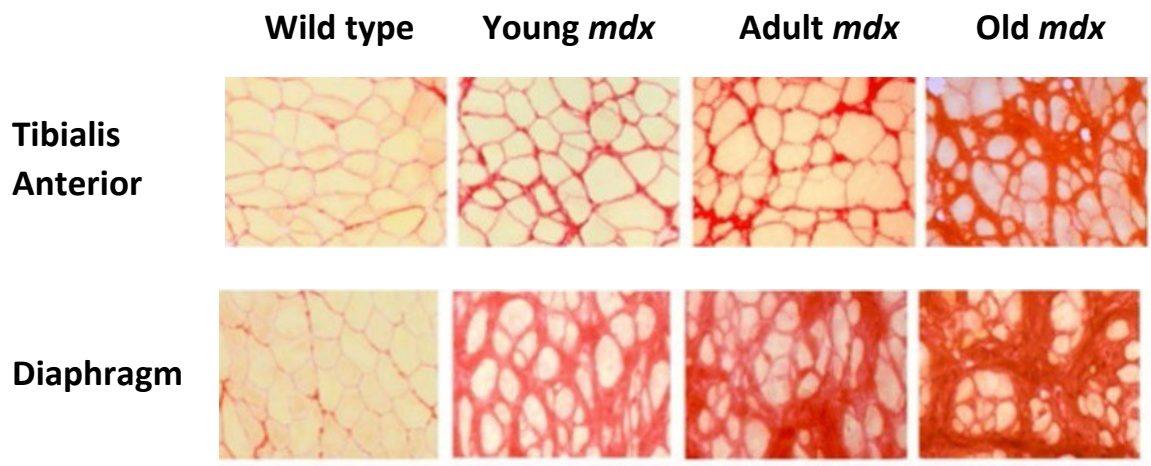

Figure 1.9: Sirius red staining of the tibialis anterior and diaphragm muscles of wild type, young *mdx* (3 months old), adult *mdx* (9 months old) and old *mdx* (18-24 months old). Modified from Pessina *et al*. (2014).

Similarly, immunofluorescence studies are used to assess various aspects of *mdx* pathology. For example, regenerating muscle fibres can be identified by using antibodies against embryonic myosin, providing an indication of how many fibres have been damaged and recently regenerated (Guiraud *et al*., 2018). Fibrosis can also be assessed in immunofluorescence studies by staining ECM components such as collagen (Gibertini *et al.,*2014) and fibronectin (Hollinger & Selsby, 2015). While inflammation can be studied by staining for inflammatory factors such as TGF-β1 and for macrophages (Gibertini *et al.,*2014).

The study of fibre type proportions via MHC profiling has become a technique of interest when studying the pathology of *mdx* mice. Studies have reported that the soleus, a slow-type muscle, is more resistant to damage and has higher dystrophin expression when compared to fast-type muscles (Omairi *et al.,* 2019*).* Interestingly, one study was able to induce a fast to slow-type switch by transgenic overexpression of peroxisome proliferator activated receptor gamma coactivator 1-alpha (PGC-1α) in *mdx* mice. It is thought that overexpression of PGC-1α made muscles more resistant to contraction-induced injury and improved their fatigue resistance via this fast to slow fibre switch (Selsby *et al*., 2012).

1.5 Muscle Specific Kinase (MuSK) signalling system

1.5.1 MuSK signalling system at the neuromuscular junction

Muscle Specific Kinase (MuSK) is transmembrane receptor tyrosine kinase responsible for the development and maintenance of the neuromuscular junction (NMJ; Ghazanfari *et al.,* 2011). At the NMJ, motor neuron terminals release acetylcholine onto postsynaptic acetylcholine receptors (AChR), allowing for muscle contraction. Effective neurotransmission relies on the agglomeration of AChRs into clusters (Ghazanfari *et al.,* 2011). During early development, AChRs are dispersed uniformly across the length of skeletal muscle fibres. The AChRs then accumulate and form clusters in the centre of the muscle fibres. This clustering, termed pre-patterning, requires MuSK but is independent of motor innervation (Ueta *et al*, 2016). It is important to note that the AChR clusters themselves contain MuSK. The AChR-MuSK clusters form in the central part of the muscle fibre where motor nerves will later form synapses (Ghazanfari *et al.,* 2011). Following targeted mutation of the MuSK gene, MuSK-null mouse embryos were unable to form stable NMJs and consequently became paralysed and died before birth (DeChiara *et al.,*1996).

MuSK is able to stabilise AChR clusters via its interaction with various other proteins that form the MuSK signalling complex: Neural agrin (hereafter referred to simply as Agrin), LRP4 (low-density lipoprotein receptor-related protein), Dok7 (downstream-of-tyrosinekinase-7), and Rapsyn (which acts downstream of MuSK) (Ghazanfari *et al.,* 2011; Pratt *et al.,* 2013). Agrin is a heparan-sulphate proteoglycan secreted from motor nerve terminals and is a potent inducer of LRP4-MuSK mediated AChR clustering. Agrin does not interact directly with MuSK, instead it induces AChR clustering via its interaction with LRP4, which interacts with MuSK via its extracellular domain (Figure 1.10; Ghazanfari *et al.,* 2011;

Ohno, Ohkawara & Ito, 2017). Dok7 binds to MuSK via its kinase domain (Figure 1.10) and helps activate MuSK by cross-linking the two MuSK monomers to form a tetramer. Active MuSK then recruits Rapsyn, a scaffolding protein to help form and stabilise the AChR clusters (Ghazanfari *et al.,* 2011).

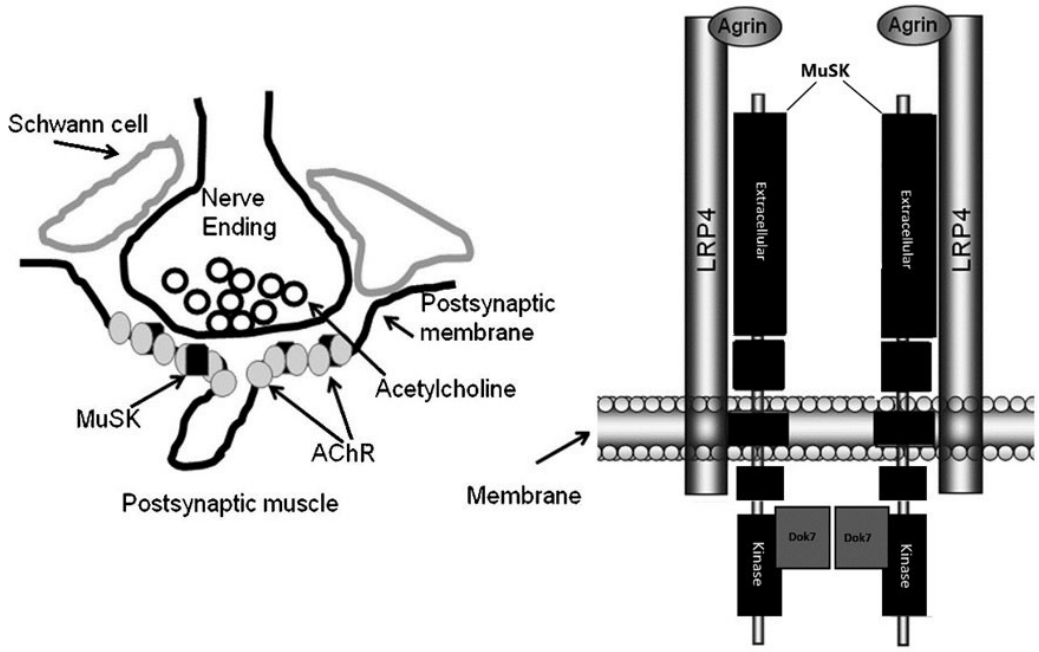

Figure 1.10: Schematic showing the location of MuSK at the neuromuscular junction and the structure of the MuSK signalling complex. MuSK is represented in black with its extracellular and kinase domains. Adapted from Ghazanfari *et al*. (2011).

Interestingly, MuSK expression levels seem to differ among different skeletal muscles in the adult mouse. One study found that high levels of MuSK were expressed in the slow-type muscle, the soleus (Punga *et al.,* 2011), which has been shown to be more resistant to contraction-induced damage (Omairi *et al.,* 2019). The fast-type EDL on the other hand, expressed only low levels of MuSK. These differences in MuSK expression between muscles may explain why some muscles suffer more in DMD than others. The same pattern of expression was found for the AChRα subunit. Interestingly, Dok7, LRP4 and Rapsyn had a similar level of expression across the EDL and soleus muscles. These differences in expression are thought to be independent of the slow/fast-type of the muscle but rather depend on the sensitivity of the muscle to Agrin (Punga *et al*., 2011).

1.5.2 Reasons for studying the influence of MuSK in *mdx* muscles

While MuSK has a well-established role in the development and maintenance of the NMJ, its role in broader muscle physiology remains unclear (Pratt *et al.,* 2013). Interestingly, the MuSK signalling complex is thought to interact with the DAPC at the NMJ where the synaptic laminins (α4, α5 and β2 laminin), residing in the synaptic basement membrane (Nishimune *et* al., 2004; Samuel *et al*., 2012, interact with α-dystroglycan, allowing for the DAPC to be brought closer to the MuSK-signalling complex (Figure 1.11B; Pilgram *et al*., 2010). However, at the sarcolemma, α-dystroglycan is known to interact with non-synaptic laminin α2 (Figure 1.11A; Pilgram *et al*., 2010). It is this close association of the MuSK complex with the DAPC which suggests that MuSK may play an important role in muscle physiology. Specifically, the two complexes are physically linked by the binding of Rapsyn to β-

dystroglycan (Figure 1.11B). Furthermore, this interaction between Rapsyn and the DAPC seems to be important for the stabilisation of AChR clusters (Pilgram *et al.,* 2010).

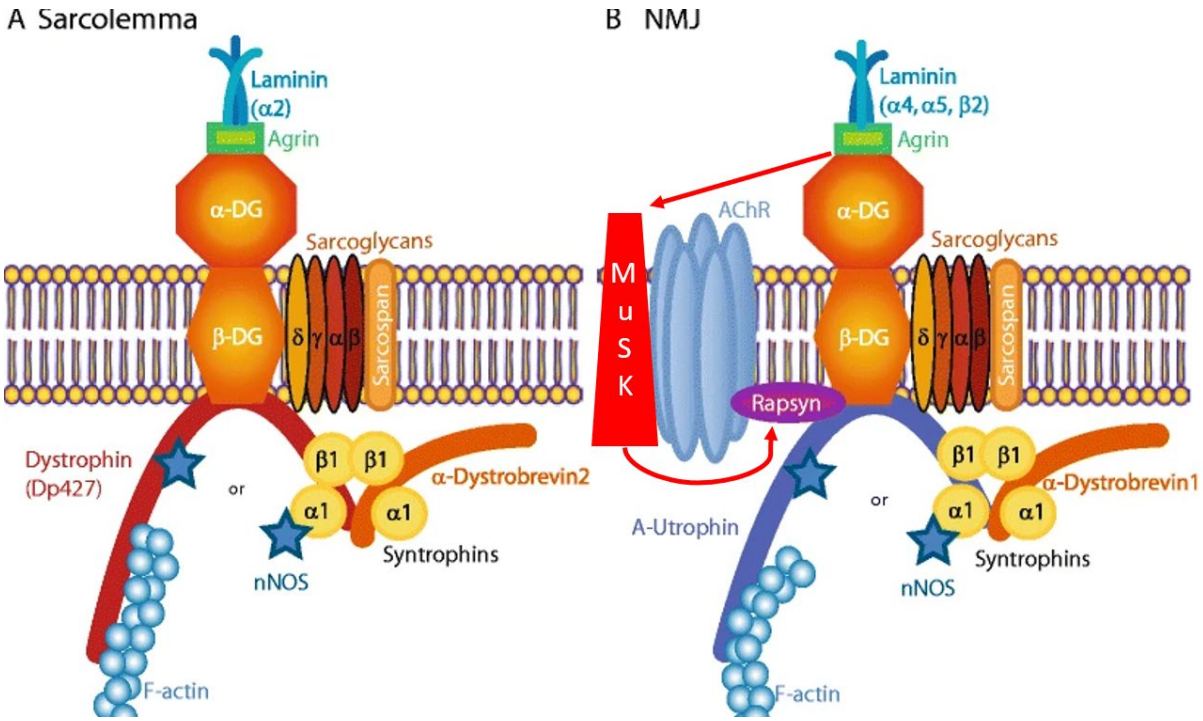

Figure 1.11: Schematic of the Dystrophin associated protein complex at the (A) sarcolemma and at the (B) neuromuscular junction, showing the interaction of MuSK and the DAPC at the neuromuscular junction. First, Agrin activates MuSK. The active form of MuSK then recruits Rapsyn to stabilise AChR clusters. The MuSK signalling complex is linked to the DAPC by the interaction between Rapsyn and β-dystroglycan. Modified from Pilgram *et al.* (2010).

Moreover, the quadriceps muscles of *mdx* mice are reported to express lower levels of MuSK than the wild type. Interestingly, no difference was reported in the expression levels of the other components of the MuSK complex: Dok7, LRP4, Agrin and Rapsyn. It is this reduced expression of MuSK that may lead to the impaired neuromuscular transmission and muscle fragility seen in *mdx* mice (Pratt *et al.,* 2013). Recent work in the Phillip's lab has used an adeno-associated viral vector (AAV) to supplement MuSK expression in the TA muscle of *mdx* mice. This supplementation was able to reduce the eccentric contraction-induced loss of force (Trajanovksa *et al*., 2019), increase specific force, reduce muscle mass (pseudohypertrophy) and reduce the number of damaged muscle fibres (Joanne Ban, PhD thesis, 2018). MuSK supplementation also increased the sarcolemmal expression utrophin and the DAPC proteins: β-dystroglycan, α-sacrcoglycan and β- sarcoglycan (Joanna Huang, Honours thesis, 2018; Trajanovska *et al*., 2019). This suggests a potential role for MuSK in protecting dystrophic muscle fibres from degeneration.

1.6 Project aims

Overall, this project aims to assess whether overexpression of MuSK in the TA muscle of *mdx* mice can reduce dystrophic muscle pathology. To do this, 4-week-old *mdx* mice were injected with an AAV encoding MuSK in the TA muscle. The contralateral TA muscle was injected with an empty AAV vector, to serve as a control. Mice were culled when they were 12-weeks-old for the first lot of experiments (chapter 3) and at 9-weeks-old for later experiments (chapter 4). Muscles were then dissected and cryosectioned for immunofluorescence analysis.

Specifically, this project is based on three findings that arose from the work of Joanne Ban (PhD thesis, 2018): 1) 12-week-old *mdx* TA muscles were heavier than that of the wild type. 2) Supplementation with AAV-MuSK reduced this muscle mass back to wild type level (Figure 1.12). 3) *Mdx* muscles expressing AAV-MuSK produced greater specific force than that of the empty vector controls (Figure 1.13). With these findings in mind, I aimed to test whether the increased muscle mass seen in *mdx* mice was due to an increase in the non-contractile components of the muscle (pseudohypertrophy) and whether MuSK supplementation was reducing the muscle mass by reducing pseudohypertrophy. To assess this, immunofluorescence staining for collagen I, and pan-myosin were used to identify the proportions of the muscle taken up by contractile machinery (myosin) and the non-contractile ECM (collagen).

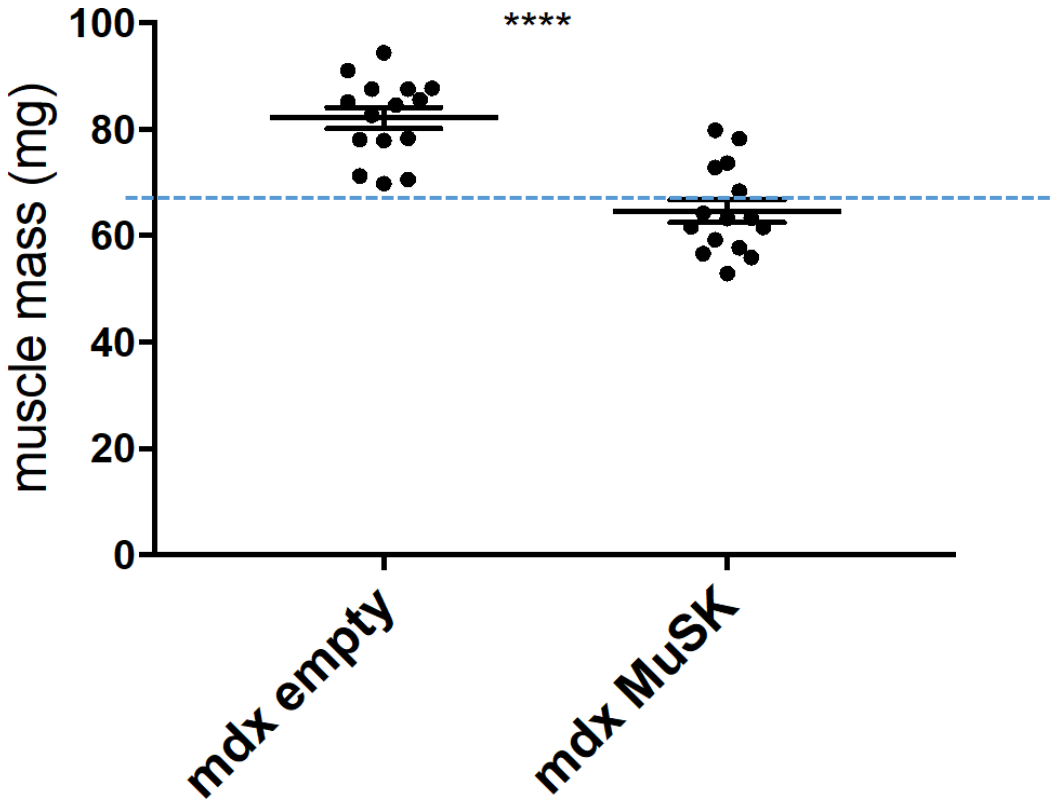

Figure 1.12: Average wet mass of 12-week-old *mdx* TA muscles injected with AAV-MuSK at 4 weeks of age (n=15). Each circle represents the mass of one *mdx* TA muscle and the error bars represent the SEM. The dotted line represents the average wet mass of 12-week-old wild type TA muscles. Data from Joanne Ban, PhD thesis, 2018.

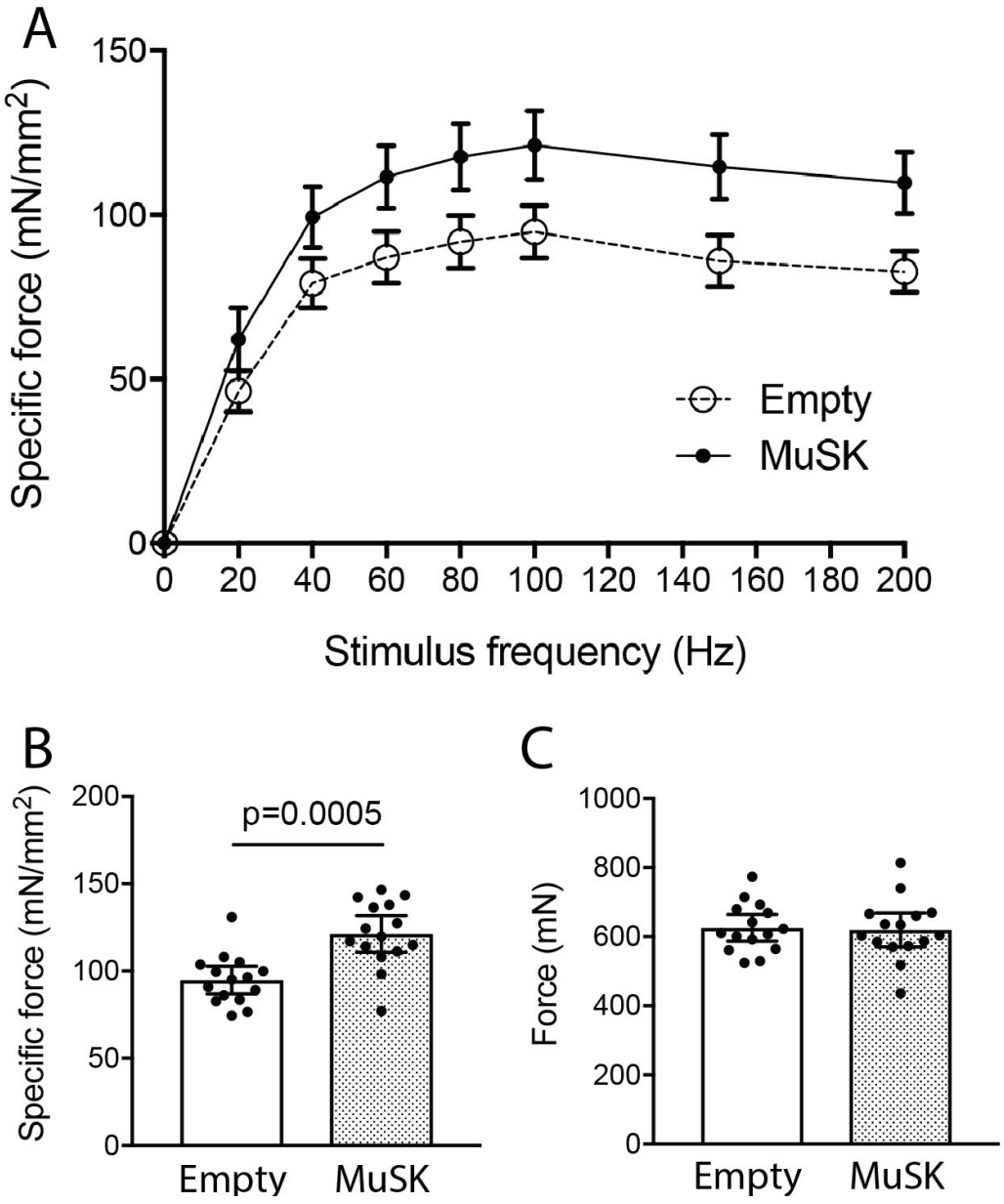

Figure 1.13: Specific force in 12-week-old *mdx* TA muscles injected with AAV-MuSK. (A) Force-frequency curve of specific force, (B) mean specific force and (C) mean force in 12-week-old *mdx* muscles injected with AAV-MuSK compared to the empty vector control (n=15). Data from Joanne Ban, PhD thesis, 2018.

Additionally, this thesis aims to test whether overexpression of MuSK causes any alterations in the fibre type proportions in the TA muscle of *mdx* mice. This will be assessed via immunostaining and fibre counts of the various slow and fast MHC isoforms (Type I, IIa, IIb& IIx). Finally, this thesis also aims to determine whether supplementation of either: MuSK, Dok7, Rapsyn or MuSK- ΔIg3 can reduce the number of fibres that have recently undergone degeneration and regeneration by staining for embryonic myosin, a marker of muscle fibre regeneration. In this way, I will test whether the MuSK-system has any capacity to reduce the extent of muscle fibre degeneration/regeneration in *mdx* mice.

CHAPTER TWO:
Materials and methods

2.1 Mice

2.1.1. Ethics and housing

All mouse experiments were approved by The University of Sydney Animal Ethics Committee (Project number: 2017/1153) in compliance with the Australian code for the care and use of animals for scientific purposes. Both our male *mdx* (C57BL/10ScSn-Dmd^{mdx}) and C57BL/10 ScSn (genetic background control) mice were ordered from Animal Resources Centre in Western Australia. The *mdx* mutation was previously bred onto a C57BL/10 ScSn background and for this reason male C57BL/10 ScSn mice were used as healthy controls (Bulfield *et* al., 1984). However, for some of my experiments there was an error in the supply chain that resulted in C57BL/6 mice being mistakenly supplied instead of C57BL/10 ScSn, without our knowledge at the time. This error impacted the experiments on pseudohypertrophy, and muscle fibre type described in chapter 3. The male *mdx* mice used in experiments from chapter 3 had been ordered and monitored by Joanne Ban as part of her PhD project. All the wild type and *mdx* mice used in chapter 4 were monitored by my supervisor and myself. The postnatal day 1 (P1) neonatal mouse muscles used for the work in chapter 4 were supplied by Prof Frank Lovicu from mice being culled under his ethics approval at the University of Sydney. All mice were held in the Bosch PC2 animal holding room and were group housed with *ad libitum* access to food and water. Each cage also included environmental enrichment items such as a plastic igloo and a refuge tube. Mice were inspected twice weekly to monitor their general welfare. This included checking the condition of their coat, behaviour and hydration. All observations were recorded on the general monitoring sheet kept in the animal holding room. In the experiments described below mice were killed with an intraperitoneal injection of pentobarbitone (30mg; Cenvet, Australia).

2.1.2 Isoflurane anaesthesia of mice

Mice were anaesthetised using an isoflurane anaesthesia machine (The Stinger, Advanced Anesthesia Specialists) connected to a medical oxygen tank. The isoflurane machine and oxygen tank were switched on, allowing for an oxygen flow of 0.7 L/min and 4% isoflurane (Cenvet, Australia) into an induction chamber. The chamber was allowed to fill with the oxygen and isoflurane for a few minutes before the mouse was placed in the chamber. The mouse was kept in the chamber until it was lying on its side and breathing steadily. Isoflurane levels were then turned down to 2-2.5%. The isoflurane machine was then connected to a nose cone and placed over the snout of the mouse. Testing of the foot withdrawal reflex, corneal reflex and monitoring of any changes in the respiratory rate were used to check that a deep anaesthesia was achieved and maintained. The mouse was considered to be deeply anaesthetised when it was breathing steadily, and the foot withdrawal and blink reflexes were fully supressed.

2.1.3 AAV injection experiments

Construction of cytomegalovirus (CMV) promoter-driven MuSK and Rapsyn expression cassettes in the pAAV-CMV plasmid, their packaging into AAV serotype 6 capsids and the intramuscular injection of the AAV preparations were detailed previously (Blankinship *et al.*, 2004; Ghazanfari *et al.*, 2015). These AAV preparations are referred to below as the original AAV batches. Additional AAV expression vectors for MuSK-ΔIg3 and human Dok7 were constructed in 2018. In each case the full-length coding sequence fused, in-frame, at its C-terminus to the coding sequence of enhanced green fluorescent protein (GFP) was synthesized commercially to our design by Genscript. The coding sequence for the fusion proteins: MuSK- ΔIg3-GFP and human Dok7-GFP were then each subcloned into pAAV-CMV

and the insertions and joins were sequenced, again by Genscript. New plasmid preps encoding AAV-MuSK-GFP, AAV-MuSK- ΔIg3 -GFP and AAV-Dok7-GFP were then grown up, purified by Qiagen plasmid maxi-prep kit (Qiagen) within the lab by my supervisor in 2018. These plasmid preps were then packaged into fresh batches of AAV serotype 6 by the laboratory of Dr Paul Gregorevic, University of Melbourne. These are referred to below as the new batches of AAV.

Series one AAV injections: The *mdx* muscles used in chapter 3 were from mice injected in January- March 2017 with the original batch of AAV-MuSK by Joanne Ban, as part of her PhD thesis (2018). The muscles had been injected at 3-4 weeks of age and the mice culled at 12 weeks of age by intraperitoneal injection of pentobarbitone (30mg; Cenvet, Australia). This allowed a period of 9-10 weeks for transgene expression, to study the long-term effect of MuSK on muscle pathology.

Series two AAV injections: the muscle blocks from *mdx* mice that were used in chapter 4 were injected with an AAV vector encoding: MuSK, mutant MuSK lacking the Ig3 domain (MuSK-ΔIg3), Dok7 (new batches) or Rapsyn (original batch). These mice were injected at 3-4 weeks of age by our post-doc Dengyun Ge in April-May 2019. The mice were culled at 9 weeks of age by an intraperitoneal injection of pentobarbitone. I dissected the muscles and snap froze them for cryosectioning (detailed below). For series two injections, no evidence of successful expression of the four transgenes is presented in this thesis. However, the AAV-Rapsyn used in chapter 4 comes from the same batch of AAV-Rapsyn used in previous work, where widespread expression of Rapsyn-GFP was shown across the entire cross-section of *mdx* TA muscles (Trajanovksa *et al*., 2019). The MuSK, MuSK-ΔIg3 AAV and Dok7 vectors were newly constructed and used for the first time in this thesis. Evidence of successful expression

of these four transgenes (via AAV injection) will be required before this work can be published.

All AAV injections were done using the following abbreviated protocol. Mice were deeply anaesthetised (as described in *2.1.2 Isoflurane anaesthesia of mice*) and the skin on the shank area of the leg was exposed by shaving. The skin was then swabbed with 80% ethanol/water. An incision through the skin of approximately 3mm in length parallel with the shank was made to expose the TA muscle. A Hamilton syringe fitted with a 32-gauge needle was then used to inject 20µl of sterile 0.9% sodium chloride containing $2x10^9$ viral genomes of AAV into the TA muscle belly. The wound was then closed with a sterile suture and the mouse was administered an analgesic, buprenorphine (0.03mg/kg; Reckitt, Benckiser, Australia) via intraperitoneal injection while the animal was still anaesthetised. The contralateral TA muscle was injected in the same way with an empty AAV vector (no gene inserted) to serve as a control. After the mouse regained mobility, it was returned to the holding cage and was inspected twice a week for general welfare as described above.

2.2 Contraction recordings and analysis

All contraction recordings were conducted by Joanne Ban as part of her PhD thesis (2018) with mice injected with AAV series one. Joanne undertook the contraction recordings when the *mdx* mice reached 12 weeks of age. In brief, the mouse was first anaesthetised (as in *2.1.2 isoflurane anaesthesia of mice*) and placed on a heating pad. The TA muscle was surgically exposed, and its distal tendon was cut and tied onto the lever arm of a dual-mode servomotor/ force transducer using a silk thread (Aurora instruments). A clamp was used to anchor the tibia to minimise any movement artefacts. For the nerve-stimulated recordings a pair of platinum wire electrodes were placed on the peroneal nerve and delivered 0.2msec

supramaximal square wave pulses in 400msec long trains. For the direct muscle stimulation, electrodes were placed on the surface of the muscle perpendicular to the long axis of the muscle fibres and trains of 0.5msec supramaximal pulses were delivered. Warm HEPES buffered Tyrode's solution was applied to the nerve and muscle to maintain moisture and recordings were visualised using Axoscope software. Each muscle was adjusted to optimal muscle length for maximum isometric tetanic force and stimulation frequency was varied to determine the maximum tetanic force. Specific force was estimated by normalising maximum tetanic force to muscle cross-sectional area [(force (N) x length (mm) x density (1.06 mg.mm 3))/muscle mass (mg)]. After the force recordings were completed, the mouse was culled by intraperitoneal injection of pentobarbitone (30mg; Cenvet, Australia). The original contraction recordings and calculated force data were both saved onto the University Research Data Store (RDS) by Joanne Ban. Tim, a volunteer in the lab at the time used the specific force data obtained by Joanne to plot force-frequency curves for the nerve-stimulated and directly stimulated *mdx* muscles. The force-frequency curves were then expressed as a percentage of maximal force in a separate graph. No muscle contraction recordings were made for the AAV series two mice.

2.3 Muscle dissection and freezing

2.3.1 Muscle dissection

Series one mice used in chapter 3 were first deeply anaesthetised with isoflurane for the contraction recordings (as described in *2.2 Isoflurane anaesthesia of mice*) and were then given an intraperitoneal injection of pentobarbitone (30mg; Cenvet, Australia). The mice were kept deeply anaesthetised until death was confirmed by the absence of heart and respiratory rate. Series two mice described in chapter 4 were restrained and culled via an intraperitoneal

injection of pentobarbitone (30mg; Cenvet, Australia). For dissection of the TA muscle, the dead mouse was positioned supine on a foam dissection board and the limbs were secured with pins. The shank area of the mouse hind limb was sprayed with ethanol and an incision in the skin was made down to the foot. The distal tendon of the TA muscle could then be identified and was cut to allow the muscle to be teased away from the surrounding tissues by gently pulling on the tendon. At the same time, any surrounding fascia was cut away from the muscle. For dissection of the soleus muscle, the mouse was positioned prone on the Styrofoam dissection board and limbs were secured with pins. An incision was made near the foot so that the tendon of the gastrocnemius muscle could be identified and cut. The gastrocnemius muscle was removed by slowly pulling on its tendon until the tendon of the soleus muscle became visible. The soleus muscle was then peeled away from the gastrocnemius by gently pulling on its tendon. For the neonatal hind limb dissection, an incision was made near the foot so that the leg could be skinned before the whole hind limb was removed. To ensure that the tissue was kept moist, phosphate buffered saline (PBS) was applied to all muscles during dissection. After dissection, muscles were immediately frozen in a mould containing Tissue-Tek O.C.T compound (Sakura Finetek, California).

2.3.2 Snap-freezing of muscles

For freezing, the dissected muscle was placed into a mould and submerged in O.C.T compound. A metal beaker was part filled with isopentane and was floated in a foam box containing liquid nitrogen. The isopentane was chilled until white pebbles formed on the bottom of the beaker. The TA muscle block was submerged in the chilled isopentane for ~12 seconds. Smaller tissue blocks such as the neonatal hindlimb were submerged in chilled isopentane for ~2 seconds. For the series one experiments described in chapter 3, moulds were prepared by folding aluminium foil into a ‘boat’ shape, with the approximate dimensions

of 20mm L x 10mm W x 10mm H. The frozen block was then removed from the mould and trimmed to fit a 1.5ml poly-propylene Eppendorf-type 1.5ml centrifuge tube. To prevent desiccation of the block during subsequent storage at -80°C, a drop of water was frozen in place at the bottom of the tube by holding the tube over liquid nitrogen. The O.C.T-muscle block was then placed into the tube which was transported on liquid nitrogen to the -80°C freezer for long-term storage. I found that, using this method, the muscle block began to partially thaw during the trimming process and was then re-freezing when transported in liquid nitrogen. This thawing and re-freezing caused substantial freezing artefact in my early tissue samples. Thus, subsequent muscle blocks were frozen by placing them in a mould made from a 0.5mL poly-propylene centrifuge tube with the conical base cut off (Figure 2.1). In this way the frozen O.C.T-muscle block could be slipped out of the mould and straight into the (larger) 1.5mL centrifuge tube for storage without any trimming and subsequent thawing.

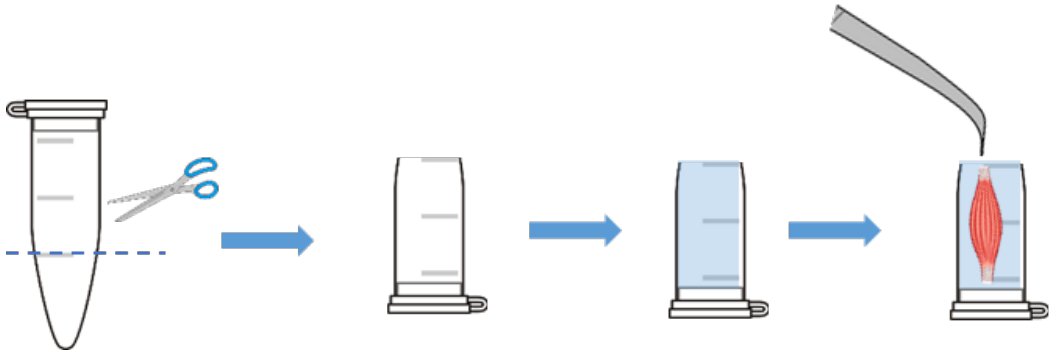

Figure 2.1: Embedding and freezing of muscles for cryosectioning. For later experiments the mould was prepared by cutting the conical tip off a 0.5mL Eppendorf tube. The lid of the Eppendorf tube was then closed, and the tube was filled with O.C.T compound. The muscle was then placed into the tube using forceps and frozen in isopentane that had been pre-chilled in liquid nitrogen. The block was removed from the tube by opening the lid and pushing the block out with a pair of blunt forceps.

2.4 General Immunolabelling procedure

Transverse cryosections of the TA muscle (10µm) were sectioned using the Leica CM3050 cryostat and were collected on a polysine coated microscope adhesion slide (Thermo Fisher Scientific, Australia). Slides were then left on the bench to air dry for 10 minutes before being washed in 3 changes of PBS for 30 minutes. The sections were then pre- blocked in 10% goat serum in PBS for one hour at room temperature. The primary antibody was diluted in 10% goat serum/PBS and 12.5µl of the diluted primary antibody was applied over each muscle section. The slides were then incubated in a humidified chamber overnight at 4°C. Each experiment included control slides that were not exposed to primary antibody (10% goat serum/PBS only). The next day sections were washed in 3 changes of PBS for 30 minutes in coplin jars. The secondary antibody was also diluted in 10% goat serum and 12.5 µl was applied to each section. The slides were incubated in a humidified chamber for 1 hour at room temperature. The slides were again washed in 3 changes of PBS for 30 minutes. Finally, the sections were mounted in DABCO anti-fade mountant (Sigma, Australia) and coverslipped. The edges of the coverslip were sealed with clear nail polish. All slides were imaged using equipment in the Bosch Institute Advanced Microscopy Facility. After imaging, slides were stored in the fridge (~4°C).

2.5 General blinding protocol

For the series one experiments described in chapter 3, I ensured that I (the operator) remained blinded during the sampling and analysis of microscope fields by passing the immunolabelled slides to a second person (the coder) to relabel with code numbers. The

coder first typed the slide label information for each slide in a row in an excel spreadsheet. The coder then erased the original label from the slide and used a random number generator to assign a 4-digit code number to re-label each slide and recorded this code in the excel spreadsheet in a column next to the original slide label. This 'secret' version of the spreadsheet was then saved as "020418_Besa_secret.xls" on the coder's computer so the operator could not access it. The coder then created a second, open, version of the same spreadsheet by deleting the original label column leaving just the code number column. The rows were sorted in numerical order according to the random code number (lowest to highest number). This was done to avoid giving the operator a clue to the identity of the slides. The open "operator/scorer" version was then saved as "020418_Besa_scorer.xls" and was sent to the operator. The slides were then placed into a plastic slide box in numerical order. The box was labelled with the date and antibody used and returned to the operator. In this way, the imaging and subsequent microscopic sampling and analysis were conducted by the operator who remained blind to the treatment group. Once all images from an experiment were analysed, the coder sent the operator the 'secret' spreadsheet, allowing the operator to break the code and analyse the data.

For series two experiments in chapter 4, a similar method of blinding was employed but the slides themselves were not blinded. Instead, whole muscle cross-section images were captured and saved with a file name that indicated the treatment group and a mouse identifier (e.g. 80470_Lt_ear_MuSK). These file names were then entered on an excel spreadsheet and the coder used a random number generator to assign a 4-digit code number to each image file. A second copy of the image file was then created after replacing the original file name with the code number so that the operator would be blinded when conducting image analysis. The 'secret' spreadsheet was then saved on the coder's computer.

The operator was then provided with access to a folder containing the numerically coded files. Once all image analysis was complete for the experiment, the 'secret' spreadsheet was sent back to the operator, allowing me to break the code and generate graphs from the data.

2.6 Collagen I and pan-myosin analysis (series one muscles)

2.6.1 Immunolabelling procedure for collagen I and pan-myosin

Cryosections of the TA muscle (10µm) were collected and immunolabelled as in the general protocol described above (see *2.4 General Immunolabelling*). Specifically, these sections were collected and double-labelled with a mixture of the following primary antibodies: rabbit polyclonal anti- collagen I (Millipore, AB765P; 1:40) and mouse monoclonal anti-MHC (Developmental Studies Hybridoma Bank, A4.1025; 1:200), hereafter referred to as 'pan-myosin' since this antibody recognises all skeletal muscle MHC isoforms (Dan-goor *et al*., 1990). After overnight incubation in the primary antibody and washing, the sections were incubated for 1 hour at room temperature with the following fluorophore-conjugated secondary antibodies: Cy3-conjugated Donkey Anti-Rabbit IgG (Jackson, 711-165-152; 1:100) and Alexa Fluor 647-conjugated Donkey Anti-Mouse IgG (Jackson, 715-605-150; 1:200).

This immunolabelling protocol was conducted in 5 batches, with each batch containing the TA muscle from one wild type mouse (C57BL/6), a TA muscle from one *mdx* mouse that had been injected at 3-4 weeks of age with AAV-MuSK and the contralateral control TA muscle (injected with the empty AAV vector). The slides were blinded so that the operator could not identify which treatment group the muscle came from (wild type, *mdx* MuSK or *mdx* empty). Each batch of immunolabelling also contained one non-blinded wild

type muscle labelling-control slide and another control slide that had been processed without the anti-MHC antibody (no-primary antibody controls).

2.6.2 Blinded confocal imaging and analysis

Fluorescent images of collagen I/pan-myosin were collected on the Zeiss 510 META confocal microscope (first 3 batches) and later on the Zeiss LSM 800 Plus Airyscan (final 2 batches), when the Zeiss 510 was out of order for repair. These images were collected using the 40x oil objective. Each session began with the non-blinded wild type slides. These were used to confirm the effectiveness of labelling and to set the gain and offset for subsequent confocal imaging. For the coded slides, sampling began at the upper left corner of each muscle section. Each field was examined moving from left to right. Any fields that contained blood vessels, tendons or ligaments were excluded to ensure that only endomysial collagen I was quantified. The microscope stage was then moved to the adjoining field and images were collected on both fluorescence channels as long as there were no blood vessels or tendons/ligaments. If the next field contained any of these structures, it was skipped and the field after that was imaged. This was repeated until 12 fields were collected for each muscle section. All images were then saved onto the University RDS (sms\researchdata. shared.sydney.edu.au\\: Besa Collagen and myosin folder) so they could be analysed in the lab.

Image J was used to quantify collagen I and pan-myosin content via threshold analysis. The threshold was used to isolate areas of positive staining and was adjusted such that only membrane staining (collagen I) or staining inside the fibre (myosin) could be seen. The Image J percentage area tool was used to determine the percentage of the total area of the field taken up by either collagen I or pan-myosin. For each muscle, 12 fields were taken, and their

percentage areas were averaged to calculate the mean collagen I and pan-myosin percentage for each muscle.

2.6.3 Blinded Axioscan imaging and analysis

After imaging on the confocal, the same slides were also imaged on the wide-field Zeiss Axioscan to obtain whole muscle cross-section virtual montages for analysis of total myosin area. These images were collected using the 20x objective starting with the non-blinded wild type slides. These non-blinded wild type sections were used to manually set the exposure time. This was done using the 'range indicator' tool on ZEN software, which shows any saturated pixels as red while any non-saturated pixels are shown in grayscale. The exposure time was increased manually until 1 pixel of red could be seen in the field of view, indicating saturation. These settings were then applied to all the subsequent slides in the imaging session. Whole cross-sections of muscle were obtained using the ZEN software which stitches together all the fields captured by the Axioscan. Scale bars were added and images were converted into TIFF files using ZEN software. The images were then saved on the University RDS (sms\research-data.shared.sydney.edu.au\\: Besa Collagen and Myosin folder) so they could be analysed in the lab.

Image J was used to quantify the pan-myosin total area via a threshold analysis. First, the selection tool on image J was used to draw as closely around the section as possible. The threshold was then used to highlight the areas of positive staining inside the fibres, ensuring that the gaps between individual muscle fibres were visible. Once the muscle fibre area was highlighted by the threshold, the muscle fibre area within the selection boundaries was measured.

2.7 Myosin fibre type analysis (series one muscles)

2.7.1 Immunolabelling procedure for myosin fibre types

Serial cryosections of the TA and soleus muscles (10µm) were collected and stained as in the general protocol described above (see *2.4 General Immunolabelling*). Specifically, each section was labelled with a single mouse monoclonal antibody against one of the following MHC isoforms obtained from the Developmental Studies Hybridoma Bank (DSHB): MHC Type I (BA-F8), IIa (SC-71), IIb (BF-F3) or IIx (6H1). After overnight incubation in the primary antibody at 4°C and washing, the sections were incubated with a fluorophore-conjugated secondary antibody for 1 hour at room temperature, according to the immunoglobulin type of the primary antibody, either Cy3-conjugated Goat Anti-Mouse IgG (Jackson, 115-165-146) or Cy3-conjugated Goat Anti-Mouse IgM (Jackson, 115-165-020) was used. The dilutions used and the combination of primary and secondary antibodies can be seen in Table 2.1.

This immunostaining protocol was conducted in batches, with each batch containing one wild type mouse TA muscle, one *mdx* mouse TA muscle supplemented with MuSK-GFP and the contralateral TA muscle from the same *mdx* mouse that was injected with the empty AAV vector. Each of the primary antibodies was applied to separate muscle sections within the batch. The wild type muscle primary antibody-labelled slide (positive control) and corresponding no-primary antibody slide (negative control) were not blinded as they were not quantitatively analysed. They were used simply to confirm effective immunolabelling of the batch before analysing the *mdx* samples. Blinding was conducted on the *mdx* slides by replacing the treatment group label with a code number (see 2.5 *General blinding protocol*). In this way, the operator was unaware of whether the muscle had been injected with AAV MuSK or the empty AAV vector. Since slow fibres are not normally found in the TA muscle

(Bloemberg & Quadrilatero, 2012) sections of wild type soleus muscle were used for optimising exposure time for the BA-F8 (slow MHC).

Table 2.1: List of primary and secondary antibody combinations used with their dilutions and the myosin heavy chain (MHC) isoform they recognise.

Primary antibody	Isotype	MHC reactivity	Dilution	Secondary antibody (1:100)
BA-F8	IgG2b	Type I, slow	1:500	Cy3 Goat anti-mouse IgG
SC-71	IgG1	Type IIa, fast	1:500	Cy3 Goat anti-mouse IgG
BF-F3	IgM	Type IIb, fast	1:500	Cy3 Goat anti-mouse IgM
6H1	IgM	Type IIx, fast	1:500	Cy3 Goat anti-mouse IgM

2.7.2 Blinded Axioscan imaging and analysis for fibre types

For the fibre type analysis all slides were imaged on the Zeiss Axioscan using the 20x objective. First, the non-blinded wild type slides were used to select the appropriate exposure time for each antibody. Exposure was set manually by increasing the exposure time until a single saturated pixel appeared inside a fibre. This exposure time was then fixed for all blinded *mdx* slides stained with that same antibody during that imaging session. This process of exposure determination was then repeated for all four antibodies. The images of the whole cross-sections were converted into TIFFs with scale bars and were saved onto the RDS (sms\research-data.shared.sydney.edu.au\\: Besa Fibre Typing folder) for later analysis.

The superficial 'white' part of the mouse TA muscle contains primarily IIb MHC positive muscle fibres while the deep 'red' part (near the bone) is made up of predominantly IIx fibres (Bloemberg & Quadrilatero, 2012; Pullen, 1977). Due to the different composition of fibre types in the red and white areas, each muscle section was segmented into a red and white component and these areas were counted and quantified independently. For example, type IIb fibres are said to occupy large proportion (~70%) of the white TA but only a small proportion (~25%) in the red TA (Bloemberg & Quadrilatero, 2012). Thus, the staining pattern observed in sections stained with BF-F3 (anti-MHC IIb) was used to identify the red and white areas of the muscle. This was then used as a template to determine the red and white components of the subsequent serial muscle sections stained with the other fibre type primary antibodies.

Once the red and white components were determined, the fibre counts could then be conducted. Using Image J software, a 400µm2 grid was used to create fields each of which contained approximately 100 fibres for counting. Fields were analysed from both the red and white regions of the muscle to ensure that about 300 fibres were sampled from each region. Any fields that included the epimysium were excluded as the fibres near the edges of the section consistently stained brightly, probably due to the damage of muscle fibres on the edge. It's likely that this damage occurred during the dissection process when the TA muscle was pulled away from its surrounding tissues. A field was also excluded if it contained a patch of intensely stained fibres as this intense staining is not typical and these occasional patches may be sites of muscle injury where *mdx* fibres have taken up endogenous IgG. Figure 2.2 shows a sample field containing typical type IIb-stained muscle fibres (cross hairs). Also shown are examples of some intensely stained cells (marked with a white tracing) that were occasionally seen and may be injured fibres that would be excluded from counts. When such

intensely stained fibres were present in a field, that field would be excluded from counting on this basis. The multipoint tool on image J was used for the counts of stained fibres. Fibres lacking staining were counted as negative for that particular fibre type. The positive fibres were then expressed as a percentage of the total fibre count in the selected fields.

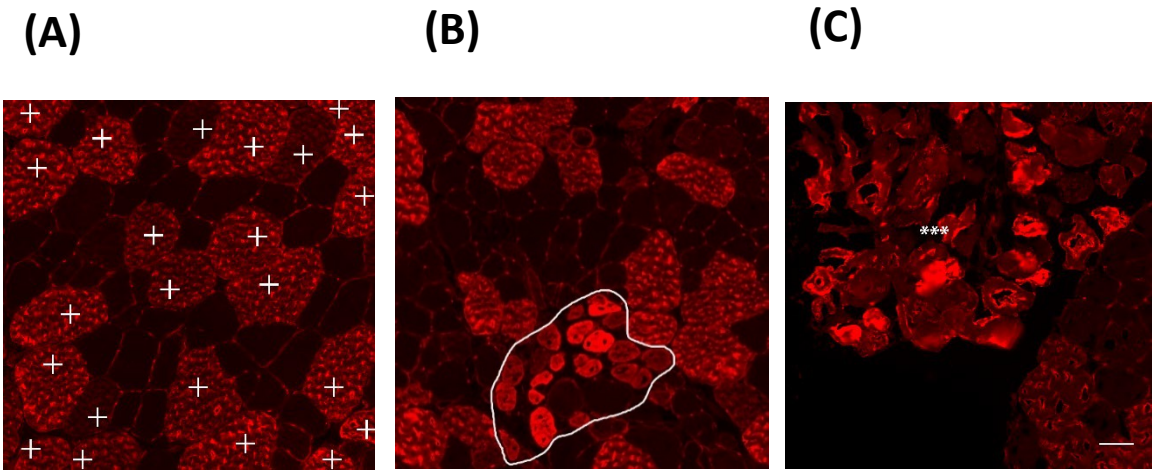

Figure 2.2: Examples of type IIb fibres (cross hairs) and intensely stained fibres that may be damaged fibres. (A) Cross hairs show examples of healthy type IIb fibres that would be counted as positive. (B) Patches of intensely stained fibres (traced around in white) that would cause a microscopic field to be excluded from counts. (C) Fields containing epimysium/edges of the section were also excluded as the fibres are often damaged and stain brightly. Some damaged fibres are indicated with the asterisks.

2.8 Embryonic myosin analysis (series two muscles)

2.8.1 Cryosectioning for embryonic myosin analysis

Cryosections of the TA muscle of series two *mdx* mice (10µm) were collected in series on 4 slides with each series labelled A, B, C and D. Cryosections of the hind limb from a wild type P1 neonatal mouse (10µm) were also collected on separate slides to be used as positive controls for embryonic myosin staining. The serial sections of TA muscles from *mdx* mice were collected at two different levels of the muscle: approximately 2mm and 3mm in from the proximal end of the muscle. To reach the point of 2mm into the muscle, approximately 200x 10µm sections were cut and discarded. The next section was then observed under a phase-contrast microscope to ensure that the muscle section contained many fibres in cross-section without any tendon. To ensure consistency, sections were collected when they took up the entire field of view on the microscope 4x objective and when all fibres appeared to be in cross-section with no fibres showing oblique attachment to a tendon. Another 100 x 10µm sections were then cut and discarded. The next section was then observed under the phase-contrast microscope again to ensure that the section was increasing in size. This was done to ensure that I had not cut past the muscle belly. Serial sections were then collected on the same slides.

2.8.2 Immunolabelling procedure for embryonic myosin analysis

Serial cryosections of the TA muscle and neonatal hind limb (10µm) were collected and stained as in the general protocol described above (see *2.4 General Immunolabelling*). Specifically, these sections were pre-blocked with Mouse on Mouse blocking reagent (Vector Laboratories Inc., US) for an hour before they were double labelled with the following mixture

of primary antibodies: mouse monoclonal anti-embryonic myosin (DSHB, BF-G6, 1:4) and rabbit polyclonal anti-laminin (Abcam, ab11575, 1:1000). After overnight incubation in a mixture of these primary antibodies at 4°C and washing, the sections were incubated for 1 hour at room temperature with the following mixture of fluorophore-conjugated secondary antibodies: Cy3-conjugated Goat anti-mouse IgG (Jackson, 115-165-146, 1:100) and FITC-conjugated Goat anti-rabbit IgG (Jackson, 111-095-144, 1:100). The DNA stain, DAPI (1:1250, Life technologies Australia Pty Ltd) was included in the incubation time to label the nuclei.

This immunostaining protocol was conducted in batches, with each batch containing three *mdx* mouse TA muscles that had been injected with MuSK-GFP and the contralateral control TA muscles from the same three *mdx* mice (injected with the empty AAV vector). The immunostaining was repeated in the same sized batches until all *mdx* muscles expressing MuSK-GFP had been processed. This procedure was then repeated for the three remaining AAV vectors encoding: MuSK-ΔIg3, Dok7 and Rapsyn. Sections from the same neonatal hind limb were also used in each batch to act as a positive control for embryonic myosin staining. Each batch also contained sections that lacked the embryonic myosin antibody (antibody-negative control slide).

2.8.3 Axioscan imaging and blinded analysis of embryonic myosin

All slides were imaged on the Zeiss Axioscan using the 20x objective to obtain images of the entire muscle cross-section. First, the neonatal hind limb slide (positive control) was used to select the appropriate exposure time for the embryonic myosin staining. This exposure time was then applied to all the adult *mdx* slides in the imaging session. The first

mdx slide was used to set the exposure time for laminin and DAPI staining. These exposure times were then applied to all subsequent slides. The images of these whole cross-sections were converted into TIFF files and saved onto the university RDS (\\research-data 2.shared.sydney.edu.au\RDS-02\PRJ-SMS\Besa\Embryonic myosin folder) for later analysis.

For the analysis of images, counting was conducted blind. To achieve this, the coder assigned and re-named each TIFF file with a 4-digit code number (see *2.5 General blinding protocol).* The original file name of the image along with its corresponding 4-digit code number were recorded in the 'secret' excel spreadsheet by the coder. The scorer did not have access to this 'secret' sheet until all image analysis was complete.

For the embryonic myosin counts, the whole cross-section images were viewed on Image J as an RGB stack so that I could move between the red (embryonic myosin) and green (laminin) channels. A 400μm^2 grid was applied to each image to aid with counting. Small fibres that stained brightly for embryonic myosin (red) were counted as positive. The green laminin staining was used to visualise the boundary of each fibre and each discrete fibre was identified based on the complete laminin ring observed around it. If there was any embryonic myosin staining within the laminin ring, that fibre was counted as positive (Figure 2.3). The monoclonal BF-G6 is selective for embryonic myosin (Schiaffino *et al*., 1986). However, in my experience a subset of large fibres with peripheral nuclei also displayed weak fluorescence with BF-G6, suggesting that it was labelling some non-regenerated fibres of a particular fibre type (Figure 2.3). The number of embryonic myosin positive fibres in each field was counted and recorded on an excel spreadsheet. After the number of positive fibres was counted, an automated analysis was conducted to determine the total number of fibres in the muscle

cross-section. The number of positive fibres was then divided by the number of total fibres in the cross-section to determine the percentage of fibres positive for embryonic myosin.

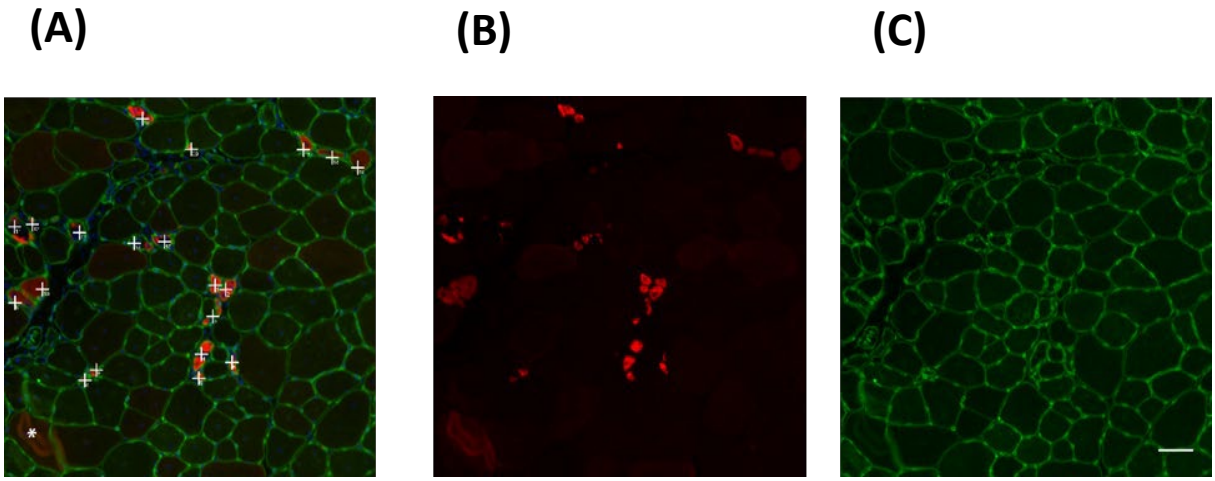

Figure 2.3: Sample image of embryonic myosin immunofluorescence used to identify regenerating muscle fibres. Muscle cross-sections were double labelled for embryonic myosin (red) and laminin (green)**.** (A) Shows a merged image containing laminin, embryonic myosin and DAPI staining. The cross hairs signify that the fibre was counted as positive for embryonic myosin. The asterisk shows diffuse staining in a large fibre (lower left corner; not counted as positive). (B) Red channel showing embryonic myosin staining. (C) Green channel showing laminin staining, marking out the boundaries of individual muscle fibres. Scale bar = 50µm.

2.8.4 Automated fibre counts & minimal Feret's diameter analysis

For the automated fibre counts and minimal Feret's diameter, the same whole cross-section images were used as in the embryonic myosin analysis. The minimal Feret's diameter is generally used to estimate muscle fibre girth to avoid distortions that occur when some of the fibres in the cross-section are not truly perpendicular to the plane of section (Grounds *et al*., 2008). The images were split into the 3 colour channels: red (embryonic myosin), green (laminin) and blue (DAPI). For this analysis, only the laminin (green) channel was used. The automated analysis was conducted using the 'analyze particles' function on Image J. Since this function requires a binary image, a fluorescence intensity threshold was manually applied to each image such that the fibre boundaries (laminin staining) showed up black on a white background, with minimal black staining inside the muscle fibres (Figure 2.4A). Once the binary images were obtained, the 'analyze particles' function was applied to the image. The output of this function was a table containing the number of muscle fibres with their minimal Feret's diameters and a binary image showing the outlines of all counted muscle fibres (Figure 2.4B). To ensure that the software was counting only muscle fibres, any objects with a diameter smaller than 10µm were excluded from the analysis. This value was selected as no *mdx* muscle fibres with Feret's diameters less than 10µm have been reported (Pertl *et* al., 2013; Trajanovska *et al.,* 2019). Each image was inspected visually after the automated analysis to ensure that no fibres were missed or that multiple fibres were not counted as one large fibre. This analysis was repeated on all cross-section images. Due to variability in the quality of the laminin staining, some muscle cross-section images had to be excluded from this analysis and were counted manually instead. For these images I did not obtain the minimal Feret's diameter. As described above, cross-sections were imaged at two levels along the length of each muscle. For the total fibre counts in the cross-section, values from both

levels were averaged to estimate the fibre number in each muscle. For the minimal Feret's diameter analysis, only fibres from the second level were used. This was done to avoid counting any oblique fibres that may skew the counts or minimal Feret's diameter

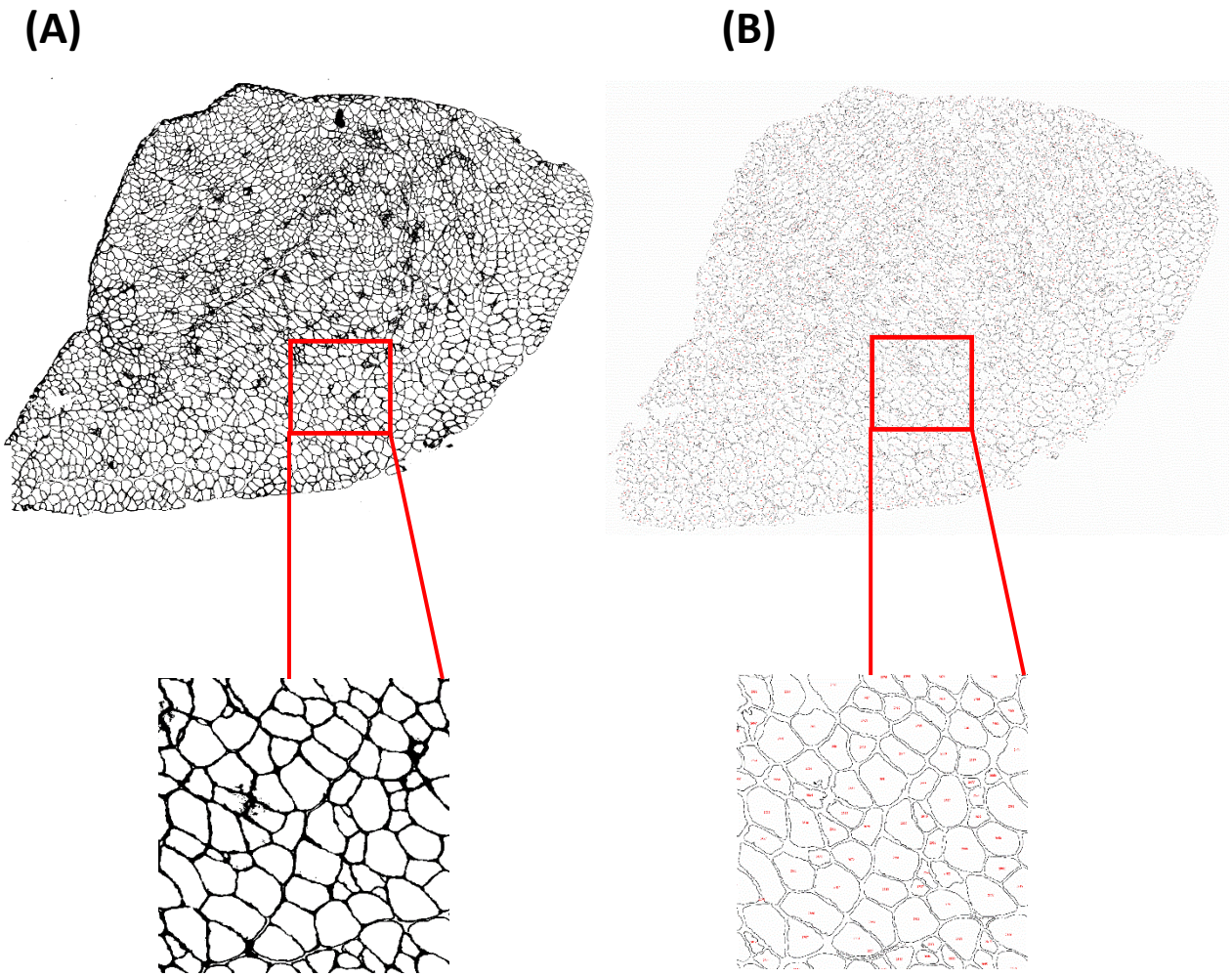

Figure 2.4: Sample images of laminin staining after thresholding and particle analysis for automated counting. (A) Shows an example of the binary image after applying an intensity threshold to the laminin staining. This thresholded image was then used to define the cell boundaries and count the muscle fibre profiles using the analyze particles function on Image J. (B) Output of the analyse particles for the muscle cross-section. The number (shown in red) in the centre of the fibre corresponds to the count. A separate table of minimal Feret's diameters were also produced but is not shown.

2.9 Statistics

To test the effects of MuSK, Rapsyn and Dok7 supplementation on *mdx* muscles, compared to contralateral empty vector control muscles, two-tailed, paired Student's t-tests were used (comparing AAV-transgene injected muscle to the contralateral empty vector control injected muscle). The level of significance was set at 0.05. GraphPad Prism version 7 was used for all data analysis and to create the graphs. For the sample size n= number of mice unless specified otherwise. All errors bars on graphs indicate mean ± 95% confidence intervals. Values for individual muscles are shown as circles on each graph. In the results text all values are represented as: Mean (SD).

CHAPTER THREE:

MuSK-GFP supplementation does not alter the composition of *mdx* muscle

3.1 Introduction

As discussed in the introduction chapter, the TA muscles of *mdx* mice are heavier than those of the age-matched wild type genetic background strain (C57BL/10 ScSn). Furthermore, recent work in the lab has suggested that MuSK-GFP supplementation was able to reduce this muscle mass back to the wild type level without any change in the maximum force capacity (Joanne Ban, 2018, PhD thesis). Hypertrophy and pseudohypertrophy of the limb muscles both occur in human DMD and in the *mdx* mouse model of DMD (Guiraud & Davies, 2017; Mazala *et al.*, 2015; Manning & O'Malley, 2015). Hypertrophy refers to an adaptive growth in muscle fibre girth to maintain effective muscle function. Pseudohypertrophy is defined as an enlarged, yet weak muscle and it occurs when muscle fibres necrotise and are subsequently replaced with fatty and fibrous deposits (Manning & O'Malley, 2015). It is this increase in non-contractile tissue that is thought to create a muscle that is heavier than normal but does not produce more force (Lynch *et al*., 2001). The first aim of this chapter is to investigate whether the greater mass of the TA muscles of *mdx* mice, compared to wild type mice (and its reversal by AAV-MuSK) involves either pseudohypertrophy or true hypertrophy. To do this, the same muscle blocks used by Joanne Ban were cryosectioned and immunostained for collagen I and pan-myosin. Immunostaining and morphometry were then used to determine the portion of the muscle taken up by ECM vs the area taken up by muscle fibres. These *mdx* muscles were injected with AAV-MuSK or an empty vector control and were dissected by Joanne Ban as part of her PhD thesis (2018). The mice were injected shortly after weaning (3-4 weeks of age) and were culled for analysis when they reached 12-13 weeks of age, allowing for a period of 9-10 weeks for gene expression (Figure 3.1). In her PhD thesis,

Joanne Ban (2018) also included sample images of these *mdx* TA muscles injected with MuSK-GFP which revealed widespread MuSK-GFP expression across the entire muscle (Figure 3.2).

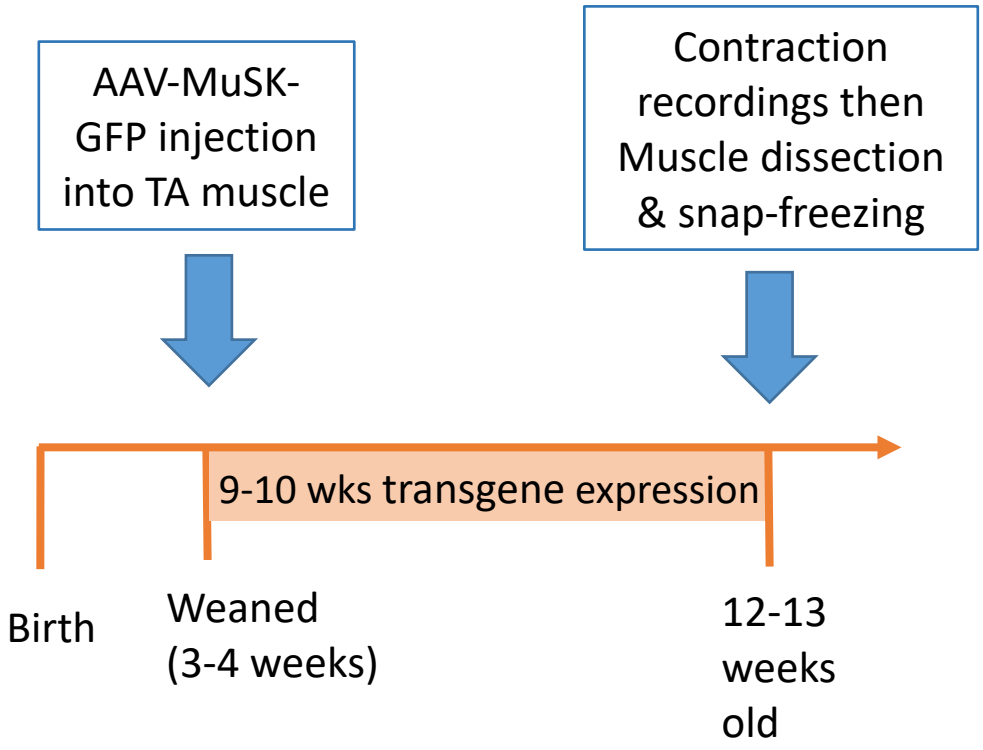

Figure 3.1: Experimental timeline for injections of AAV-MuSK at 3-4 weeks of age. At 3-4 weeks of age the TA muscles of *mdx* mice were injected with an AAV vector encoding MuSK-GFP while the contralateral TA was injected with an empty vector to serve as a control. 9-10 weeks was then allowed for expression of the MuSK transgene. At 12-13 weeks of age the mice were anaesthetised for contraction recordings. After the recordings, the mice were culled, and their TA muscles were dissected and snap-frozen for immunostaining.

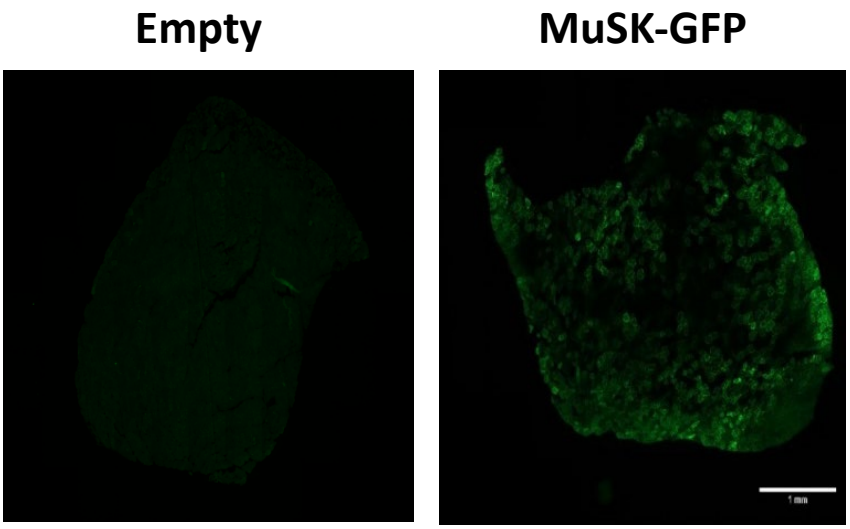

Figure 3.2: Expression of MuSK-GFP in whole cross-sections of *mdx* TA muscles treated with an AAV vector encoding MuSK-GFP or an empty vector at 3-4 weeks of age. Muscles were harvested when the mice were 12-weeks-old. The Zeiss Axioscan microscope was used to image entire sections as tiles which were stitched together to produce a scan of the whole muscle cross-section. The muscle treated with the empty vector did not show any MuSK- GFP fluorescence. Widespread GFP fluorescence can be seen for muscles treated with MuSK-GFP. Scale bar represents 1mm. Images from Joanne Ban, PhD thesis (2018).

Recent work in the lab found that the TA muscles of *mdx* mice supplemented with MuSK-GFP retained more of their original contraction strength after being challenged by a series of eccentric contractions (Joanne Ban, 2018 PhD thesis). Muscles such as the TA contain a mixture of fibre types characterised by their expression of particular forms of MHC (Type I, IIa, IIb and IIx). These four fibre types vary not only in their MHC composition but also in their speed of contraction, with type IIb being the fastest/strongest and type I the slowest (IIB > IIX > IIA > I) (Schiaffino, 2010). Conceivably, the improved retention of force in *mdx* muscles expressing MuSK-GFP might be explained by a fast to slow fibre switch, as slow fibres are thought to be more resistant to contraction-induced injury (Selsby *et al*., 2012). Therefore, in this chapter, I also investigate whether there is any change in the proportions of the four fibre types in the TA muscles of *mdx* mice after injection of AAV-MuSK. To do this, I used immunofluorescence to stain for the four MHC isoforms and undertake fibre counts.

Slow-type muscles such as the soleus are thought to produce a greater amount of their maximal force at lower frequencies, when compared to a fast-type muscle like the TA. Thus, in a force-frequency graph the curve for a slow muscle like the soleus should be shifted to the left (as shown in Figure 3.3), compared to a fast muscle like the EDL (Head & Arber 2013; Huang, Dennis & Baar, 2006; Figure 3.2). With this in mind, Tim De Solom, a volunteer in the lab used the specific force data from Joanne Ban's PhD thesis to plot force-frequency curves for nerve-stimulated and directly stimulated *mdx* muscles expressing MuSK-GFP and their contralateral empty vector controls. These force-frequency curves were then analysed qualitatively, specifically to see if the curve from the MuSK-GFP muscles was shifted to the left of the empty vector control, which may indicate a slow fibre switch.

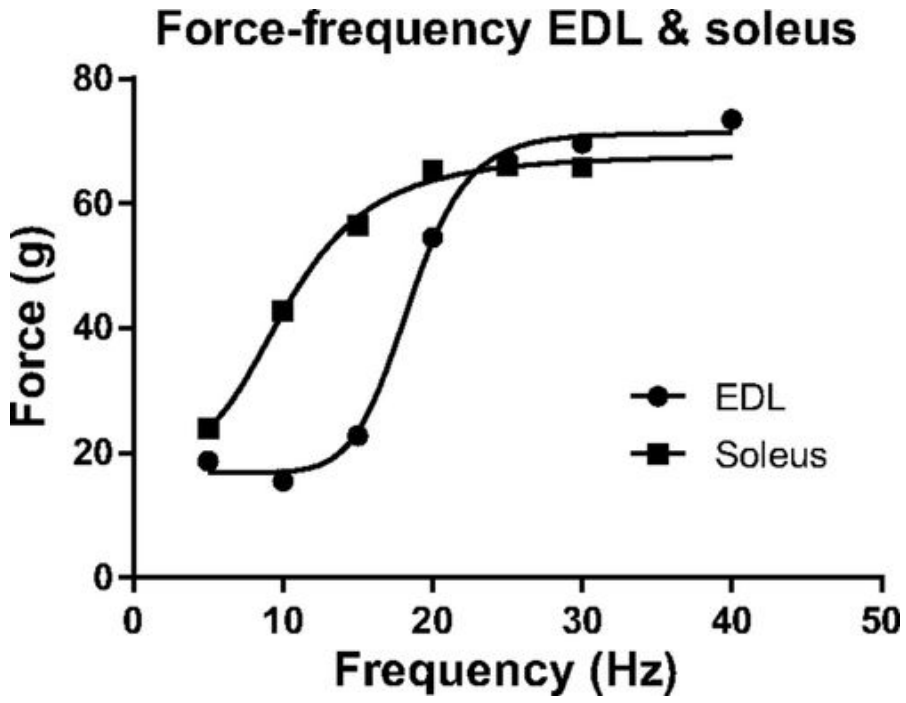

Figure 3.3: Force-frequency curve from rat EDL and soleus muscles. The lines represent the best-fit sigmoidal curves fitted to the data points. This graph shows a shift to the left for the soleus (slow-type) muscle when compared to the curve for the EDL (fast-type). From Head & Arber, 2013.

3.2 Results

3.2.1 MuSK-GFP supplementation does not significantly affect collagen content

To assess the fraction of the muscle occupied by connective tissue, cross-sections were labelled by immunofluorescence for collagen type I (Figure 3.4A). Consistent with previous findings, the age-matched C57BL/6 mice yielded a smaller percentage area that was positive for collagen I, 2.82 (0.41) %, when compared to the empty vector control which had a collagen I area of 5.05 (1.29) % (Figure 3.4B). While the average collagen I area was slightly smaller for the MuSK-GFP expressing *mdx* muscles when compared to the contralateral empty vector controls, this difference was not statistically significant (Figure 3.4B).

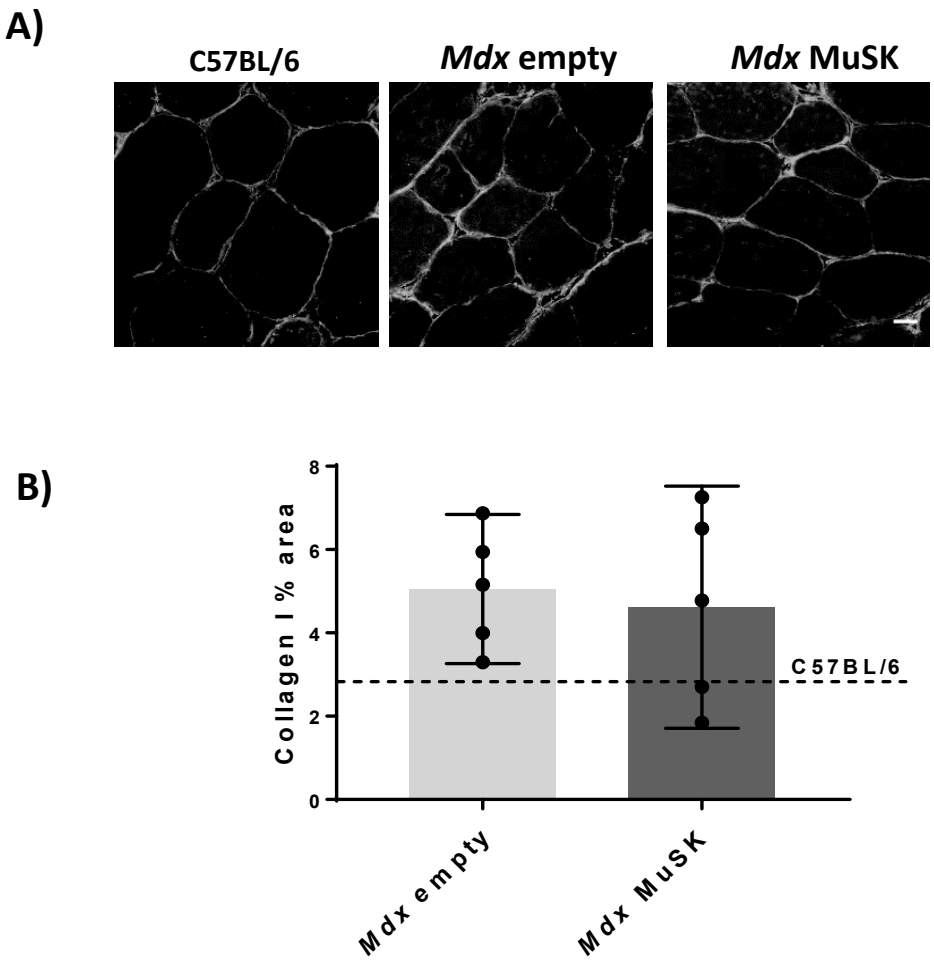

Figure 3.4: MuSK-GFP supplementation does not affect collagen I content in the TA muscle of *mdx* mice. (A) Representative immunofluorescence images stained for collagen I in wild type or *mdx* muscles injected with either empty AAV vector or AAV-MuSK-GFP respectively. Scale bar = 20 µm. (B) The percentage area occupied by collagen I was compared for MuSK-GFP and control mice (n=5) and compared to the wild type level (see chapter 2 for method). The bars represent the mean ± 95% confidence intervals. The dotted line represents the mean for wild type (n=5) mice. No significant difference was found in collagen I percentage area between MuSK-GFP injected and contralateral empty vector controls. Paired student's t-tests were used (*$p<0.05$).

3.2.2 MuSK-GFP supplementation does not significantly affect myosin-filled fibre area

To assess the fraction of the muscle occupied by contractile apparatus, cross-sections were labelled by immunofluorescence with a pan-myosin heavy chain antibody. Figure 3.5A shows sample immunofluorescence images of whole cross-sections stained for pan-myosin. As seen in Figure 3.5D, the mean myosin area was largest in the *mdx* empty vector controls at 6.98 (1.10) mm^2. For MuSK-GFP expressing *mdx* muscles the mean area was slightly lower at 6.17 (1.44) mm^2. The mean myosin area was smallest for the wild type muscles at 4.72 (1.77) mm^2. None of these differences were statistically significant but this might be due to the large variation in the total cross-sectional area for the sample sections from individual muscles.

The fraction of the muscle occupied by pan-myosin was also assessed in high magnification fields (Figure 3.5B). The MuSK-GFP expressing *mdx* muscles showed a myosin percentage area of 76.54 (4.90) %, while the *mdx* empty vector controls showed a myosin percentage area of 75.16 (3.54) % and the untreated wild type value was 74.70 (2.12) % (Figure 3.5E). Interestingly, the proportion of the muscle cross-section occupied by myosin was therefore very similar for *mdx* muscles expressing MuSK-GFP, contralateral control muscles (injected with empty vector) and untreated wild type muscles.

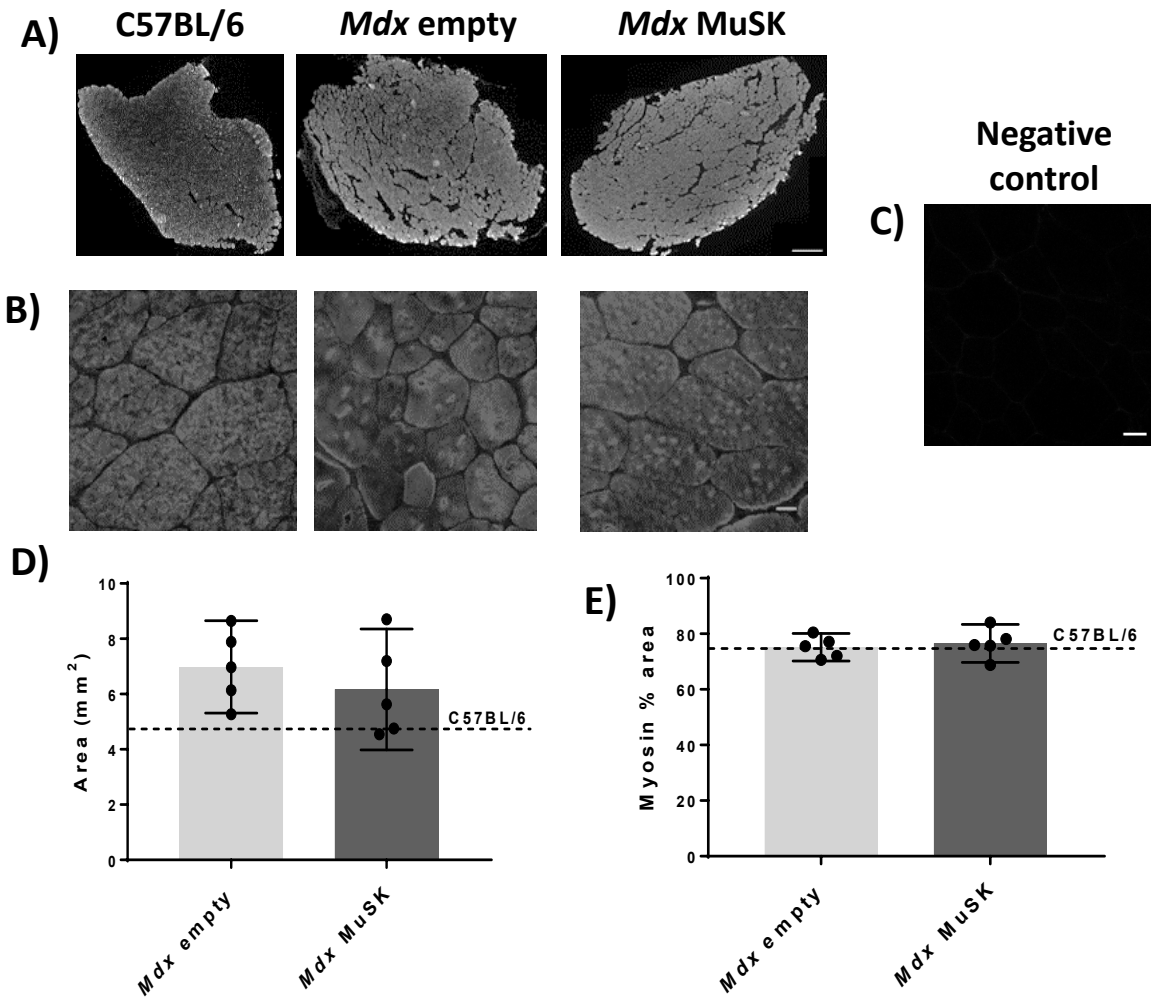

Figure 3.5: MuSK-GFP supplementation does not change myosin-filled fibre area in the TA muscle of *mdx* mice. (A) Whole cross-sections of the TA muscle of wild type, *mdx* empty vector controls and *mdx* muscles injected with AAV-MuSK-GFP respectively stained with pan-myosin antibody. Scale bar = 500µm. (B) High magnification images showing myosin labelling of individual fibres, including a negative control slide that lacks the pan-myosin primary antibody (C). Scale bars =20 µm. (D) Myosin positive area for the whole muscle cross-section. (D) Percentage area of the muscle cross-section occupied by myosin. Results for MuSK-GFP and control mice (n=5) are compared to the mean for wild type muscles (horizontal dotted line). The bars on both graphs represent the mean ± 95% confidence intervals. No significant differences were found between the *mdx* muscles injected with MuSK-GFP and the empty vector controls. Paired student's t-tests were used (*p<0.05).

3.2.3 MuSK-GFP supplementation does not affect the proportions of the muscle fibre types

Cross-sections were labelled by immunofluorescence with antibodies specific for each of the four fibre types: type I, IIa, IIb and IIx. Figure 3.6A shows sample fields from the *mdx* TA muscle labelled for IIa, IIb and IIx myosin. Very few type I fibres were detected in the TA muscle. The TA muscle consists of two distinct regions, the superficial "white" region and deep "red" region (Sréter & Woo, 1963; Bloemberg & Quadrilatero, 2012). As seen in Figure 3.6B, the white component of the TA muscle from *mdx* empty vector control muscles revealed: 0.37 (0.42) % type I fibres, 0.69 (0.57) % type IIa fibres, 53.09 (6.12) % type IIb fibres and 51.27 (6.99) % type IIx fibres. By comparison, within the white region of MuSK-GFP supplemented *mdx* muscles the proportion of fibre types was: 0.31 (0.37) % type I fibres, 0.75 (0.74) % type IIa fibres, 56.86 (9.55) % type IIb fibres and 55.92 (15.20) % type IIx fibres. When comparing AAV-MuSK to AAV-empty vector *mdx* muscles the small differences in the means were, in each case not statistically significant. As expected, the red component of the TA muscle appeared to contain fewer type IIb and slightly more type IIx fibres (Figure 3.6C). *Mdx* empty vector control muscles yielded: 0.76 (0.20) % type I fibres, 3.16 (3.47) % type IIa fibres, 24.94 (4.78) % type IIb fibres and 65.05 (4.73) % type IIx fibres. The MuSK-GFP supplemented *mdx* muscles showed the following percentages: 6.51 (4.40) % type IIa fibres, 30.64 (9.99) %, type IIb fibres, 64.49 (3.15) type IIx fibres and 0.51 (0.39) % type I fibres. When comparing AAV-MuSK to AAV-empty vector *mdx* muscles the small differences in the means were, in each case not statistically significant.

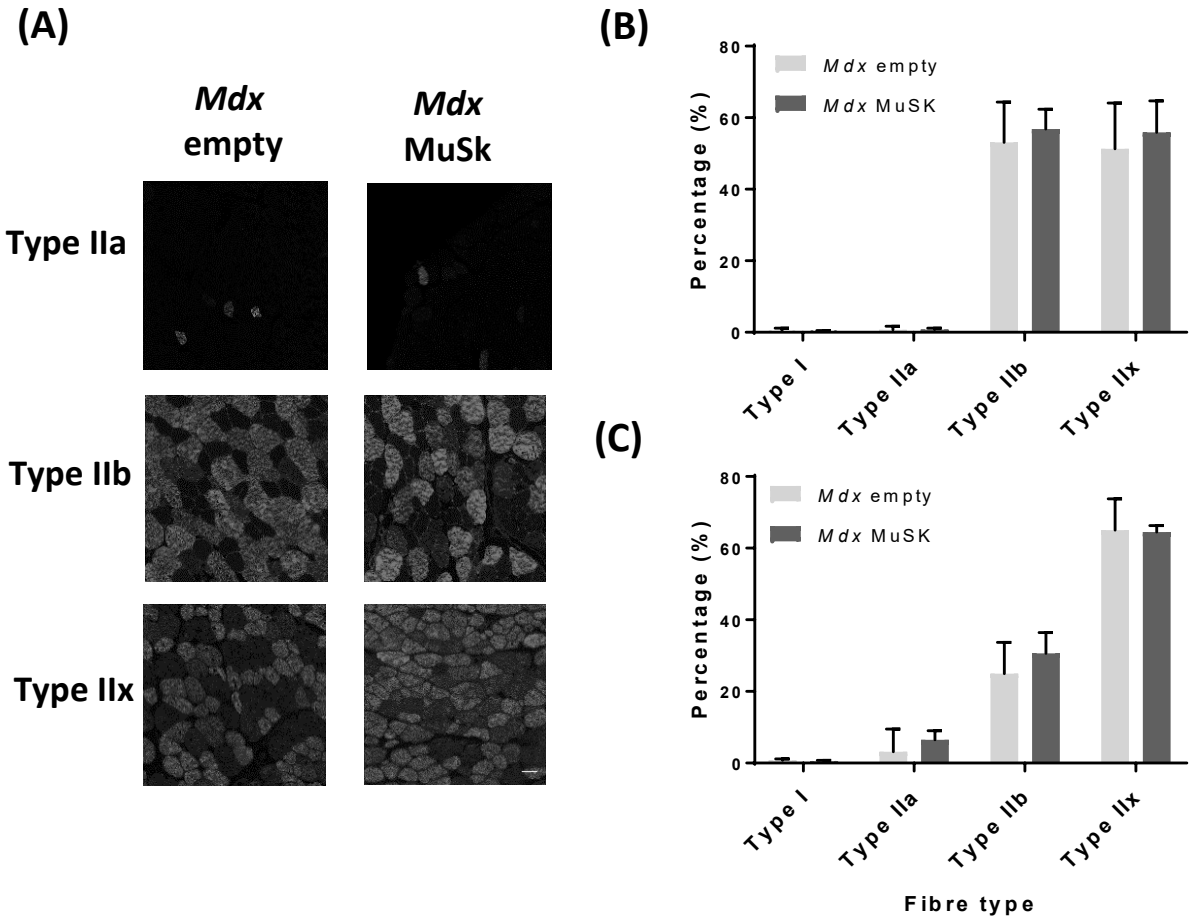

Figure 3.6: MuSK-GFP supplementation does not change fibre type proportions in the TA muscle of *mdx* mice. Cross-sections of TA muscles were stained by immunofluorescence for the four myosin heavy chain isoforms: type I, type IIa, type IIb and type IIx. (A) Representative fields from the red region of an *mdx* empty vector TA muscle labelled for type IIa, type IIb and type IIx fibres. Scale bar = 50µm. (B) The proportion of each of the four fibre types within the white region of *mdx* muscles previously injected with AAV-MuSK-GFP versus values for contralateral empty vector control muscles (n=4). (C) Comparable results for the red region of the TA muscle. The bars represent the mean ± 95% confidence interval. No significant differences were found. Multiple paired student's t-tests were used (*$p<0.05$).

3.2.4 MuSK-GFP supplementation does not produce a left shift in force-frequency curves

To assess whether MuSK-GFP supplementation was inducing a fast to slow fibre switch, force-frequency curves were plotted for *mdx* TA muscles that had been either: nerve-stimulated or directly stimulated. The responses for nerve-stimulated and directly stimulated muscles were compared to reflect any modifications in either the contractile properties of the muscle (seen in direct stimulation) or neuromuscular transmission (nerve-stimulated), as a result of supplementation with MuSK-GFP. Figure 3.7A illustrates that direct muscle stimulation of *mdx* TA muscles (injected with AAV-MuSK) produces a similar force-frequency curve to that of the AAV-empty vector controls. The nerve-stimulated *mdx* TA muscles injected with AAV-MuSK also produced a similar force-frequency curve to that of the AAV-empty vector control muscles (Figure 3.7B). For both the direct and nerve-stimulated muscles, the force-frequency curves for the AAV-MuSK expressing *mdx* muscles were overlapping with that of the AAV-empty vector control muscles, showing no shift to the left.

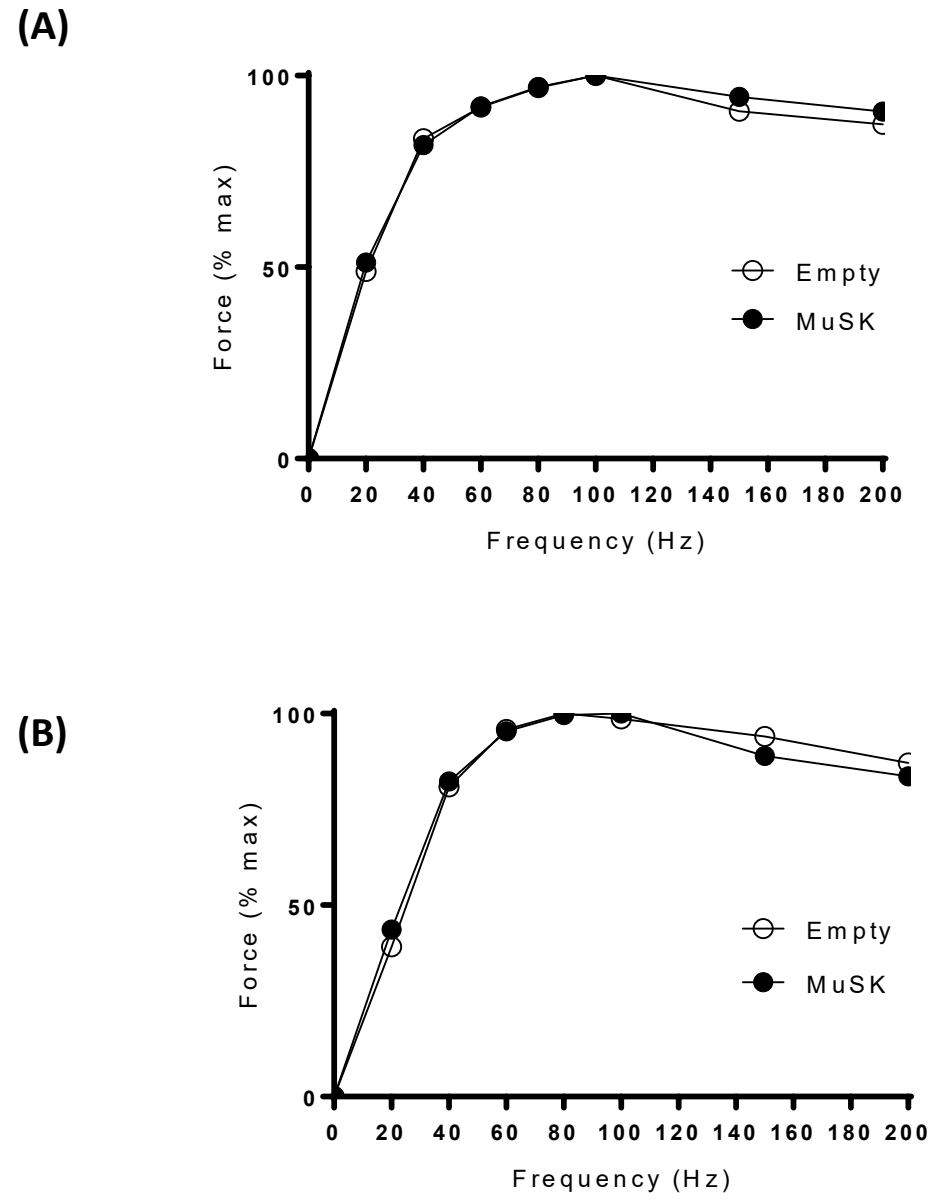

Figure 3.7: Force-frequency curves for directly stimulated and nerve stimulated *mdx* TA muscles supplemented with MuSK-GFP or an empty vector control. Force is expressed as a percentage of maximal force. (A) Direct muscle-stimulated force-frequency curve of *mdx* TA muscles supplemented with MuSK-GFP (black circle) or an AAV-empty vector control (open circle) for n=15 mice. (B) Comparable force-frequency curve for nerve-stimulated *mdx* TA muscles.

3.3 Discussion

Mdx muscles have been reported to be heavier than aged-matched wild type muscles in many different studies (Faber *et* al., 2014; Froehner *et al*., 2014 Selsby *et al*., 2012). However, the mechanisms that lead to this increase in mass remain uncertain and likely depend upon the age at which the mice are studied. Thus, the first part of this chapter aimed to determine whether the greater muscle mass that we found in 12-week-old *mdx* mice (compared to wild type) was due to increased ECM deposition (fibrosis/pseudohypertrophy) or an increase in the contractile machinery of the muscle (genuine hypertrophy). In particular, I wanted to determine whether MuSK-GFP reduces the mass of *mdx* muscles by preventing hypertrophy or pseudohypertrophy.

To assess the possibility of pseudohypertrophy, I quantified the area of the muscle cross-section taken up by collagen I. The control (empty) *mdx* muscles displayed a slightly greater proportional area of collagen I when compared to the age-matched wild type but showed no significant difference when compared to the *mdx* muscles expressing MuSK-GFP (Figure 3.4B). The 2.82% collagen I area found in wild type TA muscle is consistent with previous findings which found that collagen I occupied approximately 3% of the total cross-sectional area in 12-week-old wild type quadriceps muscle (Gibertini *et al*, 2014). This same study reported a significant increase in collagen I in their Sgcb-null mouse (knock down of β-sarcoglycan, another mouse model used to study DMD). It is important to note that the fibrosis reported in these Sgcb-null mice is more severe than that in *mdx* mice (Gibertini *et al*, 2014). The slight increase (2.2%) in collagen I content between age-matched wild type and the *mdx* empty vector controls (Figure 3.4B) cannot easily account for the much larger (18%) difference in muscle mass between wild type and *mdx* (empty vector) control muscles (Joanne Ban, PhD thesis, 2018). This suggests that it is unlikely that the increased mass seen

in *mdx* muscles is due to increased deposition of connective tissue within the muscle. Moreover, fibrosis is often measured qualitatively and consequently there are discrepancies in the literature, with some studies claiming a mild fibrosis begins from 10-13 weeks (Grounds *et al*.,2008), while others state that there is no fibrosis in 12-week-old *mdx* muscles (Latroche *et al*.,2015). With this in mind, it might be better to assess fibrosis in older *mdx* mice, with many studies reporting extensive fibrosis in the hind limb from 12-24 months of age (Grounds *et al*., 2008; Kharraz *et al.,* 2013; Latroche *et al*., 2015). In summary, it is unlikely that excessive connective tissue deposition (fibrosis) is responsible for the differences in muscle mass seen in our 12–week-old *mdx* muscles.

To assess whether the increased muscle mass was a consequence of muscle fibre hypertrophy, I analysed the absolute area of myosin in whole cross-sections. There was no significant difference between wild type and *mdx* empty vector control muscles (Figure 3.5D). While the *mdx* empty vector control muscles had a slightly larger average myosin area than for the MuSK-GFP expressing muscle this difference was not significant. This general trend is in line with the finding that the mass of *mdx* empty vector control muscles was greater than the contralateral MuSK-GFP expressing muscles and the wild type (Joanne Ban, PhD thesis, 2018). The small sample size and a high degree of variability between muscle sections may have limited my ability to properly test for a genuine difference in cross-sectional area. The high variability is probably due to differences in the precise location along the length of the muscle from which the sampled sections were taken. Some sections may have been taken right at the muscle belly and others may have been taken a little further away from the mid-belly. Due to the variability in the total area data, it is hard to make a firm conclusion on whether the greater muscle mass seen in *mdx* is due to hypertrophy.

As seen in Figure 3.5E, there was no difference in the percentage area occupied by myosin when comparing MuSK-GFP expressing *mdx* muscles and their contralateral empty vector control muscles. Moreover, there was also no difference in myosin percentage area between the wild type and the empty vector controls. The *mdx* muscle values are in both treatments very similar to the untreated wild type means, suggesting that the share of the muscle cross-section occupied by contractile machinery was not affected by the loss of dystrophin, nor by the addition of MuSK-GFP to the *mdx* muscles. Together with the collagen results described above, the myosin findings provide little support for the idea that the greater muscle mass of 12-week old *mdx* mice can be explained by pseudohypertrophy. My results, while not definitive, do not support the hypothesis that the greater mass of *mdx* muscles was due to excess ECM accumulation and that MuSK supplementation can prevent this. My results did not demonstrate a significant increase in the area of contractile machinery per muscle cross sections. However, this might simply be due to the small sample size combined with section-to-section variability in muscle cross-sectional area. To overcome this limitation, it would be good to use a power calculation to determine how many muscles are needed to find a statistical difference in a given experiment. It is also possible that the increase in muscle mass is due to hyperplasia, rather than hypertrophy (Faber *et al*, 2014). Any apparent increase in the number of fibre profiles per section might be caused by the formation of entirely new fibres, or by the branching of pre-existing myofibres (Faber *et al*, 2014). Fibre branching might lead to an increase in muscle mass without a corresponding increase in force production. Further detailed studies will be needed to determine precisely why the mass of *mdx* muscles is increased, compared to wild type muscles and how MuSK can prevent this increase.

To assess whether the improved retention of force (following eccentric contractions) found in *mdx* muscles supplemented with MuSK-GFP was due to a change in the fibre type profile of the muscle, I conducted fibre counts and assessed the proportion of each fibre type using antibodies specific for the four MHC isoforms (Figure 3.6). In general, the population percentages of each fibre type I found in the TA muscle of *mdx* mice (empty vector control muscles) were consistent with the values reported for the untreated TA muscle in wild type mice but there were some differences. For example, type IIb fibres were reported to occupy 70.9% of the total fibre population in the white TA and only 25.1% in the red TA (Bloemberg & Quadrilatero, 2012). This compared to the 51.27 (6.99) % that I found in the white TA and 24.94 (4.78) % in the red TA of my *mdx* empty vector muscles. Moreover, type IIx fibres are reported to make up 16.3% of the white and 44.7% of the red TA in wild type C57BL/6 mice (Bloemberg & Quadrilatero, 2012), compared to the 51.27% I found in the white TA and 65.05% in the red TA. It is important to note that these differences in fibre type profile, compared to previous studies might reflect on the different background genotypes of the wild type and *mdx* mice in the different studies.

Mdx muscles expressing MuSK-GFP showed no differences in fibre type profile when compared to the empty-AAV vector contralateral controls in both the white (Figure 3.6B) and red TA (Figure 3.6C). These findings suggest that supplementing *mdx* TA muscles with MuSK does not change the fibre type profile of the muscle. It is important to note that each section was single-labelled with antibody specific for just one fibre type. This means that so called "hybrid" fibres which can express multiple MHC isoforms (Bloemberg & Quadrilatero, 2012), if present, could not be identified. Such hybrids may have been counted as positive for more than one fibre type. Additionally, expression of MuSK-GFP did not result in a shift in the force-frequency curve for the direct (Figure 3.7A) or nerve-stimulated (Figure 3.7B) contractions.

Together with the fibre type count results described above, these contraction findings provide little support for any changes in the myosin fibre type of *mdx* muscles supplemented with MuSK.

These findings are of particular interest as they indicate that it is unlikely that the improved retention of force after eccentric contractions observed after MuSK-GFP supplementation is due to a fast to slow fibre switch. However, it is possible that MuSK supplementation is simply causing the fibres to adopt a more aerobic phenotype, rather than altering the MHC composition. For example, the 'slower' soleus muscle consists of a larger proportion of type I fibres (30-40%), when compared to muscles like the TA which have no type I fibres (Bloemberg & Quadrilatero, 2012; Kammoun *et all., 2014)*)and it is the soleus muscle which is thought to be more resistant to contraction-induced injury when compared to other fast-type muscles such as the TA (Punga *et al*., 2011). Interestingly, muscle fibres from the soleus muscle are also reported to express high levels of MuSK and utrophin on their sarcolemma (Punga *et al*., 2011). Moreover, supplementation with MuSK-GFP was also able to increase sarcolemmal expression of utrophin and β- dystroglycan (Trajanovska *et al*., 2019), both of which were found to be elevated in the soleus when compared to TA muscle of *mdx* mice (Joanna Huang, Honours thesis, 2018). Supplementation of fast-type TA muscles with MuSK-GFP may be preventing contraction-induced damage by causing fibres to adopt more of an aerobic phenotype (rich in utrophin and β- dystroglycan) without altering the MHC composition. In conclusion, my results do not support the hypothesis that MuSK-GFP reduced eccentric contraction-induced loss of force by inducing a fast to slow fibre type switch.

CHAPTER FOUR:

Effect of MuSK-system on muscle fibre regeneration

4.1 Introduction

Due to the lack of dystrophin, *mdx* muscle fibres are fragile and are susceptible to contraction-induced injury. This fragility is thought to predispose *mdx* muscles to the repeated cycles of muscle fibre necrosis and subsequent regeneration that ultimately lead to muscle atrophy and weakness (Manning & O'Malley, 2015). One marker of muscle fibre regeneration and therefore muscle damage is embryonic myosin, an isoform of myosin that is expressed transiently during development and is re-expressed in adult muscle that has been injured (Schiaffino *et al*., 2015). Typically, embryonic myosin begins to be expressed 2-3 days after injury and is thought to persist for an additional 2-3 weeks (Guiraud *et al*., 2018). In this chapter, staining for embryonic myosin (Emb-MHC) is used as a marker of muscle fibre regeneration, to assess the extent of recent damage to muscle fibres in TA muscles of *mdx* mice.

Previous work indicated that MuSK supplementation was able to protect muscle fibres from acute contraction-induced injury (Trajanovksa *et al*., 2019). This chapter aims to see whether MuSK and other members of the MuSK signalling pathway (Dok7 and Rapsyn) can protect muscles from injury, and if so, in what way. While the role of the MuSK signalling complex at the NMJ is well-established, little is known about the role MuSK plays beyond the NMJ. Interestingly, AAV-Dok7 enlarged NMJs in Dok7 myasthenia model mice (Arimura et al., 2014) and another study has shown that AAV-Dok7 was able to increase myofibre size relative to the atrophied fibres of untreated Amyotrophic Lateral Sclerosis (ALS) mice. The same study also reported supressed motor nerve terminal degeneration and muscle atrophy (Miyoshi et al., 2017). Recent work has suggested that MuSK is a co-receptor for Bone Morphogenetic Protein (BMP) and BMP receptors. Specifically, MuSK is thought to interact with BMPs and their receptors via its extracellular Ig3 domain (Figure 4.1). Conceivably, this

MuSK-dependent BMP signalling might modify the expression of genes that regulate myofibre size (Yilmaz *et al*., 2016). The interaction of MuSK with BMP4 was shown by these researchers to be mediated by the third extracellular Ig domain of MuSK. With this finding in mind, an AAV vector encoding a mutant MuSK that lacked the third Ig domain (MuSK-ΔIg3) was produced to test whether the ability of MuSK to mediate BMP signalling might influence MuSK's ability to protect the muscle fibres of *mdx* mice from injury.

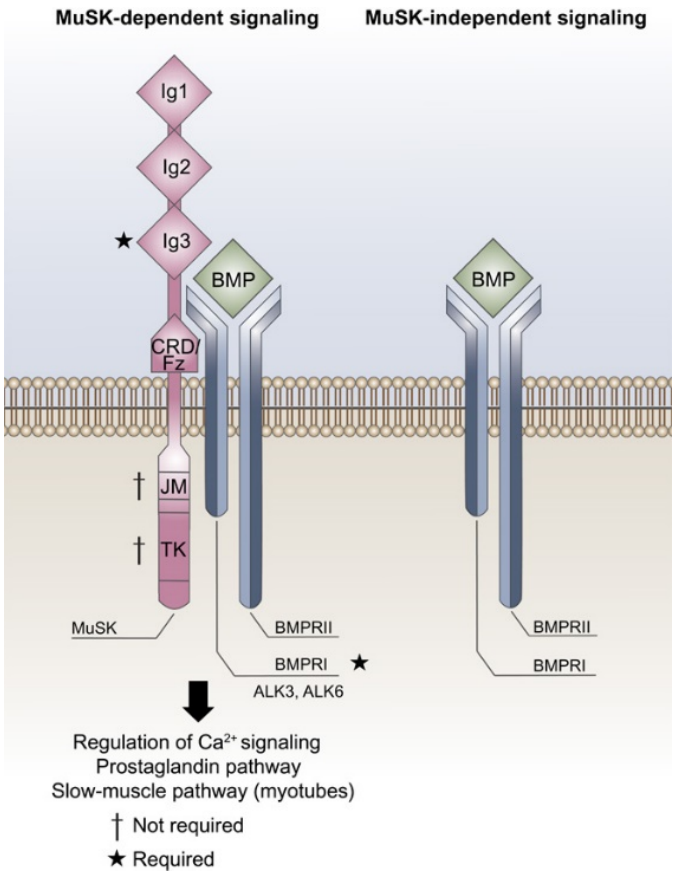

Figure 4.1: Schematic showing the interaction of MuSK with BMP4 and BMP receptors. MuSK binds to BMP4 and BMP receptors via its Ig3 extracellular domain. This results in the expression of genes that are thought to regulate myofibre size and composition. Tyrosine kinase activity of MuSK is not required for MuSK-mediated BMP signalling. CRD/fz, Cysteine rich domain/frizzled-like domain; JM, juxtamembrane; TK, tyrosine kinase. Image from Yilmaz *et al.* (2016).

This chapter investigates the effect of four AAV vectors encoding: MuSK, MuSK-ΔIg3, Dok7 or Rapsyn (each fused to GFP) on the percentage of fibres that stained positive for embryonic myosin (regenerating fibres) in transverse sections through the TA muscle of *mdx* mice. In the previous chapter, mice were injected with an AAV vector encoding MuSK-GFP at 3-4 weeks of age and culled at 12 weeks of age. In this chapter, mice were injected with one of the four AAV vectors (MuSK, MuSK-ΔIg3, Dok7 or Rapsyn) at 3-4 weeks of age and allowed 5-6 weeks for transgene expression before being culled at 9 weeks of age for analysis (Figure 4.2).

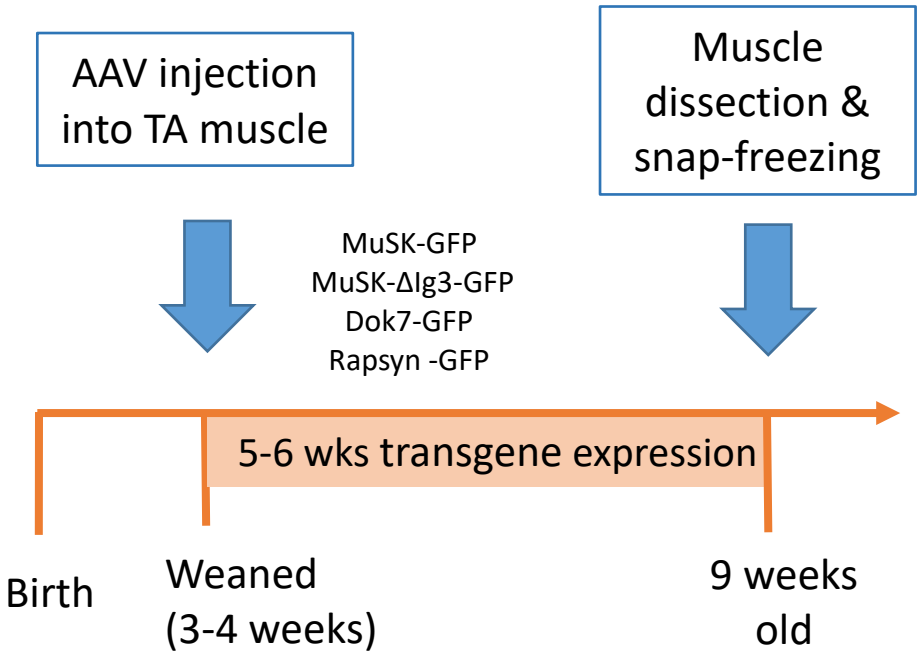

Figure 4.2: Experimental timeline for the injections of AAV-MuSK, AAV-MuSK-ΔIg3, AAV-Dok7 and AAV-Rapsyn at 3-4 weeks of age. At 3-4 weeks of age the TA muscle of *mdx* mice were injected with one of the four AAV vectors (MuSK, MuSK-ΔIg3, Dok7, Rapsyn) while the contralateral TA was injected with an empty vector to serve as a control. The mice were culled after 5-6 weeks of transgene expression so muscles could be dissected and snap-frozen for histological analysis.

Mice were analysed at the younger age of 9 weeks, as opposed to the 12-week-old mice used in the previous chapter, because 9 weeks is just after the period of florid degeneration and regeneration seen in *mdx* mice from about 3-7 weeks of age (Duddy *et al*., 2015). A recent study reported larger percentages of emb-MHC positive cells in *mdx* EDL muscles at 7 weeks of age (12.8%), when compared to 14-week-old *mdx* EDL muscles which yielded 1.7% emb-MHC positive cells (Guiraud et al*.,* 2018). With this in mind, a pilot study was conducted, where the number of emb-MHC positive cells were counted in whole cross-sections of the TA muscle from 7 and 9-week-old *mdx* mice. The counts conducted for the 9-week- old *mdx* yielded slightly higher percentages of emb-MHC positive cells when compared to 7-week-old *mdx* (Table 4.1). For this reason, the *mdx* mice injected with AAV vectors encoding one of MuSK, MuSK-ΔIg3, Dok7 or Rapsyn at 3-4 weeks were culled at 9 weeks of age for embryonic myosin analysis.

In order to express the number of emb-MHC positive cells as a percentage of the total number of muscle fibres, sections were double labelled for laminin, to mark out the basement membrane boundaries of each muscle fibre. The staining with laminin was also used to collect additional data on muscle fibre counts and muscle fibre girth (minimal Feret's diameter). In this way, I also examined the effects of the MuSK-system on fibre size and the number of fibres after treatment with one of the four AAV vectors.

Table 4.1: Pilot experiments: Embryonic myosin (emb-MHC) positive cells in whole cross-sections of *mdx* tibialis anterior (TA) muscle. Values are expressed as the number of positive fibres as well as the fraction of positive fibres in the whole cross-sections. Counts were conducted on the left and right TA muscles of 7-week-old *mdx* (n=2 mice) and 9-week-old *mdx* (n=2 mice).

Mouse	Leg	# emb-MHC positive cells	% emb-MHC positivity
7 week old mdx	Left TA	78	1.51
	Right TA	87	0.96
7 week old mdx	Left TA	244	3.31
	Right TA	136	2.07
9 week old mdx	Left TA	61	0.68
	Right TA	194	4.16
9 week old mdx	Left TA	664	6.45
	Right TA	374	7.08

4.2 Results

4.2.1 Overexpression of MuSK-system components does not alter muscle mass

Previous work in the lab suggested that elevating the expression of MuSK (but not Rapsyn) in the TA muscle of *mdx* mice beginning at 3-4 weeks was able to reduce the mass of the muscle at 12 weeks of age down to that of the wild type level (Joanne Ban, PhD thesis, 2018). In agreement with previous studies, the untreated TA muscles of 9-week-old *mdx* mice used in this chapter weighed in at about 60mg (Barker *et al.,* 2017; Gehrig *et al*., 2010). In these 9-week-old *mdx* mice I found no differences in the mass of the TA muscles supplemented with any of the four AAVs, compared to contralateral empty vector control muscles. The *mdx* TA muscles supplemented with MuSK-GFP had a muscle mass of 59.49 (6.45) mg, while their empty vector control TA muscles were not significantly different at 60.08 (6.10) mg (Figure 4.3A). After the weights were normalised to body mass there was still no significant difference (MuSK: 0.21 (0.01) %, control: 0.22 (0.01) %, Figure 4.3B). Moreover, there was no significant difference in the muscle mass (MuSK-ΔIg3: 57.8 (5.00) mg, Control: 59.84 (4.89) mg, Figure 4.3A) or normalised muscle mass (MuSK-ΔIg3: 0.21 (0.02) %, Control: 0.22 (0.008) %, Figure 4.3B) of the MuSK-ΔIg3-GFP treated *mdx* TA muscles when compared to the empty vector controls. For Dok7-GFP treated *mdx* mice, there was also no significant difference between the treated and empty vector control TA muscles for both muscle mass (Dok7: 62.1 (5.88) mg, control: 62.99 (7.12) mg, Figure 4.3A) or normalised muscle mass (Dok7:0.23 (0.02) %, control: 0.23 (0.01) %, Figure 4.3B). Finally, for Rapsyn-GFP treated *mdx* mice, there was no significant difference in the mass (Rapsyn: 60.56 (3.59) mg, control: 60.5 (4.13) mg, Figure 4.3A) or normalised mass (Rapsyn: 0.22 (0.005) %, control: 0.22 (0.01) %, Figure 4.3B) between the treated and empty vector control muscles.

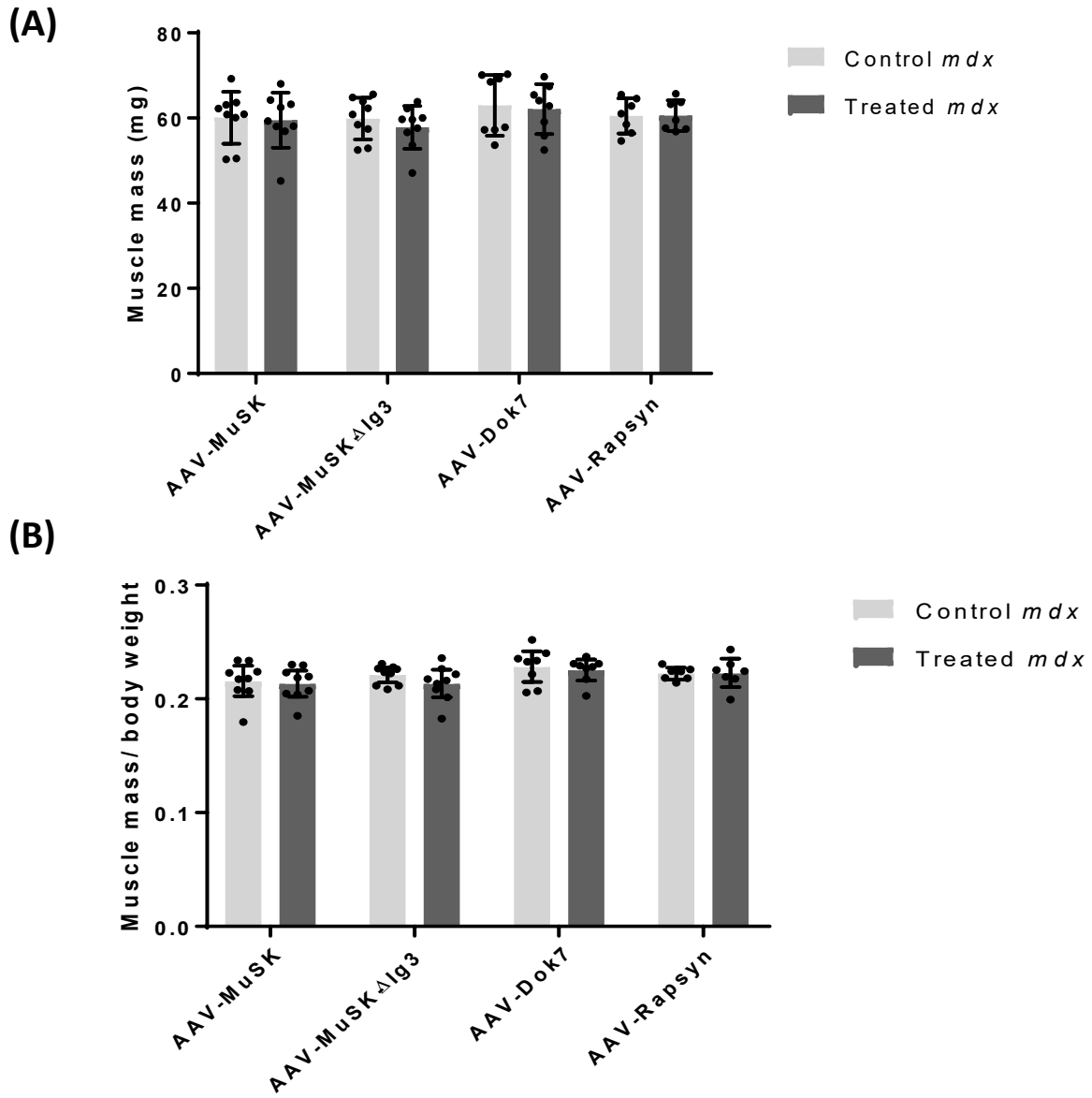

Figure 4.3: Overexpression of MuSK-system components does not alter muscle mass. (A) Wet weight of the tibialis anterior muscle from 9-week-old *mdx* mice treated with one of the following AAV vectors: MuSK, MuSK-ΔIg3, Dok7 or Rapsyn. The contralateral TA muscle of each mouse was also injected with an empty AAV vector as a control. (B) Tibialis anterior muscle mass from same mice relative to body weight. The bars in panels A and B represent means ± 95% confidence intervals and the circles represent the mass of an individual muscle (n= 9 per group except Rapsyn where n=7). Multiple paired student's t-tests were used (*p<0.05).

4.2.2. Overexpression of MuSK-system components does not alter muscle fibre number

To assess the total number of muscle fibres in a whole muscle cross-section, sections were labelled by immunofluorescence for laminin (Figure 4.4A), to visualise the muscle fibre boundaries for automated counting (see 2.8.4 *Automated fibre counts*)**.** No significant differences in the number of fibres were found when comparing the TA muscles of *mdx* mice treated with one of the four AAV vectors and their empty vector control muscles (Figure 4.4B). Counts of the *mdx* TA muscles supplemented with MuSK-GFP yielded 2687 (363) muscle fibres per cross-section, while the empty vector control cross-sections contained 2705 (285) muscle fibres. The *mdx* muscle cross-sections supplemented with MuSK-ΔIg3-GFP contained 2136 (533) muscle fibres compared to 2232 (238) in the contralateral empty vector controls. Cross-sections of TA muscles treated with Dok7-GFP contained 2518 (418) muscle fibres, while their contralateral empty vector control muscle cross-sections contained 2386 (304). Finally, Rapsyn-GFP treated *mdx* muscle cross-sections contained 2593 (363) muscle fibres compared to 2393 (263) in the empty vector controls (Figure 4.4B).

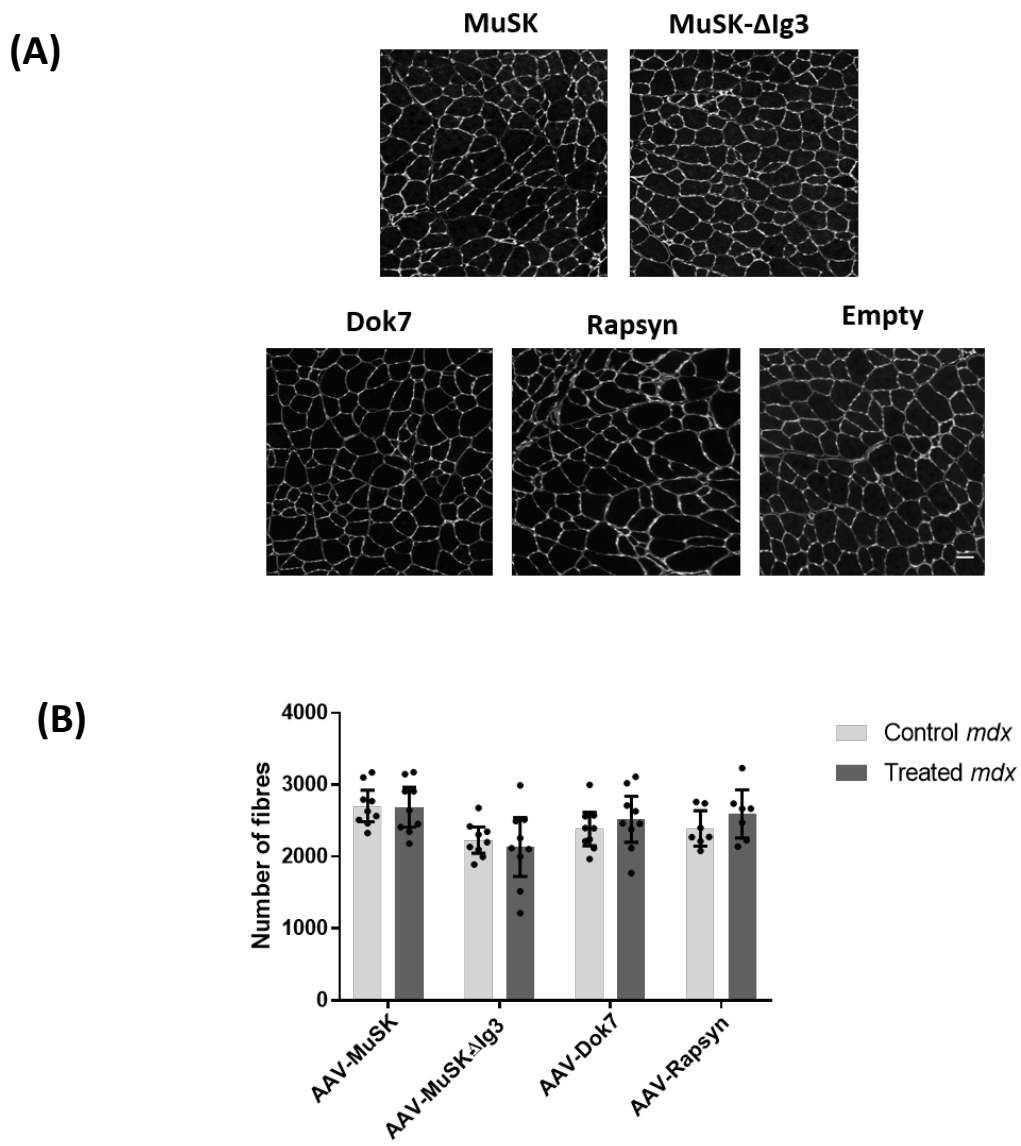

Figure 4.4: Overexpression of MuSK-system components does not alter muscle fibre number. (A) Representative immunofluorescence images of laminin staining in 9-week-old *mdx* TA muscles injected with one of the following AAV vectors: MuSK, MuSK-ΔIg3, Dok7 or Rapsyn. The contralateral TA muscle of each mouse was also injected with an empty AAV vector as a control. Scale bar = 50µm. (B) Number of fibres in whole cross-sections of *mdx* TA muscles. The bars represent the mean fibre number ± 95% confidence intervals and the circles represent the fibre count from individual muscles. (n= 9 per group except Rapsyn where n=7). Multiple paired student's t-tests were used (*p<0.05).

4.2.3 Overexpression of MuSK and Rapsyn decreased muscle fibre diameter

Immunolabelling for laminin was also used to determine muscle fibre girth (minimal Feret's diameter) of all muscle fibres in whole muscle cross-sections. Figure 4.5 shows pooled frequency distributions of muscle fibre girth (minimal Feret's diameter) for the four groups of mice treated with one of the following AAV vectors: MuSK-GFP, MuSK-ΔIg3-GFP, Dok7-GFP or Rapsyn-GFP. As seen in Figure 4.6A, the mean minimal Feret's diameter for *mdx* TA muscles treated with MuSK-GFP was significantly smaller than for the empty vector control muscles (MuSK: 36.74 (2.26) µm; Empty: 39.67 (3.43) µm). The minimal Feret's diameter for muscles treated with MuSK-ΔIg3 was not significantly reduced compared to their empty vector controls (MuSK-ΔIg3: 39.84 (9.05) µm; Empty: 43.84 (3.46) µm; Figure 4.6B). It should be noted that the animal-to-animal variation was greater for muscles injected with AAV-MuSK-ΔIg3 compared to other treatment groups (Figure 4.6). Overexpression of Dok7-GFP did not produce any significant difference in minimal Feret's diameter when compared to the empty vector controls (Dok7: 46.51 (2.82) µm; Empty: 46.6 (1.71) µm; Figure 4.6C). Overexpression of Rapsyn-GFP significantly reduced the mean minimal Feret's diameter when compared to the empty vector control (Rapsyn: 44.99 (1.57) µm; Empty: 47.04 (1.80) µm; Figure 4.6D). In summary, these results suggest that expression of elevated levels of either MuSK or Rapsyn in the TA muscle of *mdx* mice for 5 weeks, beginning about a week after weaning, resulted in a small reduction in the average girth of muscle fibres when examined at 9 weeks of age.

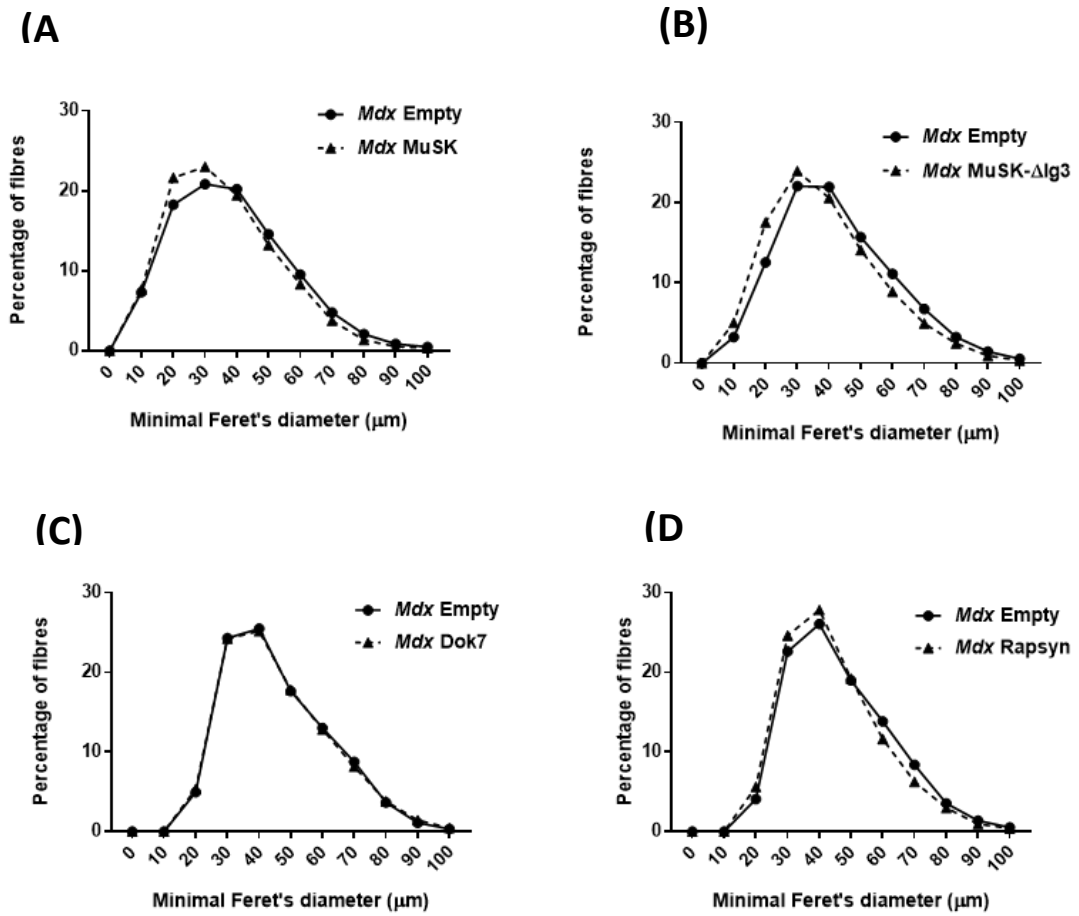

Figure 4.5: Frequency distributions of muscle fibre girth in *mdx* TA muscles. Frequency distributions of muscle fibre girth (minimal Feret's diameter) for pooled fibres from *mdx* TA muscles supplemented with one of the following AAV vectors: (A) MuSK-GFP (n=8), (B) MuSK-ΔIg3-GFP (n=5), (C) Dok7-GFP (n=9) or (D) Rapsyn-GFP (n=7). The contralateral TA muscle of each mouse was injected with an empty AAV vector to serve as a control. The triangle shows results for *mdx* muscles injected with one of the four AAV vectors while the circles show results from the contralateral empty AAV vector controls. Each curve consists of >10,000 muscle fibres pooled from multiple muscles (MuSK: n= 8 muscles, MuSK-ΔIg3: n= 5 muscles, Dok7: n = 9 muscles and Rapsyn: n=7 muscles).

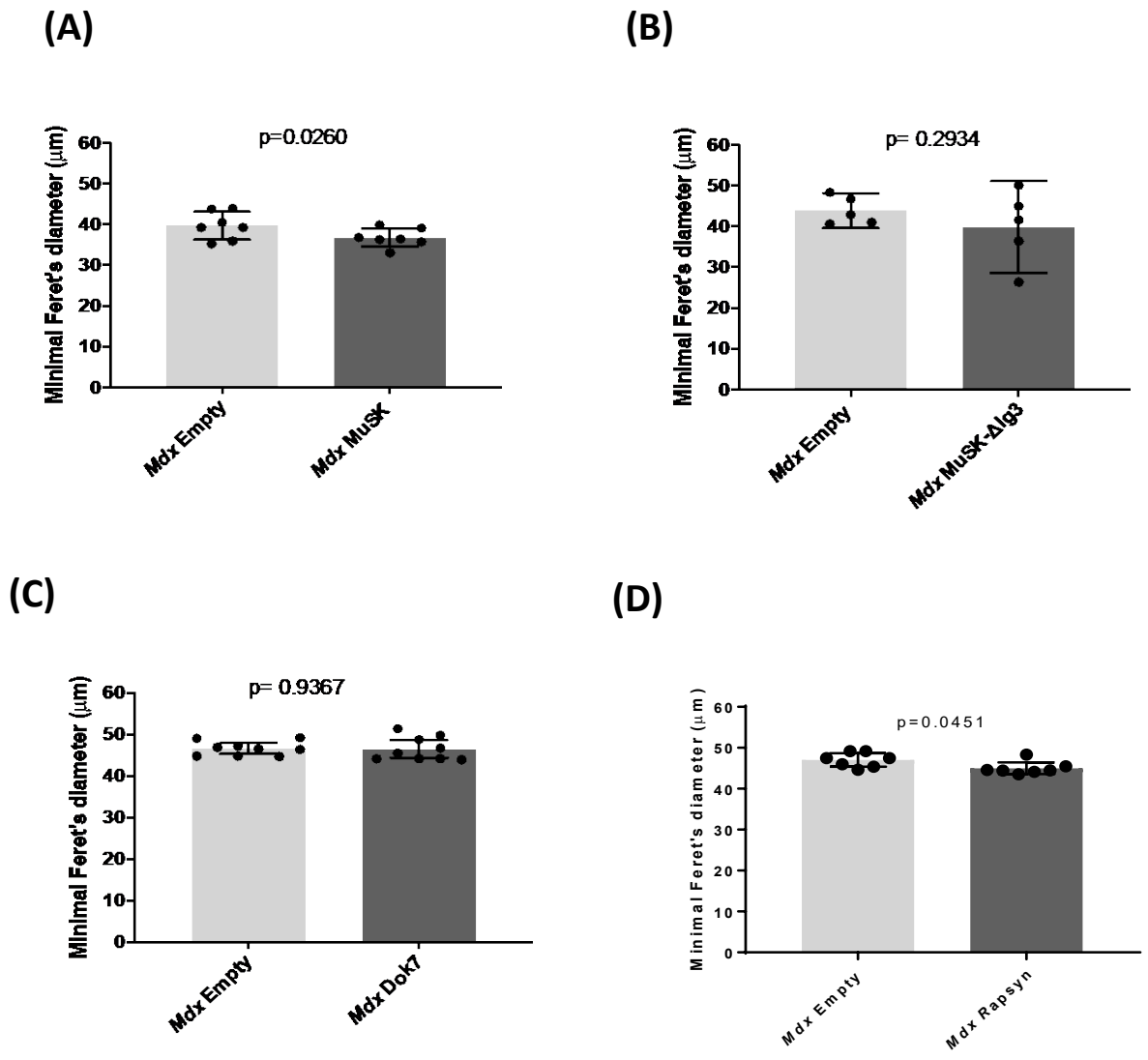

Figure 4.6: Overexpression of MuSK and Rapsyn reduce mean muscle fibre girth. Histograms show the mean minimal Feret's diameter from *mdx* TA muscles supplemented with one of the following AAV vectors: (A) MuSK-GFP (n=8), (B) MuSK-ΔIg3-GFP (n=5), (C) Dok7-GFP (n=9) or (D) Rapsyn-GFP (n=7). The contralateral TA muscle of each mouse was injected with an empty AAV vector to serve as a control. The bars in all panels represent the mean ± 95% confidence interval and the circles represent results from an individual muscle. Paired student's t-tests were used (*p<0.05).

4.2.4 MuSK-GFP overexpression does not affect the number of regenerating fibres

To assess the fraction of the muscle occupied by regenerating fibres, cross-sections of the TA muscle were labelled by immunofluorescence for emb-MHC, a marker of regenerating muscle fibres (Figure 4.7A). The percentage of emb-MHC positive fibres was slightly lower for MuSK-GFP treated *mdx* muscles (2.50 (1.70) %), compared to the empty vector controls (3.39 (2.91) %). However, this difference was not statistically significant (p=0.4965 paired t-test; Figure 4.7B).

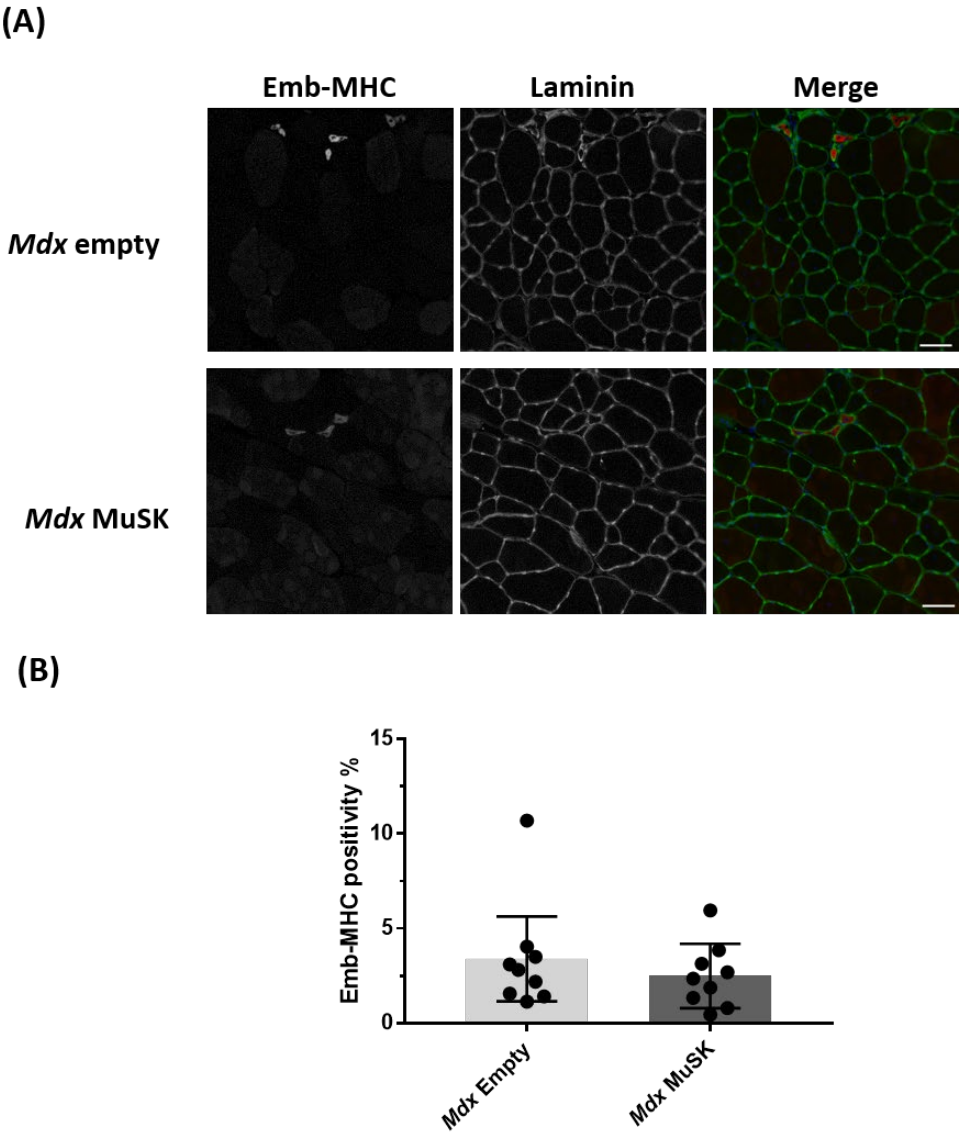

Figure 4.7: Overexpression of MuSK does not significantly affect fibre regeneration in the TA muscle of 9-week-old *mdx* mice. (A) Representative immunofluorescence images of *mdx* TA muscles stained for embryonic myosin (emb-MHC), laminin and DAPI injected with either AAV-MUSK or empty AAV vector. In the third column (merged images) emb-MHC, laminin and DAPI are shown in red, green and blue respectively. (B) The fraction of muscle fibres expressing emb-MHC was compared for MuSK-GFP and control mice (n=9). No significant difference was found. Paired student's t-tests were used (*p<0.05).

4.2.5 MuSK-ΔIg3-GFP overexpression does not affect the number of regenerating fibres

Mdx muscles treated with an AAV vector encoding MuSK-ΔIg3-GFP or an empty AAV vector were also labelled by immunofluorescence for emb-MHC (Figure 4.8A). Interestingly, Emb-MHC positive (regenerating) fibres made up a larger component of the cross-section in the MuSK-ΔIg3-GFP treated *mdx* muscles at 3.70 (3.20) %, compared to 2.18 (1.62) % of the cross-section in the empty AAV vector control *mdx* muscles. However, this difference was not statistically significant (p=0.2052; Figure 4.8B).

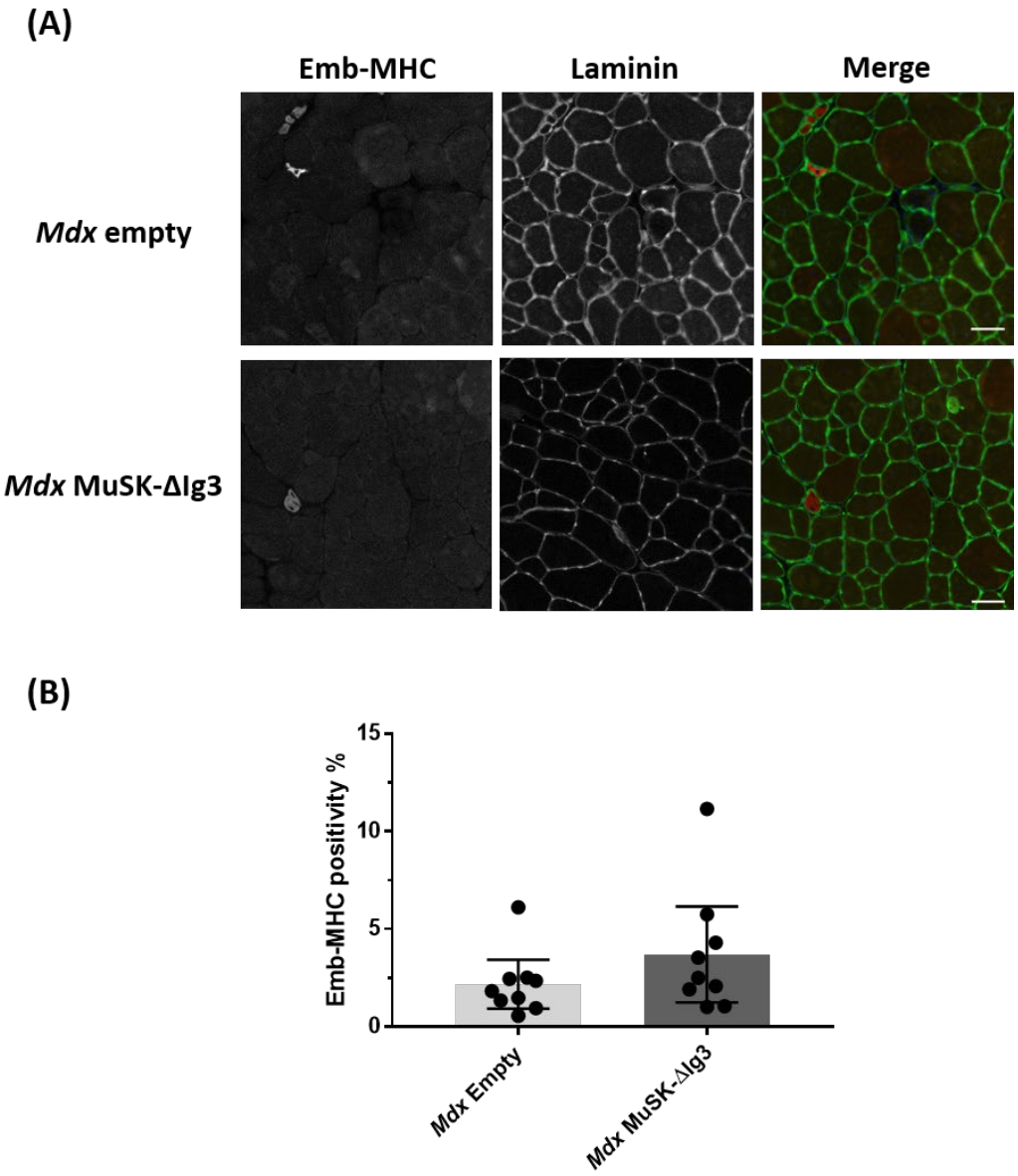

Figure 4.8: Overexpression of MuSK-ΔIg3 does not significantly affect fibre regeneration in the TA muscle of *mdx* mice. (A) Representative immunofluorescence images of *mdx* TA muscles stained for embryonic myosin (emb-MHC), laminin and DAPI injected with either AAV-MUSK-ΔIg3 or empty AAV vector. In the third column (merged images) emb-MHC, laminin and DAPI are shown in red, green and blue respectively. (B) The fraction of muscle fibres expressing emb-MHC was compared for MuSK-GFP and control mice (n=9) and no significant difference was found. Paired student's t-tests were used (*$p<0.05$).

4.2.6 Dok7-GFP overexpression reduced the number of regenerating fibres

Mdx muscles treated with an AAV vector encoding Dok7-GFP or an empty AAV vector were also labelled by immunofluorescence for emb-MHC (Figure 4.9A). The percentage of fibres in the cross-section that were positive for emb-MHC in the Dok7-GFP treated *mdx* muscles was 1.59 (0.70) %, which was significantly reduced when compared to the 3.40 (2.23) % for the contralateral empty AAV vector controls (p= 0.0437; Figure 4.9B).

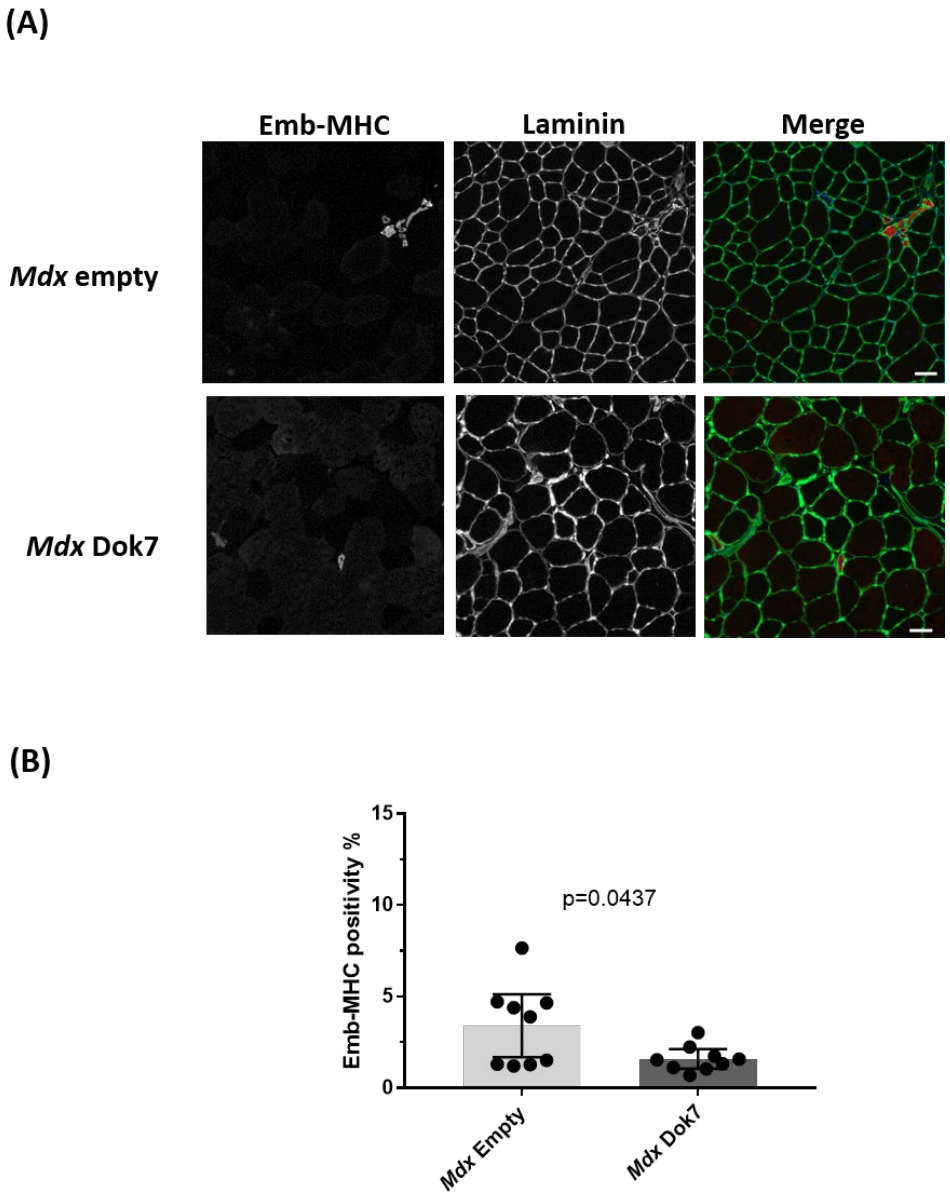

Figure 4.9: Overexpression of Dok7 reduces the number of regenerating muscle fibres in the TA muscle of *mdx* mice. (A) Representative immunofluorescence images of *mdx* TA muscles stained for embryonic myosin (emb-MHC), laminin and DAPI injected with either AAV-Dok7 or empty AAV vector. In the third column (merged images) emb-MHC, laminin and DAPI are shown in red, green and blue respectively. (B) The fraction of muscle fibres expressing emb-MHC was compared for Dok7-GFP and control mice (n=9) and a significant reduction in the number of regenerating fibres was found. Paired student's t-tests were used (*p<0.05).

4.2.7 Rapsyn-GFP overexpression does not affect the number of regenerating fibres

Mdx muscles treated with an AAV vector encoding Rapsyn-GFP or an empty AAV vector were also labelled by immunofluorescence for emb-MHC (Figure 4.10A). Emb-MHC positive (regenerating) fibres made up a smaller component of the cross-section in the Rapsyn-GFP treated *mdx* muscles at 2.16 (0.78) %, compared 2.90 (1.80) % of the cross-section in the empty AAV vector control *mdx* muscles. This difference between the Rapsyn-GFP treated and empty AAV vector controls was not statistically significant (p=0.3896; Figure 4.10B).

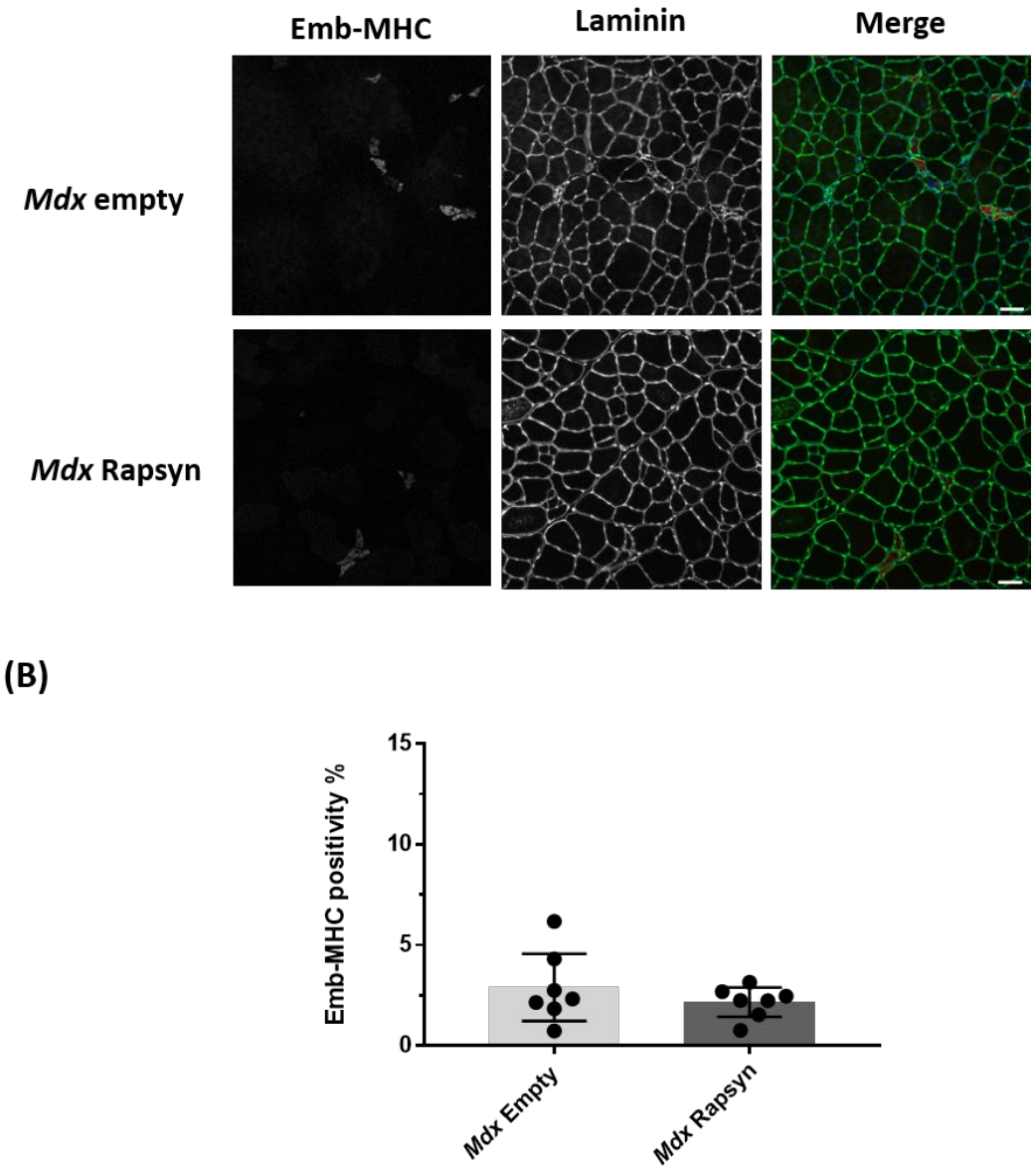

Figure 4.10: Overexpression of Rapsyn does not significantly affect fibre regeneration in the TA muscle of *mdx* mice. (A) Representative immunofluorescence images of *mdx* TA muscles stained for embryonic myosin (emb-MHC), laminin and DAPI injected with either AAV-Rapsyn or empty AAV vector. In the third column (merged images) emb-MHC, laminin and DAPI are shown in red, green and blue respectively. (B) The fraction of muscle fibres expressing emb-MHC was compared for Rapsyn-GFP and control mice (n=7 mice) and no significant difference in the number of regenerating fibres was found. Paired student's t-tests were used (*$p<0.05$).

4.3 Discussion

Experiments from chapter 3 suggested that the greater mass of the TA muscle in 12-week-old *mdx* mice, compared with age-matched C57BL/10 wild type controls (Joanne Ban, PhD thesis, 2018) was probably due to an increase in the contractile mass of the muscle, rather than fibrosis and that this *mdx*-specific muscle growth could be prevented by injecting AAV-MuSK shortly after weaning. In this chapter, muscle growth was assessed again but this time in 9-week-old *mdx* TA muscles.

Pastoret and Sebille (1995) have quantified the time course of TA muscle growth during postnatal life in *mdx* mice (Figure 4.11). Their data showed the mass of *mdx* TA muscles to be the same as that of the wild type at each age examined up until 8 weeks. However, by 13 weeks the *mdx* muscles had grown 20% heavier than for the age-matched wild type. Thus, we might expect 9 weeks to be too early to detect any substantial compensatory hypertrophy in *mdx* muscles. The mass of the TA muscle found in the present study was consistent with that of the literature (8-10-week-old *mdx* TA mass= 60mg; Barker *et al*., 2017). Although it should be noted that the absolute muscle weights reported by Pastoret and Sebille (1995) were lower at both 8 and 13 weeks when compared to my weights (at 9 and 13 weeks) and those of Barker *et al*., (2017). At 9 weeks, I found no significant difference in mean muscle mass between *mdx* muscles injected with any one of the four AAV vectors (MuSK, MuSK-ΔIg3, Dok7 and Rapsyn) when compared to their contralateral empty vector control muscles. Similarly, no significant differences were found in the average number of muscle fibres per muscle cross-section for MuSK, MuSK-ΔIg3, Dok7 and Rapsyn. Interestingly, *mdx* muscles supplemented with MuSK or Rapsyn had slightly smaller minimal Feret's diameters when compared to their empty vector controls. Perhaps, MuSK and Rapsyn were working to begin

to decrease *mdx* muscle mass by reducing the growth of muscle fibre diameter and this might help explain the lower mass of the MuSK-expressing TA muscles that Joanne Ban reported at 12 weeks of age.

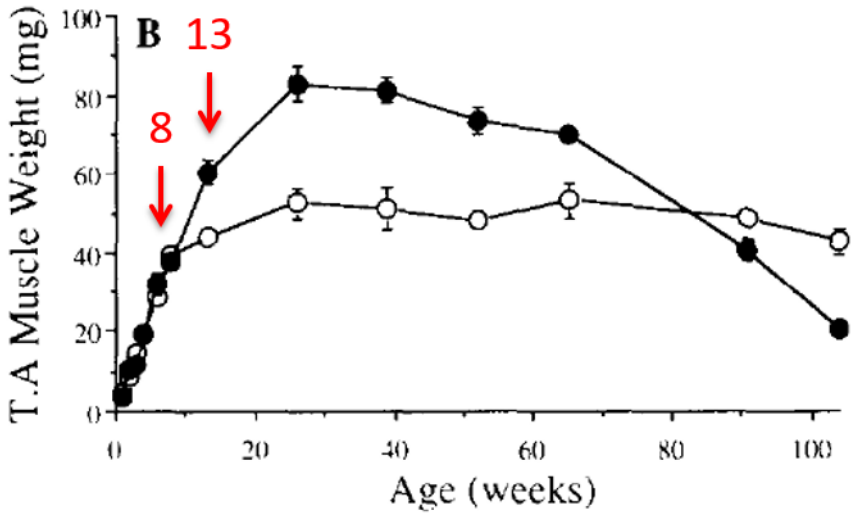

Figure 4.11: TA muscle weight as related to age in C57BL/10 and *mdx* mice. The TA was weighed at 13 different time points beginning at 2 weeks of age and ending at 104 weeks of age. The red numbers and arrows indicate the age (in weeks) that corresponds to the particular data point. The black circles represent *mdx* TA muscles, while the open circles represent the wild type. Figure modified from Pastoret & Sebille (1995).

In this chapter, staining for embryonic myosin was used as a marker of recently degenerated/regenerated fibres to assess the extent of damage in *mdx* TA muscles and to see if supplementation of the MuSK-system components can lessen the damage. A study by Mozzetta *et al.* (2013) reported that, within the TA muscle of untreated 8-week-old *mdx* mice, approximately 3% of muscle fibres were stained positive for embryonic myosin, consistent with the findings in this chapter for *mdx* empty vector muscles (MuSK: 3.39%, MuSK-ΔIg3: 2.18%, Dok7: 3.40%, Rapsyn: 2.90% - empty vector side values for the indicated treatment groups). Supplementation with the AAV vectors encoding MuSK, MuSK-ΔIg3 and Rapsyn did not significantly alter the percentage of embryonic myosin positive fibres (Figure 4.7B, Figure 4.8B and 4.10B). The mean percentage of embryonic myosin positive fibres for *mdx* muscles supplemented with MuSK (Figure 4.7B) and Rapsyn (Figure 4.10B) were slightly lower compared to their empty vector controls but these differences were not statistically significant. It is worth noting that there are many fewer embryonic myosin positive fibres in the TA muscle when compared to other hind limb muscles such as the quadriceps and EDL. For example, a recent study reported 18.5% embryonic myosin positive fibres in the quadriceps muscle and 12.8% embryonic myosin positivity in the EDL muscle of 7-week-old *mdx* mice (Guiraud *et al*., 2018). Thus, it might be more informative to repeat this set of experiments on the quadriceps muscle, where the baseline average numbers of fibre degeneration/regeneration are more substantial, relative to animal-to-animal variation.

Interestingly, the *mdx* TA muscles supplemented with MuSK-ΔIg3 displayed a higher mean percentage of embryonic myosin positive fibres when compared to the empty vector controls (Figure 4.8B) but this difference was not statistically significant. The higher mean for the MuSK-ΔIg3 treated *mdx* may be due to sampling error, especially since the mean for the empty vector controls was at a lower 2.18% when compared to the averages from the other

empty vector muscle groups. This experiment will need to be repeated with a larger sample size before any firm conclusion can be made in relation to MuSK-ΔIg3.

A key finding in this chapter was that supplementation of TA muscles of *mdx* mice with Dok7 was able to significantly reduce the number of muscle fibres that were positive for embryonic myosin from 3.40% to 1.59% (Figure 4.9B). This is of particular interest as other members of the MuSK pathway (MuSK and Rapsyn) had no effect on regenerating fibres. Interestingly, one study reported that MuSK reduced motor end plate size in *mdx* TA muscles (Trajanovksa *et al*, 2019). In contrast, AAV-Dok7 has been shown to increase NMJ size (Arimura *et al*., 2014). Thus, the effects elevating MuSK and elevating Dok7 do not always replicate. Dok7 supplementation has also been shown to reduce motor nerve terminal degeneration, reduce muscle atrophy and even prolong the lifespan of ALS model mice (Miyoshi et al., 2017). While the role of Dok7 at the NMJ is well established, the findings in this chapter indicate that Dok7 may also play a role in the muscle regenerative process (perhaps by reducing the frequency of muscle fibre injury) and potentially other pathways in muscle biology. A characteristic of Dok7 is that it can strongly increase the tyrosine kinase activity of MuSK (Arimura et al., 2014). The published findings mentioned above, along with the findings in this chapter seem to indicate that Dok7 is a potential therapeutic target for neuromuscular diseases. It would be beneficial for future studies to investigate the effects of Dok7 supplementation in DMD and to establish how supplementing each component of the MuSK-system affects muscle physiology and pathology. While these findings on Dok7 are promising, it is important to note that no experiments were conducted to show successful Dok7-GFP expression in this thesis. Thus, further experiments will be needed to check for the successful expression of Dok7-GFP. The same applies to the other AAV vectors used in this chapter (MuSK, MuSK-ΔIg3 and Rapsyn).

CHAPTER FIVE:
Conclusions

5.1 Summary of findings

The role of the MuSK-system in stabilising and maintaining the NMJ is well-established but its broader role in muscle biology remains unclear. While a mutation in the dystrophin gene is known to cause DMD, a study by Pratt *et al.* (2013) found that the dystrophin-null quadriceps muscles of *mdx* mice also express lower levels of MuSK when compared to wild type mice. Recent work in the lab found that supplementation with MuSK using an AAV vector was able to improve the retention of force after the muscle was challenged with a bout of eccentric contractions. Extra MuSK also reduced the number of damaged/regenerated muscle fibres (fibres with centralised nuclei) and reduced the muscle mass in 12-week-old *mdx* mice. In light of these findings, this thesis examined in more detail the effect of enhancing the expression of the MuSK-system components on muscle composition and upon muscle fibre regeneration.

By 12 weeks of age the TA muscle of *mdx* mice had grown heavier than that of age-matched wild type (C57BL/10 ScSn) mice. Joanne Ban found that the injection of AAV-MuSK prevented this excessive growth of the TA muscle in *mdx* mice. The experiments I describe in chapter 3 indicate that the increased muscle mass characteristic of 12-week-old *mdx* TA muscle is not the result of inflammation or substantial fibrosis and instead is likely due to genuine muscle fibre hypertrophy. Interestingly, when I examined TA muscles of 9-week-old *mdx* mice, I found no difference in the muscle mass between muscles injected with AAV-MuSK and empty vector control muscles (chapter 4). At 9 weeks of age the mass of the TA muscle was not affected by overexpression of MuSK, MuSK-ΔIg3, Dok7 or Rapsyn when compared to their contralateral empty vector controls. This is consistent with the time course of hypertrophy reported in *mdx* TA muscles, where there is no difference between the mass of

wild type and *mdx* muscles until after 8 weeks of age, when the TA muscles of *mdx* mice undergo rapid growth while the mass of the wild type muscles reaches a plateau (Figure 4.11). At 13 weeks the *mdx* TA muscle had grown 20% heavier when compared to its last measured time point at 8 weeks of age (Pastoret & Sebille, 1995). It is important to note that this rapid growth was not observed in wild type TA muscles after 8 weeks. They grew less than 5% heavier between the ages of 8 and 13 weeks (Pastoret & Sebille, 1995). It has been suggested that the rapid muscle growth in *mdx* muscles after 8 weeks is a form of compensatory hypertrophy where healthy fibres grow larger to compensate for any damaged fibres that contract synergistically with the healthy fibres. According to this idea, hypertrophy allows damaged *mdx* muscles to maintain the same absolute force output as the wild type (Lynch *et al*., 2001). Perhaps, MuSK is working to prevent or reduce this compensatory muscle growth and the beginnings of this can be seen by the slightly smaller mean minimal Feret's diameter of *mdx* TA muscles treated with either MuSK or Rapsyn when compared to their contralateral empty vector controls at 9 weeks of age (chapter 4).

By 12-13 weeks compensatory growth is well under way but supplementation with MuSK was able to reduce this, so that the mass of the TA muscle was no greater than that of age-matched wild type mice (Figure 1.12). BMP signalling has been shown to promote muscle hypertrophy (Sartori *et al*., 2013) and it has been suggested that the interaction of MuSK with BMP-receptor signalling (mediated via the Ig3 domain of MuSK) may be involved in the regulation of myofibre size (Yilmaz *et al*., 2016). Perhaps, in the case of compensatory hypertrophy in *mdx* muscles, the MuSK-BMP pathway may have a contrasting effect, causing a reduction in muscle mass and myofibre size in a bid to restore the muscle back to that of the wild type. If so, then the injection of AAV encoding MuSK-ΔIg3 would not be expected to

produce the same reduction in fibre diameters as full-length MuSK. My results on this remain equivocal (Figure 4.6). Further experiments with MuSK-ΔIg3 examining muscle mass at 12 weeks of age might help clarify this issue.

My results are relevant to two previously reported effects of AAV-MuSK upon muscle contractile function in *mdx* mice: 1) Specific force was greater in muscles expressing MuSK-GFP (Joanne Ban, PhD thesis, 2018) and 2) *mdx* muscles expressing MuSK-GFP were more resistant to injury (Trajanovska *et al*., 2019). Supplementation of MuSK-GFP in 3-4-week-old *mdx* TA muscles did not produce any change in the proportions of type I, type IIa, type IIb or type IIx fibres, nor did it alter the contractile properties (force-frequency curve) of 12-week-old *mdx* TA muscles (chapter 3). Both these findings are consistent with each other, since the contractile properties of a muscle are thought to depend entirely on the MHC composition of the muscle (Schiaffino, 2010). Together, these findings suggest that the greater specific force and greater resistance to eccentric contraction-induced injury seen in *mdx* muscles expressing MuSK-GFP were not due to any change in fibre type. Conceivably, the improved retention of force after eccentric contraction challenge in MuSK-expressing *mdx* TA muscles could be explained by a change in muscle metabolism, with fibres adopting a more aerobic phenotype (without any change in myosin type). Alternatively, MuSK might be protecting muscle fibres from eccentric contraction-induced damage by increasing the expression of utrophin and β-dystroglycan, as previously demonstrated (Trajanovska *et al*., 2019).

Another important finding was that the injection of AAV-Dok7 at 3-4 weeks of age was able to significantly reduce the number of regenerating (embryonic myosin-positive) fibres in the TA muscle of 9-week-old *mdx* mice (chapter 4). This is consistent with the reduced number

of centralised nuclei reported in 12-week-old *mdx* TA muscles expressing MuSK-GFP (Joanne Ban, PhD thesis, 2018). Moreover, Dok7 is a known activator of MuSK kinase signalling (Bergamin *et al*., 2010) and injection of AAV-Dok7 has been shown to increase the phosphorylation of MuSK in wild type mouse muscles (Miyoshi *et al*., 2017). Perhaps, Dok7 is acting to reduce the number of degenerating fibres by enhancing the tyrosine kinase activity of MuSK. On the other hand, the AAV vectors encoding: MuSK, MuSK-ΔIg3 and Rapsyn had no significant effect upon the number of embryonic myosin-positive fibres counted at 9 weeks of age (chapter 4). This result for Rapsyn is consistent with previous findings in the lab which showed no effect of Rapsyn-GFP on the percentage of muscle fibres with centralised nuclei (Joanne Ban, PhD thesis, 2018). The finding that supplementation of *mdx* muscles with MuSK-GFP had no significant effect on the number of fibres undergoing regeneration is surprising, given that, by 12 weeks, muscles expressing MuSK-GFP showed slightly fewer centralised nuclei (Joanne Ban, PhD thesis, 2018). Perhaps, under the conditions of my experiment, AAV-Dok7 was able to reduce degeneration by greatly enhancing activation of endogenous MuSK.

5.2 Caveats

Several caveats need to be considered when interpreting the results in this thesis. Firstly, the *mdx* mouse is the most commonly used animal model of DMD (McGreevy *et al*., 2015) but it is worth mentioning that the pathology seen in *mdx* mice is much less severe than that of human DMD. In this thesis, all experiments were conducted on the TA muscle, which is often used in DMD research as it is easily accessible (Grounds *et al*., 2008). However, it is important to note that the pathology in *mdx* limb muscles is much less severe than in the limb muscles of boys with DMD (Manning & O'Malley, 2015). Even among the limb muscles of *mdx* mice, the extent to which the muscles are affected is variable. For example, the quadriceps

muscle is thought to be more severely affected in terms of muscle fibre necrosis when compared to other limb muscles such as the EDL and TA (Grounds *et al*., 2008; Guirard *et al*., 2018; Mozzetta *et al.,* 2013). Of all the studied muscles, the diaphragm of *mdx* mice is said to have the most severe pathology, showing extensive fibrosis and muscle fibre necrosis by 16 months of age (Grounds *et al*., 2008; Pessina *et al*., 2014). Thus, the diaphragm muscle is thought to most closely resemble human DMD (Grounds *et al*., 2008). For these reasons, findings in the limb muscles of *mdx* mice do not directly reflect the pathology of human DMD. Future studies may benefit from using the diaphragm muscle, as this muscle is thought to most closely resemble the severe pathology seen in human DMD.

Another factor that should be considered is the age of the mice at the time of AAV injection. In this thesis, all mice were injected just after weaning (3-4 weeks of age) and culled at either 9 (chapter 4) or 12 weeks of age (chapter 3). Since necrosis is thought to peak at 25-26 days of age in *mdx* mice (Grounds *et al*., 2008), future experiments, injecting the mice with MuSK prior to this period of florid degeneration might be more informative. For example, Wang *et al*. (2000) injected an AAV encoding human mini dystrophin into the gastrocnemius muscle of 10 and 50-day old *mdx* mice. When studied at 3 months postnatal, both treatments reduced the number of muscle fibres with centralised nuclei. However, the *mdx* mice treated at 10 days postnatal showed a much smaller proportion of fibres with centralised nuclei (~1%) when compared to the mice treated at 50 days postnatal (~35%). This suggests that it might be more beneficial to inject *mdx* mice with AAV-MuSK at a younger age, before this period of florid degeneration/regeneration has occurred. In this way, we would be able to see whether supplementing with MuSK can actually prevent the massive fibre degeneration/regeneration event seen in the first few weeks of life.

Another factor that needs to be considered in this thesis is the variable transduction efficiency of AAV vectors. The transduction efficiency of AAV vectors is thought to vary between the different AAV serotypes and again between different species. Specifically, the AAV serotype 6 used in this thesis is thought to have variable expression in different skeletal muscles and in different sized myofibres (Riaz *et al*., 2015). For this reason, all AAV vectors in this thesis were fused to GFP, so that expression of the transgene could be easily visualised. All muscles from chapter 3 of this thesis showed widespread GFP fluorescence. (Figure 3.2). However, due to time constraints, the muscles in chapter 4 were not imaged for GFP fluorescence. For this reason, we cannot rule out whether the negative results seen in chapter 4 are due to: 1) the AAV vector treatment having no effect on the measured variables or 2) the AAV vector treatment did not result in overexpression of the transgene.

Finally, the conclusions drawn in this thesis assume that AAV-MuSK is expressed in the muscle only and that the effects of MuSK are specific to muscle. The AAV serotype 6 has been shown to efficiently transduce skeletal muscle tissue via intramuscular injection (Blankinship *et al*., 2004) but is also known to transduce a wide variety of cell types (Ellis *et al.,* 2013). Interestingly, Miyoshi *et al.* (2017) reported some GFP fluorescence in the spinal cord and cerebellum after intravenous injection of an AAV encoding Dok7 fused with GFP. This indicates that the Dok7 transgene may be taken up and expressed in tissues other than the muscle. With this in mind, we cannot rule out the possibility that the MuSK transgene has been expressed in non-muscle tissues. To overcome this issue, Wang *et al.* (2000) used a muscle-specific creatinine kinase (MCK) promoter to selectively target muscle fibres when injecting *mdx* mice with an AAV encoding human mini dystrophin. It would be beneficial to use MCK promoters when constructing an AAV encoding MuSK to ensure that MuSK is

expressed in muscle fibres only. In this way, we might rule out any effect of MuSK supplementation beyond the muscle.

5.3 Future directions

The experiments in this thesis found that supplementation of Dok7 in the TA muscles of 9-week-old *mdx* mice was able to significantly reduce the number of degenerating/regenerating (embryonic myosin positive) muscle fibres. This finding is of particular interest as it suggests a novel role for Dok7 in muscle regeneration and potentially muscle biology. Published findings in ALS model mice have shown that AAV-Dok7 is able to reduce motor nerve terminal degeneration, muscle atrophy and even prolong the lifespan of the mice (Miyoshi *et al.,* 2017). These published findings, together with the findings in this thesis suggest that Dok7 may be a good therapeutic target for neuromuscular diseases such as DMD. Due to time restraints, I was unable to test the effects of Dok7 on the structure of the NMJ. However, previous work in the lab has shown that overexpression of MuSK in *mdx* muscles can reduce the size of motor endplates (Trajanovska *et al*., 2019). In contrast, a previous study reported an increase in NMJ size when ALS model mice were treated with Dok7 (Miyoshi *et al*., 2017). It would be interesting to see if this effect of Dok7 translates to *mdx* mice. Since the effects of Dok7 supplementation on *mdx* muscle function have not been tested, it would also be useful to conduct eccentric contraction-induced injury protocols to determine whether Dok7 can improve the resistance of *mdx* muscles to injury.

Another key finding was that MuSK and Rapsyn were able to significantly reduce muscle fibre girth when *mdx* mice were injected at 3-4 weeks of age and culled at 9 weeks of age. No effect of the MuSK-system was found on the mass of TA muscles in 9-week-old *mdx* mice but by 12 weeks, hypertrophy was evident in the empty vector control *mdx* muscles. The

cause of this hypertrophy and how MuSK might reduce it remains unclear. Some studies have suggested that the branching of pre-existing myofibres is responsible for the growth seen in *mdx* muscles (Faber *et al*., 2014). It would be interesting to test our *mdx* TA muscles for the extent of fibre branching and to see if perhaps AAV-MuSK was reducing the muscle mass by reducing the number of fibre branches. While significant decreases in fibre girth were reported for MuSK and Rapsyn, no differences were reported for muscles expressing Dok7 and MuSK-ΔIg3 at 9 weeks. It would be interesting to repeat these experiments, particularly for MuSK-ΔIg3 as the results for this AAV construct were quite variable from animal-to-animal. In this way, we could test whether the reduced fibre girth seen in MuSK-expressing animals is dependent upon MuSK-BMP4 signalling.

Due to time constraints, I was unable to examine the role of inflammation in dystrophic muscles. As mentioned previously (see 1.3.1 *Inflammation in skeletal muscle repair*), it is thought that the persistent inflammation in older *mdx* muscles results from an imbalance in the M1/M2 macrophage phenotypes (Nitahara-Kasahara *et al.,* 2013). It would be interesting to look at the expression of pro (M1) - and anti-inflammatory (M2) cytokines in dystrophic muscles and see if AAV-MuSK is able to alter their expression. Specifically, it would be good to look at the expression of TGF-β1 as it is known to be up-regulated in *mdx* mouse muscles, has been implicated in inflammation-driven fibrosis and is thought to interact with muscle satellite cells (Kharraz *et al.,* 2014; Narola *et al.,* 2013).

Overall, little is known about the role of the MuSK-system in the muscles of wild type and *mdx* mice. This thesis, together with previous findings in the lab, suggest that supplementation of MuSK-system components (MuSK, Rapsyn, Dok7) might hold potential to

improve pathology in the TA muscles of *mdx* mice. This suggests a novel role for the MuSK-system outside the NMJ and represents a potential therapeutic target for DMD and other neuromuscular disorders.

References

Arechavala-Gomeza, V, Kinali, M, Feng, L, Guglieri, M, Edge, G, Main, M, Hunt, D, Lehovsky, J,Straub, V, Bushby, K, Sewry, CA, Morgan, JE and Muntoni, F 2010. 'Revertant fibres and dystrophin traces in Duchenne muscular dystrophy: implication for clinical trials', *Neuromuscular Disorders*, vol. 20, no. 5, pp. 295-301.

Arimura, S, Okada, T, Tezuka, T, Chiyo, T, Kasahara, Y, Yoshimura, T, Motomura, M, Yoshida, N, Beeson, D, Takeda, SI and Yamanashi, Y 2014, 'Dok7 gene therapy benefits mouse models of diseases characterized by defects in the neuromuscular junction', *Science,* vol. 345, no. 6203, pp. 1505.

Ban, J 2018, 'Novel Effects of the MuSK System in Muscles of Wild-Type and Mdx mice' ,*PhD thesis,* University of Sydney.

Barker, RG, Horvath, D, van der Poel, C and Murphy, RM 2017, 'Benefits of prenatal taurine supplementation in preventing the onset of acute damage in the Mdx mouse', *PLoS currents*, vol. 9.

Bergamin, E, Hallock, PT, Burden, SJ and Hubbard, SR 2010, ' The cytoplasmic adaptor protein Dok7 activates the receptor tyrosine kinase MuSK via dimerization', *Molecular cell*, vol. *39, no.* 1, pp.100-109.

Blankinship, MJ, Gregorevic, P, Allen, JM, Harper, SQ, Harper, H, Halbert, CL, Miller, DA and Chamberlain, JS 2004, 'Efficient transduction of skeletal muscle using vectors based on adeno-associated virus serotype 6' *Molecular therapy*, vol. 10, no. 4, pp.671-678

Bloemberg, D and J Quadrilatero 2012, 'Rapid determination of myosin heavy chain Expression in rat, mouse, and human skeletal muscle using multicolor immunofluorescence analysis', *PLoS One,* vol. 7, no.4, pp. e35273.

Bulfield, G, Siller, WG, Wight, PA and Moore, KJ 1984, 'X chromosome-linked muscular dystrophy (mdx) in the mouse', *Proceedings of the National Academy of Sciences*, vol. *81, no*. 4, pp.1189-1192.

Chang, N, Chevalier, F and Rudnicki, M 2016, 'Satellite Cells in Muscular Dystrophy – Lost in Polarity', *Trends in Molecular Medicine*, vol. *22*, no. 6, pp. 479–496.

Chaturvedi, V, Dye, DE, Kinnear, BF, Van Kuppevelt, TH, Grounds, MD and Coombe, DR 2015, 'Interactions between skeletal muscle myoblasts and their extracellular matrix revealed by a serum free culture system', *PloS one*, vol. *10*, no. 6, pp.e0127675.

Cros, D, Harnden, P, Pellissier, JF and Serratrice, G 1989, 'Muscle hypertrophy in Duchenne muscular dystrophy', *Journal of neurology*, vol. 236,no. 1, pp.43-47.

Dan-Goor, M, Silberstein, L, Kessel, M and Muhlrad, A 1990, 'Localization of epitopes and functional effects of two novel monoclonal antibodies against skeletal muscle myosin', *Journal of Muscle Research & Cell Motility*, vol. *11, no.* 3, pp.216-226.

DeChiara, TM, Bowen, DC, Valenzuela, DM, Simmons, MV, Poueymirou, WT, Thomas, S, Kinetz, E, Compton, DL, Rojas, E, Park, JS and Smith, C 1996, 'The receptor tyrosine kinase MuSK is required for neuromuscular junction formation in vivo', *Cell*, vol. *85, no.* 4, pp.501-512.

Duddy, W, Duguez, S, Johnston, H, Cohen, TV, Phadke, A, Gordish-Dressman, H, Nagaraju, K, Gnocchi, V, Low, S and Partridge, T 2015, 'Muscular dystrophy in the mdx mouse is a severe myopathy compounded by hypotrophy, hypertrophy and hyperplasia', *Skeletal muscle*, vol. *5, no.* 1, pp.16.

Ellis, BL, Hirsch, ML, Barker, JC, Connelly, JP, Steininger, RJ and Porteus, MH 2013, 'A survey of ex vivo/in vitro transduction efficiency of mammalian primary cells and cell lines with Nine natural adeno-associated virus (AAV1-9) and one engineered adeno-associated virus serotype', *Virology journal*, vol. *10*, no. 1, pp.74.

Faber, RM, Hall, JK, Chamberlain, JS and Banks, GB 2014, 'Myofiber branching rather than myofiber hyperplasia contributes to muscle hypertrophy in mdx mice', *Skeletal muscle*, vol. *4*, no. 1, pp.10.

Fairclough, R.J, Wood, MJ and Davies, KE 2013, 'Therapy for Duchenne muscular dystrophy: renewed optimism from genetic approaches', *Nature Reviews Genetics*, vol. 14, no.6, pp. 373-378.

Farup, J, Madaro, L, Puri, P L, and Mikkelsen, UR 2015, 'Interactions between muscle stem cells, mesenchymal-derived cells and immune cells in muscle homeostasis, regeneration and disease', *Cell Death and Disease,* vol. 6, pp. e1830.

Froehner, SC, Reed, SM, Anderson, KN, Huang, PL and Percival, JM 2014, 'Loss of nNOS inhibits compensatory muscle hypertrophy and exacerbates inflammation and eccentric contraction-induced damage in mdx mice', *Human molecular genetics*, vol. *24, no.*2, pp.492-505.

Gehrig, SM, Koopman, R, Naim, T, Tjoakarfa, C and Lynch, GS 2010, 'Making fast-twitch dystrophic muscles bigger protects them from contraction injury and attenuates the dystrophic pathology', *The American journal of pathology*, vol. *176, no.* 1, pp.29-33.

Gelse, K, Pöschl, E and Aigner, T 2003, 'Collagens—structure, function, and biosynthesis', *Advanced drug delivery reviews*, vol. *55, no.* (12), pp.1531-1546.

Ghazanfari, N, Fernandez, KJ, Murata, Y, Morsch, M, Ngo, ST, Reddel, SW, Noakes, PG and Phillips, WD 2011, 'Muscle specific kinase: organiser of synaptic membrane domains' *The international journal of biochemistry & cell biology*, vol. *43, no.*3, pp.295-298.

Ghazanfari, N, Linsao, EL, Trajanovska, S, Morsch, M, Gregorevic, P, Liang, SX, Reddel, SW and Phillips, WD 2015, 'Forced expression of muscle specific kinase slows postsynaptic acetylcholine receptor loss in a mouse model of MuSK myasthenia gravis', *Physiological reports*, vol. 3*, no.* 12, pp.e12658.

Gibertini, S, Zanotti, S, Savadori, P, Curcio, M, Saredi S, Salerno, F, Andreetta, F, Bernasconi, P, Mantegazza, R and Mora, M 2014, 'Fibrosis and inflammation are greater in muscles of beta-sarcoglycan-null mouse than mdx mouse', *Cell and tissue research*, vol. 356, no.2, pp.427-443.

Gillies, AR and Lieber, RL 2011, 'Structure and function of the skeletal muscle extracellular matrix', *Muscle & nerve*, vol. *44*, no. 3, pp.318-331.

Guiraud, S and KE Davies 2017, 'Pharmacological advances for treatment in Duchenne muscular dystrophy', *Current Opinion in Pharmacology*, vol. 34(Supplement C): pp. 36-48.

Guiraud, S, Edwards, B, Squire, SE, Moir, L, Berg, A, Babbs, A, Ramadan, N, Wood, MJ and Davies, KE 2018, 'Embryonic myosin is a regeneration marker to monitor utrophin-based therapies for DMD', *Human molecular genetics*, vol. *28*, no. 2, pp.307-319.

Grounds, MD 2008, 'Complexity of Extracellular Matrix and Skeletal Muscle Regeneration', *Skeletal Muscle Repair and Regeneration*, vol. 3, Springer, Dordecht, p. 269-302.

Grounds, MD, Radley, HG, Lynch, GS, Nagaraju, K and De Luca, A 2008 , 'Towards developing standard operating procedures for pre-clinical testing in the mdx mouse model of Duchenne muscular dystrophy' , *Neurobiology of disease*, vol. 31, no. 1, pp.1-19.

Grounds, MD 2014, 'Quantification of histopathology in Haemotoxylin and Eosin stained muscle sections', *Treat-NMD Neuromuscular Network,* [Pdf] retrieved from: https://treat-nmd.org/wp-content/uploads/2016/08/MDX-DMD_M.1.2.007-28.pdf

Head, SI and Arber, MB 2013, 'An Active Learning Mammalian Skeletal Muscle Lab Demonstrating Contractile and Kinetic Properties of Fast- and Slow-Twitch Muscle', *Advances in Physiology Education,* vol. 37, no.4, pp. 405.

Hollinger, K and Selsby, JT 2015, 'PGC-1α gene transfer improves muscle function in dystrophic muscle following prolonged disease progress', *Experimental physiology*, vol. *100*, no. 10, pp.1145-1158.

Huang, YC, Dennis, RG and Baar, K 2006, 'Cultured slow vs. fast skeletal muscle cells differ in physiology and responsiveness to stimulation', *American Journal of Physiology-Cell Physiology*, vol. *291, no.* 1, pp.C11-C17.

Jones Jr, HR, Srinivasan, J, Allam, G.J and Baker, RA 2011, '*Netter's Neurology E-Book*' Elsevier Health Sciences.

Kammoun, M, Cassar-Malek, I, Meunier, B and Picard, B 2014, 'A Simplified Immunohistochemical Classification of Skeletal Muscle Fibres in Mouse', *European Journal of Histochemistry,* vol. 58, no.2.

Kemaladewi, DU, 't Hoen, PA, Ten Dijke, P, Van Ommen, GJ and Hoogaars, WM 2012, 'TGF-β signaling in Duchenne muscular dystrophy', *Future Neurology*, vol. *7*, no. 2, pp.209-224.

Kharraz, Y, Guerra, J, Mann, CJ, Serrano, AL and Muñoz-Cánoves, P 2013, 'Macrophage Plasticity and the role of inflammation in Skeletelal Muscle Repair', *Mediators of inflammation*, vol. 2013, pp. 1-9.

Kharraz, Y, Guerra, J, Pessina, P, Serrano, AL and Muñoz-Cánoves, P 2014, 'Understanding the process of fibrosis in Duchenne muscular dystrophy', *BioMed research international*, vol. 2014.

Kole, R and Krieg, A 2015, 'Exon skipping therapy for Duchenne muscular dystrophy', *Advanced Drug Delivery Reviews*, vol. *87*.

Kornegay, JN, Childers, MK, Bogan, DJ, Bogan, JR, Nghiem, P, Wang, J, Wagner, KR 2012, 'The paradox of muscle hypertrophy in muscular dystrophy', Physical *medicine and rehabilitation clinics of North America*, vol. 23, no. 1, pp. 149–xii.

Latroche, C, Matot, B, Martins-Bach, A, Briand, D, Chazaud, B, Wary, C, Carlier, PG, Chrétien, F and Jouvion, G 2015, 'Structural and functional alterations of skeletal muscle microvasculature in dystrophin-deficient mdx mice', *The American journal of pathology*, vol. *185, no.* 9, pp.2482-2494.

Lemos, DR, Babaeijandaghi, F, Low, M, Chang, CK, Lee, ST, Fiore, D, Zhang, RH, Natarajan, A, Nedospasov, SA and Rossi, FM 2015, 'Nilotinib reduces muscle fibrosis in chronic muscle injury by promoting TNF-mediated apoptosis of fibro/adipogenic progenitors', *Nature medicine*, vol. *21, no.* 7, p.786.

Lynch, GS, Hinkle, RT, Chamberlain, JS, Brooks, SV and Faulkner, JA 2001, 'Force and power output of fast and slow skeletal muscles from mdx mice 6-28 months old' , *The Journal of physiology*, vol. *535, no.* 2, pp.591-600.

Mann, CJ, Perdiguero, E, Kharraz, Y, Aguilar, S, Pessina, P, Serrano, AL and Muñoz-Cánoves, P 2011, 'Aberrant repair and fibrosis development in skeletal muscle', *Skeletal muscle*, vol. *1*, no. 1, p.21.

Manning, J and O'Malley, D 2015, 'What has the mdx mouse model of duchenne muscular dystrophy contributed to our understanding of this disease?', *Journal of muscle research and cell motility*, vol. 36, no. 2, pp. 155-167.

Mázala, DA, Pratt, S, Chen, D, Molkentin, JD, Lovering, RM and Chin, ER 2015, 'SERCA1 overexpression minimizes skeletal muscle damage in dystrophic mouse models', *American Journal of Physiology-Cell Physiology*, vol. 308*, no.*9, pp.C699-C709.

McGreevy, J, Hakim, C, McIntosh, M and Duan, D 2015, 'Animal models of Duchenne muscular dystrophy: from basic mechanisms to gene therapy', *Disease models & mechanism*, vol. 8, no.3, pp. 195-213.

Miyoshi, S, Tezuka, T, Arimura, S, Tomono, T, Okada, T and Yamanashi, Y 2017, 'DOK7 gene therapy enhances motor activity and life span in ALS model mice', *EMBO molecular medicine,* vol. 9, no. 7, pp. 880-889.

Mozzetta, C, Consalvi, S, Saccone, V, Tierney, M, Diamantini, A, Mitchell, KJ, Marazzi, G, Borsellino, G, Battistini, L, Sassoon, D and Sacco, A 2013, 'Fibroadipogenic progenitors mediate the ability of HDAC inhibitors to promote regeneration in dystrophic muscles of young, but not old Mdx mice', *EMBO molecular medicine*, vol. *5*, no. 4, pp.626-639

Narola, J, Pandey, SN, Glick, A and Chen, YW 2013, 'Conditional expression of TGF-β1 in skeletal muscles causes endomysial fibrosis and myofibers atrophy', *PloS one*, vol. *8*, no. 11, pp .e79356.

Nigro, V and Piluso, G 2015, 'Spectrum of muscular dystrophies associated with sarcolemmal-protein genetic defects', *Biochimica et Biophysica Acta (BBA)-Molecular Basis of Disease*, vol. *1852*, no. 4, pp.585-593.

Nitahara-Kasahara, Y, Hayashita-Kinoh, H, Chiyo, T, Nishiyama, A, Okada, H, Takeda, SI and Okada, T 2013, 'Dystrophic mdx mice develop severe cardiac and respiratory dysfunction following genetic ablation of the anti-inflammatory cytokine IL-10', *Human molecular genetics*, vol. *23, no.* 15, pp.3990-4000.

Ohno, K, Ohkawara, B and Ito, M 2017, 'Agrin-LRP4-MuSK Signalling as a Therapeutic Target for Myasthenia Gravis and Other Neuromuscular Disorders', *Expert Opinion on Therapeutic Targets,* vol. 21, no.10.

Omairi, S, Hau, KL, Collins-Hooper, H, Scott, C, Vaiyapuri, S, Torelli, S, Montanaro, F, Matsakas, A and Patel, K 2019, 'Regulation of the dystrophin-associated glycoprotein complex composition by the metabolic properties of muscle fibres', *Scientific reports*, vol. *9, no.* 1, p.2770.

Pastoret, C and Sebille, A 1995, 'Mdx mice show progressive weakness and muscle deterioration with age', *Journal of the neurological sciences*, vol. *129*, no.2, pp.97-105.

Pertl, C, Eblenkamp, M, Pertl, A, Pfeifer, S, Wintermantel, E, Lochmuller, H, Walter, M, Krause, S and Thirion, C 2013, 'A new web-based method for automated analysis of muscle histology', *BMC Musculoskeletal Disorders,* vol. 13, no. 26, pp. 26.

Pessina, P, Cabrera, D, Morales, MG, Riquelme, CA, Gutiérrez, J, Serrano, AL, Brandan, E and Muñoz-Cánoves, P 2014, 'Novel and optimized strategies for inducing fibrosis in vivo: focus on Duchenne Muscular Dystrophy', *Skeletal muscle*, vol. 4, no. 1, pp.7.

Pilgram, GS, Potikanond, S, Baines, RA, Fradkin, LG and Noordermeer, JN 2010, 'The roles of the dystrophin-associated glycoprotein complex at the synapse', *Molecular neurobiology*, vol. *41, no.* 1, pp.1-21.

Polla, B, D'antona, G, Bottinelli, R and Reggiani, C 2004, 'Respiratory muscle fibres: specialisation and plasticity', *Thorax*, vol. 59, no. 9, pp.808-817.

Pratt SJ, Shah SB, Ward CW, Inacio MP, Stains JP and Lovering, RM 2013, 'Effects of in vivo injury on the neuromuscular junction in healthy and dystrophic muscles', *The Journal of Physiology*, vol. 591, no. 2 559-570

Pullen, AH 1977, 'The distribution and relative sized of fibre types in the extensor digitorum longus and soleus muscles of the adult rat', *Journal of Anatomy*, vol. 123, no. 2, pp.467.

Punga, AR, Maj, M, Lin, S, Meinen, S and Rüegg, MA 2011, 'MuSK levels differ between adult skeletal muscles and influence postsynaptic plasticity', *European Journal of Neuroscience*, vol. 33, no. 5, pp.890-898.

Riaz, M, Raz, Y, Moloney, EB, van Putten, M, Krom, YD, van der Maarel, SM, Verhaagen, J, and Raz, V 2015, 'Differential myofiber-type transduction preference of adeno-associated virus serotypes 6 and 9' *Skeletal Muscle*, vol. 5, no. 37, p. 37.

Samuel, MA, Valdez, G, Tapia, JC, Lichtman, JW, Sanes, JR, and Samuel, MA 2012, 'Agrin and synaptic laminin are required to maintain adult neuromuscular junctions.' *PloS One*, vol. 7, no. 10, pp. e46663–e46663.

Sanes, JR 2003, 'The Basement Membrane/basal Lamina of Skeletal Muscle' *The Journal of biological chemistry,* vol. 278, no. 15, p. 12601–12604.

Sartori, R, Schirwis, E, Blaauw, B, Bortolanza, S, Zhao, J, Enzo, E, Stantzou, A, Mouisel, E, Toniolo, L, Ferry, A and Stricker, S 2013, 'BMP signaling controls muscle mass', *Nature genetics*, vol. 45, no. 11, pp.1309.

Schiaffino, S, Gorza, L, Sartore, S, Saggin, L and Carli, M 1986, 'Embryonic myosin heavy chain as a differentiation marker of developing human skeletal muscle and rhabdomyosarcoma: a monoclonal antibody study', *Experimental cell research*, vol. *163*, no. 1, pp.211-220.

Schiaffino, S, Gorza, L, Pitton, G, Saggin, L, Ausoni, S, Sartore, S and Lømo, T 1988, 'Embryonic and neonatal myosin heavy chain in denervated and paralyzed rat skeletal muscle', *Developmental biology*, vol. *127*, no. 1, pp.1-11.

Schiaffino, S, 2010, 'Fibre types in skeletal muscle: a personal account', Acta *physiologica*, *199*(4), pp.451-463.

Schiaffino, S and Reggiani, C 2011, 'Fiber types in mammalian skeletal muscles', *Physiological reviews*, *91*(4), pp.1447-1531.

Schiaffino, S, Rossi, AC, Smerdu, V, Leinwand, LA and Reggiani, C 2015. 'Developmental myosins: expression patterns and functional significance', *Skeletal muscle*, vol. *5*, no. 1, pp.22.

Selsby, JT, Morine, KJ, Pendrak, K, Barton, ER and Sweeney, HL 2012, 'Rescue of dystrophic skeletal muscle by PGC-1α involves a fast to slow fiber type shift in the mdx mouse',*PloS one*, vol. *7, no.* 1, p.e30063.

Sréter, FA and Woo, G 1963, 'Cell water, sodium, and potassium in red and white mammalian muscles', *American Journal of Physiology-Legacy Content*, vol. 205.no. 6, pp. 1290–1294.

Theocharis, AD, Skandalis, SS, Gialeli, C and Karamanos, NK 2016, 'Extracellular matrix structure', *Advanced drug delivery reviews*, *97*, pp.4-27.

Trajanovska, S, Ban, J, Huang, J, Gregorevic, P, Morsch, M, Allen, D, and Phillips, WD 2019, 'Muscle specific kinase protects dystrophic mdx mouse muscles from eccentric contraction-induced loss of force-producing capacity', *Journal of Physiology*, vol. 597, no. 18, pp. 4831–4850.

Ueta, R, Tezuka, T, Izawa, Y, Miyoshi, S, Nagatoishi, S, Tsumoto, K and Yamanashi, Y 2016, 'The carboxyl-terminal region of Dok-7 plays a key, but not essential, role in activation of muscle-specific receptor kinase MuSK and neuromuscular synapse formation', *The Journal of Biochemistry*, vol. *161*, no. 3, pp.269-277.

Uezumi, A, Ito, T, Morikawa, D, Shimizu, N, Yoneda, T, Segawa, M, Yamaguchi, M, Ogawa, R, Matev, MM, Miyagoe-Suzuki, Y and Takeda, SI 2011, 'Fibrosis and adipogenesis originate from a common mesenchymal progenitor in skeletal muscle', *Journal of Cell Science*, vol. 124, no. 21, pp.3654-3664.

Urso, ML, 1985, 'Anti-inflammatory interventions and skeletal muscle injury: benefit or detriment?', *Journal of applied physiology*, vol. *115, no.* 6, pp.920-928.

Vidal B, Ardite E , Suelves, M, Ruiz-Bonilla, V, Janué, A, Flick, MJ, Degen, JL, Serrano, AL, and Muñoz-Cánoves, P 2012, *'*Amelioration of Duchenne muscular dystrophy in mdx mice by elimination of matrix-associated fibrin-driven inflammation coupled to the $\alpha_M\beta_2$ leukocyte integrin receptor', *Human Molecular Genetics*, Volume 21, Issue 9, p.1989–2004.

Villalta, SA, Nguyen, HX, Deng, B, Gotoh, T and Tidball, JG 2008, 'Shifts in macrophage phenotypes and macrophage competition for arginine metabolism affect the severity of muscle pathology in muscular dystrophy', *Human molecular genetics*, vol. 18, no. 3, pp.482-496.

Wallace, GQ and McNally EM 2009, 'Mechanisms of Muscle Degeneration, Regeneration, and Repair in the Muscular Dystrophies', *Annual Review of* Physiology, vol. 71, no. 1, pp. 37-57.

Wang, B, Li, J and Xiao, X 2000, 'Adeno-associated virus vector carrying human minidystrophin genes effectively ameliorates muscular dystrophy in mdx mouse model', Proceedings *of the National Academy of Sciences*, vol. *97*, no. 25, pp.13714-13719.

Yilmaz, A, Kattamuri, C, Ozdeslik, RN, Schmiedel, C, Mentzer, S, Schorl, C, Oancea, E, Thompson, TB and Fallon, JR 2016, 'MuSK is a BMP co-receptor that shapes BMP responses and calcium signaling in muscle cells', *Science Signalling,* vol. *9*. No. 444, pp.ra87-ra87.